1997

Vibration balancing analysis of a dual face mill eccentric grinder machine head.

Jason Kyle. Kushniruk
University of Windsor

INFORMATION TO USERS

This manuscript has been reproduced from the microfilm master. UMI films the text directly from the original or copy submitted. Thus, some thesis and dissertation copies are in typewriter face, while others may be from any type of computer printer.

The quality of this reproduction is dependent upon the quality of the copy submitted. Broken or indistinct print, colored or poor quality illustrations and photographs, print bleedthrough, substandard margins, and improper alignment can adversely affect reproduction.

In the unlikely event that the author did not send UMI a complete manuscript and there are missing pages, these will be noted. Also, if unauthorized copyright material had to be removed, a note will indicate the deletion.

Oversize materials (e.g., maps, drawings, charts) are reproduced by sectioning the original, beginning at the upper left-hand corner and continuing from left to right in equal sections with small overlaps. Each original is also photographed in one exposure and is included in reduced form at the back of the book.

Photographs included in the original manuscript have been reproduced xerographically in this copy. Higher quality 6" x 9" black and white photographic prints are available for any photographs or illustrations appearing in this copy for an additional charge. Contact UMI directly to order.

UMI

A Bell & Howell Information Company
300 North Zeeb Road, Ann Arbor MI 48106-1346 USA
313/761-4700 800/521-0600

VIBRATION BALANCING ANALYSIS OF A DUAL FACE MILL ECCENTRIC GRINDER MACHINE HEAD

Jason K. Kushniruk

A Thesis
Submitted to the Faculty of Graduate Studies and Research
through the Department of Mechanical Engineering
in Partial Fulfilment of the Requirements for
the Degree of Master of Applied Science at the
University of Windsor

Windsor, Ontario, Canada

1997

ABSTRACT

Balancing of machinery is a well known technical aspect of engineering which is practiced throughout the world. Many studies have been performed to optimize the models and methods used to make rotor balancing faster and more efficient. This thesis deals with the unique problems associated with the balancing of eccentrically designed spindles for the machine tool industry. Cobra Machine Tool Limited has designed and patented the newest form of combination face mill and grinder operation in North America. The study performed in this analysis provides a benchmark for further vibration studies by the company in the future.

Standard vibration measurement equipment, available at the University of Windsor, was used to develop a testing and balancing procedure for this specific machining head and to demonstrate the method to others in the field. The methods employed as well as the final balancing procedures are outlined in the study for various areas of interest.

The conclusions for the study were based on the *in situ*, balancing performed at Cobra Machine Tool for the prototype machine. Engineering design changes have been identified that will make any subsequent machines produced in the future, operate more smoothly and efficiently than the prototype machine. Other studies relating noise and vibration measurements and dynamic modeling, have been included for the completeness of the study.

DEDICATION

Dedicated to my family:

William, Deanna, Nicole, Lana,

and to those family members not present to witness our accomplishments

ACKNOWLEDGMENTS

The author would like to express his sincere gratitude to the people of Cobra Machine Tool Ltd. for making available to students, prototype machines for research and development. Special thanks to Dick Lunn and the owner of Cobra for their patience and practical knowledge in the machine tool area, they were a huge help for fabricating materials used for the project.

The author is also grateful to his advisor, Dr. R. Gaspar, for his guidance and encouragement for the duration of this project, and for supplying reference materials. Also thanks to Dr. Z. Reif for finding this project, and giving valuable advise in certain areas of uncertainty.

Special thanks to N. Chana, Dr. E. Liasi and my colleagues for advice and patience waiting for equipment to return, supplying reference materials, and for scanning in material. Also thanks to my parents and sisters for their patience and support throughout this period of studies.

TABLE OF CONTENTS

LIST OF FIGURES

LIST OF TABLES

NOMENCLATURE

TERM	*Meaning*
A	Area [in^2]
D	Diameter of specified component [inch]
F	Out of balance force of specified plane [lb_f]
K_a	Acceleration constant conversion factor [g / mV]
L/D	Length by diameter ratio [unitless]
L, *l*	Length or depth of the specified hole or other [inch]
N	Operational Speed [rpm]
W	Weight [lbf , oz]
m	Mass of a specified object [lb]
r	Radius measured from the center of rotation to the center of mass [inch]
t	Thickness of specified material [inch]
t_{os}	Optical sensor time [s]
w	Width of the specified material [inch]
x, **i**	x-directional vector symbol
y, **j**	y-directional vector symbol
α, β, θ	Influence Coefficient, Angular Values [radians, degrees]
α_{ij}	Influence Coefficient matrix entry
ρ	Density of the specified material [lb / in^3]
φ	Mechanical timing lag [degrees]
ω	Angular velocity of a specific rotor [rad/s]

Other definitions and acronyms are defined in the Glossary of Terms

I. INTRODUCTION

1.1 Background

Unbalance is the most common cause of vibration problems in many machines. Vibration problems cost companies millions of dollars every year to keep machines running smoothly and efficiently, especially as a machine ages. The main purposes of reducing machine vibration are to minimize noise, increase part quality, increase bearing life, decrease the machine stress of operation, consume less energy and provide greater customer satisfaction [32]. All of these aspects of machine performance have become increasingly more important in present day manufacturing.

Vibration considerations can be primarily linked to sources of unbalance, electromagnetic energy, looseness, gear meshing, aerodynamic forces, poor bearings, shaft misalignment, maintenance and upkeep, operating conditions and the type of operation performed by the machine. These areas are the main focus of any vibration analysis and the factors presented previously are often the results of poor machine operating conditions.

Balancing spindles dates back to about 1934 when the first references to rotor balancing appeared in engineering literature. The scope of this study includes a discussion of some of the concepts used in rigid and flexible rotor balancing and the advancements made in these areas over the past decades. These aspects will be introduced in the literature survey found in Chapter II of the study. The contribution to this area will be the primary focus of this study for dual eccentric machine spindle balancing.

There exist many methods for balancing rotors as well as classifications of rotors in terms of the type of unbalance. Balancing dual spindles is a unique and important area in engineering. Some individuals have completed mathematical and dynamic studies specific to this area, but this machine tool head is the first of its kind in North America; therefore, it is necessary to develop a working vibration model, as well as set a benchmark for balancing the operating characteristics of a dual eccentric spindle-in-spindle design.

1.2 The Super Finish Machine

The Super Finish machine consists of five primary components, a face mill, an eccentric cup faced grinder offset by one inch, a four stage planetary gear system, and a internal lubrication channel. Figure 1.1 details the entire side view of the machine demonstrating the orientation of the machine tool assembly. The ten inch face mill consists of 21 teeth 180 degrees about the front face and is fastened to the barrel spindle drive. This spindle revolves internally on two main roller bearings. The seven inch diamond grinder is seated directly to the grinder spindle as shown in Figure 1.1. The grinder spindle revolves in a one inch offset cavity though the barrel spindle on five angular contact bearings. The motor operates using an induction drive which turns the motor spindle at the desired speed. The three spindles are linked together by a four stage gear system. This gear system is shown in Appendix D as Figures D1 and D10 to D14, in which a full explanation is provided for referral.

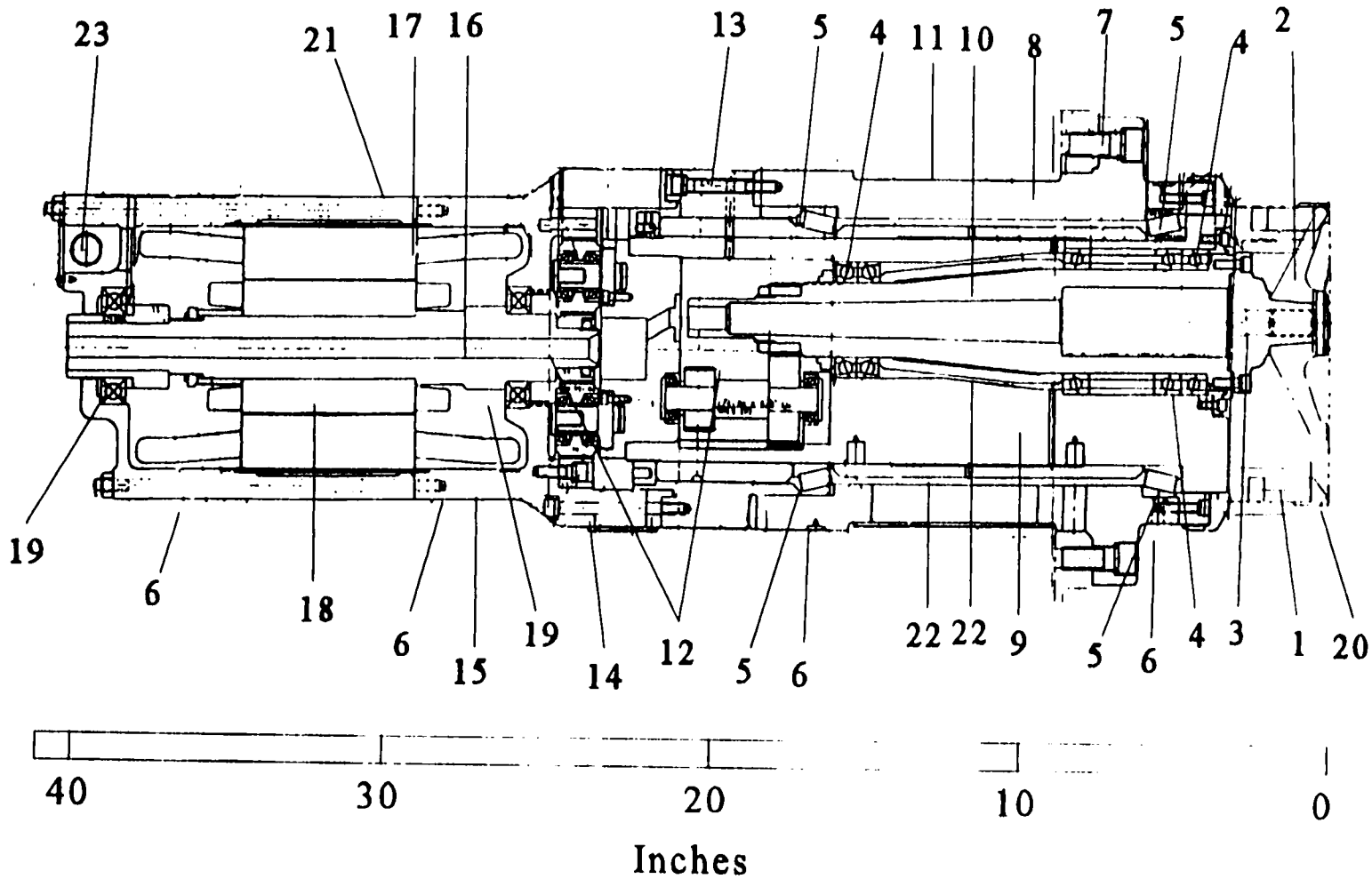

Figure 1.1 The Super Finish Machine

Table 1.1 Super Finish Machine Legend Key	
Key	**Description**
1	Face Mill Cutter Head
2	Diamond Cup Face Grinder
3	Grinder Seat
4	Angular Contact Bearings
5	Roller Bearings
6	Accelerometer Mount Location
7	Machine Fixture Mounting Location Bolt
8	Machine Spindle Housing
9	Barrel Spindle
10	Grinder Spindle
11	Machine Spindle Housing Access Panel
12	Multi-stage Gearing Location
13	Rear Mounting Bolt
14	Motor Mounting Bolt
15	Motor Housing or Shell
16	Motor Spindle Rotor
17	Stator and Coils
18	Rotor Bar and Inductors
19	Motor Bearings
20	Machine Head Inserts
21	Motor Shell Parting Line
22	Machine Steel Spacers

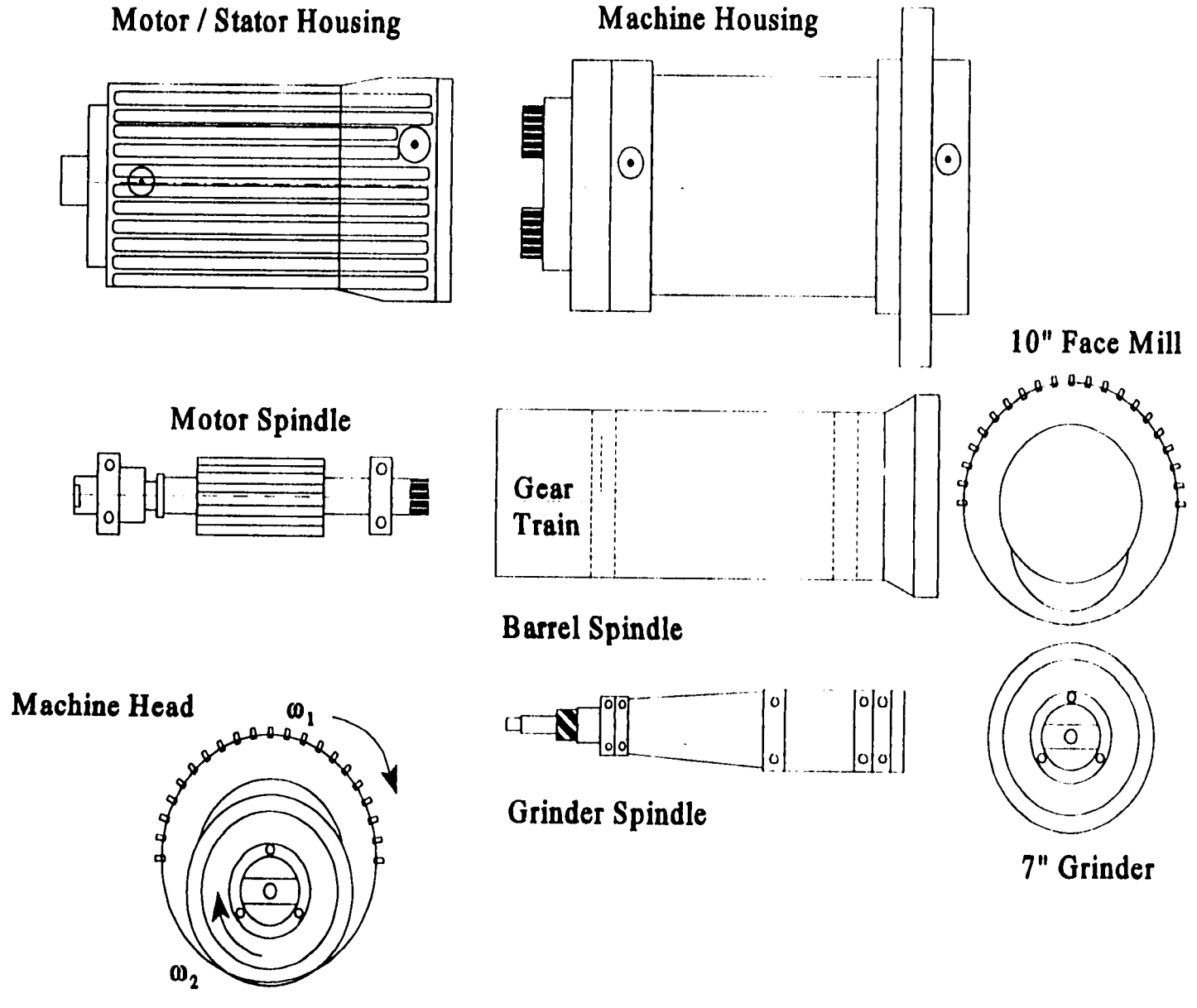

Figure 1.2 The Super Finish Machine Primary Components

1.3 Vibration Analysis

The objective of a vibration analysis is to determine the machine's operating characteristics. The first step in accomplishing this objective is a vibration analysis to determine the natural frequencies of the machine tool components. This is accomplished by performing frequency response testing (or F.R.F. testing). This testing provides valuable data for defining the behavior of the spindles in operation and for determining the natural frequency for each spindle.

The second step in meeting this objective is a vibration analysis to balance the machine. The main balancing procedure for most spindles consists of adding or subtracting a known amount of material, at specific angular locations, and radial distances. A undoubtedly symmetric rotor will always have some unbalance due to non-uniformities in the rotor material. By carefully examining the design of a non-symmetric rotor, balancing can be performed statically to eliminate the non-symmetric eccentricity in a rotor. This will be demonstrated in Chapter V of this study. A statically balanced rotor does not mean that the rotor is balanced dynamically. If all static considerations are balanced, there still may exist a *couple unbalance*, dynamically. A method of eliminating the couple generated by the rotation of the rotor is the impetus behind dynamic balancing, and the methods to accomplish this will be discussed in the literature survey. Finally, the methods utilized for this study can be found in Chapter VI.

Included in this study is a rotor acceleration (run up and run down) analysis, a full spectrum sound power level determination, and a noise spectrum analysis for the gear system

used in the machine. These studies were crucial for machine diagnostics provided to any purchasing company. Some of the data in the noise analysis was used indirectly, but it will not be included in the main body of the study which will focus primarily on balancing procedures.

Conclusions and recommendations will be discussed for the modeling found in Appendix E. This section deals with the mathematical development of the dynamic vibration forces for the machine type that is the subject of this study. Calculations and variables must be carefully solved using engineering concepts in advanced dynamics and concepts in multi-frequency vibration. These areas will be discussed before applying the governing equations to the system.

II. LITERATURE REVIEW

2.1 Spindle Balancing

According to Wowk [32], the common definition of unbalance is the unequal distribution of the weight of a rotor about its rotating centerline. The formal definition of unbalance is that condition which exists in a rotor when vibratory force or motion is imparted to its bearings as a result of centrifugal forces. The basic force which describes this phenomenon for a disk is simply, $F = m\ r\ \omega^2$. This is shown in Figure 2.1. The most important aspect of this equation is that the force is directly proportional to the mass, and the eccentric radius, and is directly proportional to the square of the constant angular velocity about its rotating centerline. This directly implies that as the mass or the radius doubles in value, the centrifugal force doubles, but as the speed doubles, the centrifugal force increases by a factor of four. This is the fundamental theory behind the dynamics of a rotating body about its center of gravity.

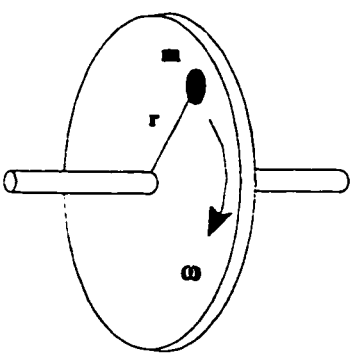

Figure 2.1 Rotational Unbalance of a Simple Disk

2.1.1 Rigid Rotor Balancing Using Influence Coefficients

Rigid rotor balancing has been dated back to 1934 when Thearle [3] published some of the earliest methods of two plane balancing using influence coefficients. Many studies were performed by others in the early 1940s but, a practical influence coefficient method was formalized only in 1964 by Goodman [9] using a least squares method for computing balance corrections. He introduced the mathematical background, the selection of balancing planes, and organized the data and results. The main focus of his paper was confined to rigid rotor balancing or rotors which operate well below their first critical speed. The critical speed of a rotor occurs at the rotating speed coinciding with a peak in the dynamic forces experienced by the rotor bearing system. This situation exists when the rotating speed of the system coincides with a natural frequency of vibration of the supporting shaft.

Goodman was the pioneer to influence coefficient balancing even when instrumentation accuracy to perform testing was questionable. Before early 1970, instrumentation and analysis methods were inaccurate and very expensive. Today, instrumentation such as accelerometers, signal analyzers and photoelectric probes are much more accurate than their forerunners, but are still very expensive.

2.1.2 Flexible Rotor Balancing Using Influence Coefficients

A flexible rotor differs from a rigid rotor in that the operating frequency is above the first critical speed of the rotor. Flexible rotor balancing using the influence coefficient

method was first introduced by Tessarik, Badgley, and Anderson [25] in 1972. They developed balancing methods which allowed for safe passage through all critical speeds after a reasonable number of balancing runs. However, this was only achievable because of superior equipment and the accuracy of phase measurement during the test runs. Lund and Tonnesen [16] documented an analysis and experiment on multi-plane balancing of a flexible rotor also in 1972. The conclusions for the study were that influence coefficients are an accurate method for the balancing of a rotor for a linear system: the magnitude and phase angle must not have error more than 3 to 4 percent; and that the influence coefficient method can accurately be expanded to more then two balancing planes.

In 1974 Tessarzik and Badgley [24] introduced the exact point-speed method and the least squares procedure for flexible rotor balancing by influence coefficients.

After the development of two plane balancing, many companies, such as Hewlett Packard, developed calculator cards and subroutines to calculate the results from the many measurements needed to perform two plane balancing with influence coefficients. These studies were simplified to a workable method and setup for performing balancing.

2.2 Rotor Classification

It is necessary to classify rotors into different categories to determine the best method to apply weights about the rotor. For example, a thin disk of thickness t, and diameter D, can be classified as a static unbalance problem. Other types of unbalance conditions exist when

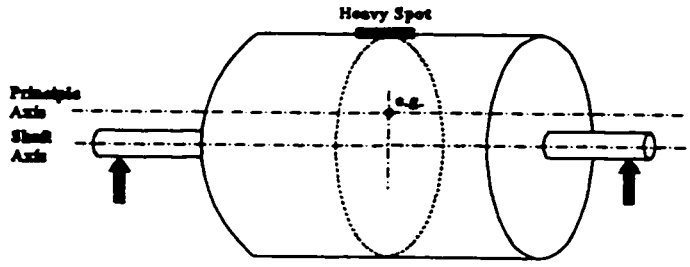

Figure 2.2 Static Unbalance Rotor Condition

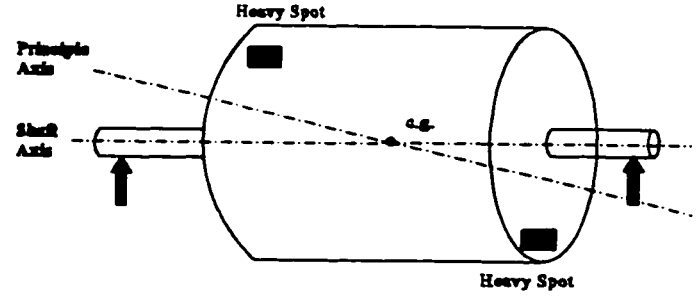

Figure 2.3 Couple Unbalance Rotor Condition

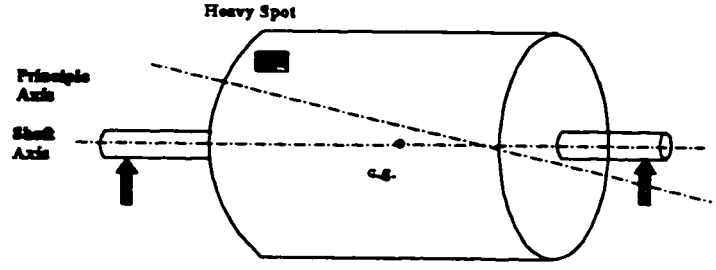

Figure 2.4 Quasi-static Unbalance Rotor Condition

the diameter and axial length are greater. As shown in Figures 2.2 through 2.4, there are three basic rotor conditions. Figure 2.2 shows a rotor in a static unbalance condition. A static rotor is defined as a rotor which the principle axis is parallel to the center of rotation and the center of gravity acts through this axis. A pure couple unbalance condition, shown in Figure 2.3, exists when the principle mass axis intersects the shaft axis at the center of gravity. This condition is very rare and only exists when two heavy spots exist 180 degrees apart on opposite ends of the rotor. The quasi-static unbalance position is the most common type of rotor unbalance. This is shown in Figure 2.4. Wowk [32] and others [3,17,19,30], nicely outline conditions and corrective methods for balancing each type of rotor. Balancing methods were introduced in section 2.1 and will be discussed in the next section.

2.3 Spindle Balancing Methods

There are several methods which exist to perform practical balancing in the field or in the shop. Having practical knowledge of all the methods available is an invaluable tool for anyone performing a balancing analysis.

2.3.1 Single-Plane Balancing

A single plane through the cross section of a rotor is needed to perform this type of analysis. The method is always applicable for thin disks and also works well for long rotors if a static unbalance condition exists as in Figure 2.2. There are only three assumptions for single plane balancing. Vibration amplitudes are related to unbalance mass linearly; the phase lag or the angular vector, in which the force rotates about the center of rotation remains constant for all measured amplitudes. The measurements are effected only by unbalance and not by any other disturbances.

2.3.2 Two-plane and Multi-plane Balancing

Two-plane balancing is an extension of single plane balancing. As the name implies, balance corrections are performed in more than one axial position along the rotor. According to Wowk [32], two plane balancing should only be attempted after single-plane balancing has proven to be unsuccessful and the following conditions are met:

1) The rotor is rigid.

2) The supports are flexible, or semi-flexible, but not resonant.

3) Either serious cross-effect or serious couple unbalance is present.

Two plane balancing has been studied by many individuals including Darlow [3], and others [6,7,9,10,16,17,24,25]. A Borland C++ program segment used in calculating the correction weights for the two plane balancing method with phase is included in Appendix B.

2.3.3 Static Couple Method

A similar procedure was performed on the machine rotor in this study. The method consists of separating the static unbalance from the dynamic couple unbalance. The static unbalanced is first corrected by the addition of weights 180 degrees opposite to the known heavy spot. The residual unbalance of any other form is balanced dynamically. This method has two great advantages. The first is that it will reduce the static unbalance before rigorous planar balancing takes place, and the second is that it is possible to visually comprehend the vector positions of the unbalance.

2.3.4 Four Run Method

The four run method was first developed when phase sensors did not exist and the ability to measure phase was very difficult. The method uses graphical methods to solve for the angular positions of unbalance and is outlined in Wowk [32]. This method was limited to single plane balancing until 1987 when Everett [6], combined the two plane balancing

method, and the four run method, into two plane balancing without phase response. This led to another study in 1988 when Foiles [7], developed a method for balancing with phase only in single or multi-plane. Both methods are applicable for many types of rotors but require a number of trial runs, or stops and starts of the rotor. In an industrial production setting, when the most efficient method must be used, minimizing the number of runs for balancing the machine must be foremost. A Qbasic program used to calculate the correction weights for two plane balancing without phase is also included in Appendix B. Both programs included in Appendix B were used to calculate correction weights, and were used to generate the balancing data tables in Appendix B.

2.3.5 Dual Rotor Balancing Methods

As the main focus of this study, dual rotor balancing is a somewhat new area of balancing technology. The first experimental analysis for an unbalance response of a dual rotor system, was performed by Gupta, Gupta and Athre [10]. They developed a rig which was capable of simulating the two spool aero-engine. They demonstrated that the rotor exhibits *cross-excitation*, or the vibration of rotor one effects the vibration of rotor two and vica versa. These effects are analyzed in the dynamic modeling section of the report for the displacements of multi-frequency excitation. The literature used for experiment is discussed in the next section.

2.4 Experimental Literature

The main literature for balancing methods came from numerous texts. Balancing setups and methods for analysis were studied to grasp the basic concepts for experimentation. Diagrams for single-plane and two-plane balancing setups were found in [11,17,27,30,31]. Hewlett Packard manuals also supplied valuable information for data acquisition, calibration, frequency window selection and much more. The various experimental setups will be demonstrated in the dynamic balancing section of the study.

2.4.1 Modal Analysis Literature

The methods used in analyzing the frequency response plots have been described by numerous authors. Singleton [21] introduces experimental modal analysis and its applications in solving machinery and structural vibration problems. Modal analysis requires knowledge of frequency response functions, reciprocity, significance of the hammer tip hardness, calibration of hammer, frequency windows, degrees of freedom and assumptions. Acceleration or g-force is given in terms of acceleration and forces. Reciprocity is assumed for a system to vary linearly, and that the components exhibit symmetry. Leakage, is also eliminated or minimized by using an exponential window, or log-scale, which allows noise to be included in the measurement. Leakage is formally defined as a smearing of energy across the frequency spectrum caused by non-periodic signals being transformed across the time spectrum [18].

Crawley [2], suggests using coherence accuracy in measurements. Coherence is derived from a series of averaged frequency response measurements. Coherence defines a range from 0 to 1 in the real domain. This will give a percentage accuracy in the impacts and demonstrates reproducibility in the impact force. The computed coherence for impact tests is approximately unity at all frequencies except the anti-resonance frequencies which exist as a sharp spike downwards between two resonance frequencies.

Other authors have also suggested using real and imaginary plots to determine the natural frequency spikes. Some literature used for this analysis was found in Broch [1].

2.4.2 Noise Experiment Literature

The information used for the noise analysis was found in Ellison and Yang [5,33]. Other information describing reverberation and setups were found in Bruel and Kjaer Review manuals [13,15]. This section is included in Appendix C for the experiment determining machine sound power level.

2.4.3 Gear Experiment Literature

The information used for the gearing analysis was found in Dudley's Gear Handbook [4]. Other information for calculations, microphone and analyzer setup have been described in [4, 14, 28]. This section is included in Appendix D for the experiment determining gear noise and vibration.

The theoretical concepts presented in this chapter provide a fundamental background in rigid rotor balancing.

III. EQUIPMENT

3.1 Accelerometers

The accelerometers used to perform the modal analysis or frequency response testing, and the balancing procedures, were Quartz accelerometers (with built in amplifiers) Series 300 type 303A02 summarized as follows:

Table 3.1 Accelerometer Specifications Type PCB 303A02			
Sensitivity Peak	10 mV / g	Transverse Sensitivity	5 % max
Range (±5Vout)	±500 g pk	Strain Sensitivity	0.05 g/μin/in
Range (±10Vout)	N/A	Temperature Range	-40 to 200° F
Resolution	0.01 g pk	Temp. Coefficient	0.3 % / °F
Resonant Frequency	70 kHz	Vibration	±1000g pk max
Freq Range ±5%	1 to 10000 Hz	Shock	2000 g pk max
Freq Range ±10%	0.7 to 20000 Hz	Structure	upright
Overload Recovery	10 μs	Size (hex by height)	0.281 x 0.48 in
Discharge Time Constant	0.5 s @ 70° F	Weight	1.9 grams
Amplitude Linearity	1 %	Case Material	316 SS
Output Impedance	100 Ω	Sealing / Ground Isol.	Epoxy / No

The accelerometer was calibrated using the Calibration Exciter Bruel and Kjaer Type 4294 at a frequency of 159.2 Hz (or 1000 rad/s) at an r.m.s. amplitude of 10 m/s^2. It was assumed that the calibration for the accelerometer would be maintained throughout the

testing. This value was measured for both accelerometers and a value of 152.6 mV / g was the calibration factor used for all the testing.

3.2 Signal Amplifiers

The accelerometers were connected to signal amplifiers by PCB Model 480 D06 Power Unit with a gain of 1X - 10X - 100X. These units condition and amplify the vibration signals from the accelerometers.

3.3 Digital Signal Analyzer

The acquired vibration signals throughout the testing were analyzed using the dual channel Hewlett Packard 35660A Dynamic Signal Analyzer (DSA, see the Glossary of Terms). It uses the Fast Fourier Transform (FFT) algorithm to convert the analog input signal, in the time domain, to the frequency domain. The analyzer is capable of making one channel measurements from 488 μHz to 102.4 kHz, or two channel measurements from 244 μHz to 51.2 kHz. The analyzer is also equiped with an IEEE 488 interface, on-board memory, an internal disk and is programmable using the HPBasic language.

The DSA was used throughout the testing for modeling FRF, balancing, noise analysis and cutting vibration. The DSA has an internal calibration factor which automatically resets the analyzer at regular intervals.

3.4 Photoelectric Probe

The Photoelectric Probe Bruel and Kjaer type MM0012 was used to obtain the required phase angle measurements during balancing. It was tested for accuracy at the University of Windsor Electronics Center and verified by a qualified technician. It was powered by a 9 Volt source.

3.5 Noise measurement equipment

The measurements for noise were taken by a sound level meter and the DSA was setup with the Bruel and Kjaer noise amplifier and microphone. The meter was the Modular Precision Sound Level Meter Type 2231 Plus Integrating SLM Module BZ 7110. It was calibrated with a Sound Level Calibrator Bruel and Kjaer Type 4230 that produced an acoustic calibration output of 94dB at a frequency of 1000 Hz.

The amplifier was attached to the DSA was the Measuring Amplifier Bruel and Kjaer Type 2606 with a frequency range of 2 to 200 kHz. This amplifier has various filters which allow for A,B,C,D and linear frequency weighting of the measured sound. This amplifier was fitted with a 1 inch diameter Condenser Microphone Bruel and Kjaer Cartridge Type 4144 serial number 499199 calibrated to 48.4 mV/(N/m^2). The calibration curve for this microphone shows a useful range to about 5500 Hz within an accuracy of 1 dB. After 5500 Hz the microphone has no discernable accuracy. Therefore, higher order mesh frequencies cannot be accurately measured past 5500 Hz using this particular microphone. It was assumed that the microphone calibration factor was constant throughout the frequency range. A value of 334 mV / 93.6 dB was the calibration factor for the microphone and DSA setup which was kept constant throughout the testing.

IV. FREQUENCY RESPONSE TESTING

4.1 Introduction

Frequency response characteristics of five major components of the machine tool drive were investigated to determine their natural frequencies, or resonance frequencies. The five components in the study were: the internal grinder spindle, the barrel spindle, the motor spindle, the motor stator housing and machine spindle housing, all shown in Figure 1.2. Each spindle, and the other components within the machine, are operating at different angular velocities; therefore, it is very important to determine the resonance characteristics to distinguish if any of these resonances will coincide with operational frequencies of the spindles. A spindle that is operating at or near its own natural frequency will exhibit excessive vibrations, and this is detrimental to optimal machine operation. A spindle can also be forced to experience excessive vibrations if excited to its natural frequency, by the operational frequency of another spindle within the same machine.

Modal analysis, or impact testing, is utilized to determine the characteristics of a spindle. A plot of amplitude verses frequency is generated by striking the spindle with an instrumental hammer at selected locations along its length. By performing impacts longitudinally, the first, second, third and higher mode shapes can be determined from the amplitude verses frequency plot generated by the digital signal analyzer. The digital signal analyzer or *DSA*, uses a Fast Fourier Transform or FFT, algorithm to generate these plots. Crawley [2] investigated the accuracy of frequency response functions using the FFT-based

analyzers with transient excitation to demonstrate the accuracy of the methods used to accurately predict resonance frequencies. It was suggested to generate the frequency response functions using coherence accuracy and using this data, compare the real and imaginary plots to determine the natural frequency peaks. Coherence is a measure of how well multiple measurements correlate themselves for each frequency within the selected measurement range. For an ideal impact test, one must strike the component at one location a number of times, with the exact same force. If this is performed correctly the coherence accuracy is unity. During real testing, not all impacts will be exactly the same as the others; therefore some of the coherence values will be less then unity while others will still exhibit high correlation values. This allows the investigator to use statistical methods for comparison to this data.

Modal testing of the components should be the first analysis performed in a vibration study for a machine. For this analysis various components were tested and found to produce a variety of results. One of the most important aspects of modal analysis is the type of supports used with the component under test. The components had a tendency to exhibit their resonance frequencies more accurately when soft bearing supports were used. In general, supports are classified as *fixed-fixed*, *fixed-free* or *free-free* type beam supports. Each type of support will interact with the same test specimen to produce different natural frequencies. Therefore, it is necessary to analyze each component in its most natural setting on the machine. For example, if the component rides on bearings, the modal analysis should be performed using these supports.

The following sections provide the results of the impact testing performed on the various components during the investigation.

4.2 F.R.F. Motor Spindle

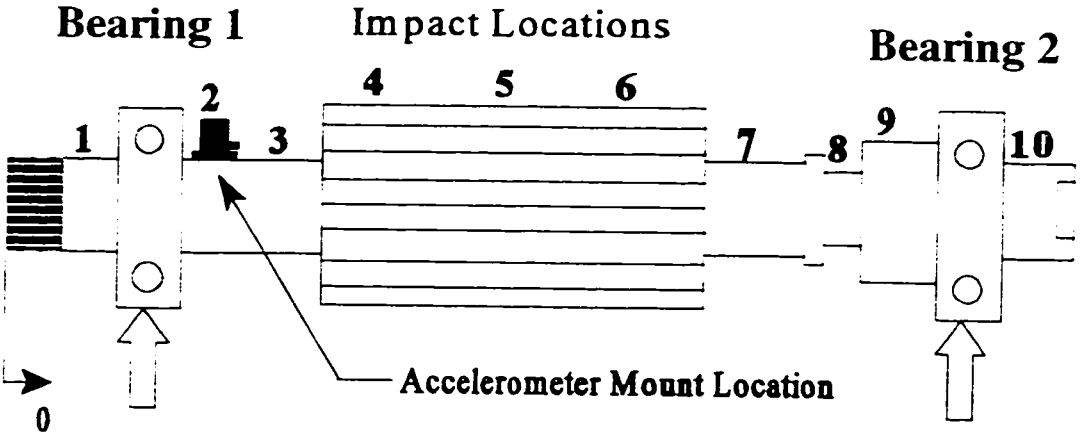

Figure 4.1 Motor Spindle F.R.F. Layout

Table 4.1.1 Impact Location Measurements (inches)									
1.75	3.75	4.88	5.88	8.75	12.0	13.5	14.4	15.1	17.0

Table 4.1.2 F.R.F. Motor Spindle Natural Frequencies		
Operating Speed	1800 rpm (30 Hz)	
Mode Number	Natural Frequency	Coherence Accuracy
Mode 1	116± 8 Hz	82.54 %
Mode 2	190 ± 8 Hz	88.93 %
Mode 3	1016 ± 8 Hz	97.14 %
Mode 4	2016 ± 8 Hz	97.48 %
Operational Mode	Rigid Rotor	

4.3 F.R.F. Internal Grinder Spindle

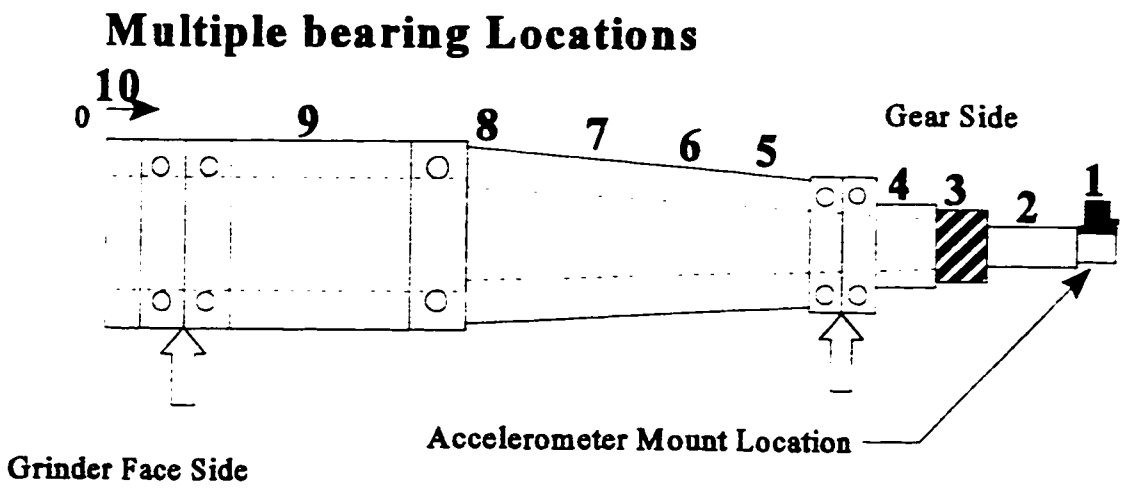

Figure 4.2 Grinder Spindle F.R.F. Layout

Table 4.2.1 Impact Location Measurements (inches)									
0.50	3.75	6.63	7.88	9.25	11.1	14.0	15.0	16.5	18.0

Table 4.2.2 F.R.F. Grinder Spindle Natural Frequencies		
Operating Speed	5820 rpm (97 Hz)	
Mode Number	Natural Frequency	Coherence Accuracy
Mode 1	40 ± 8 Hz	73.61 %
Mode 2	176 ± 8 Hz	79.24 %
Mode 3	216 ± 8 Hz	85.87 %
Mode 4	2032 ± 8 Hz	97.77 %
Operational Mode	Flexible Rotor	

4.4 F.R.F. Machine Spindle Housing

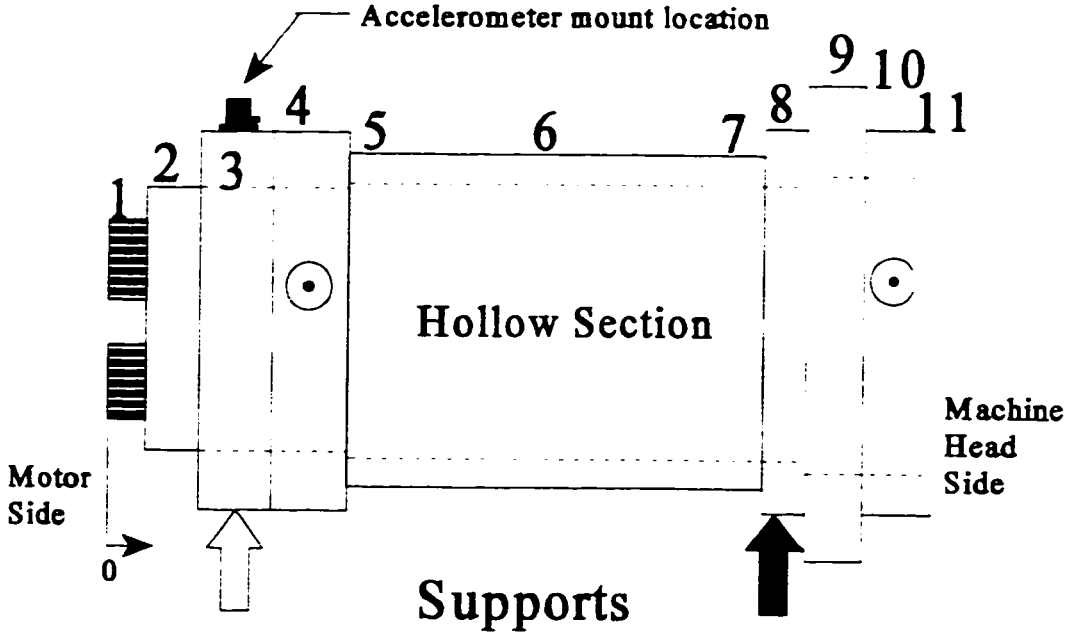

Figure 4.3 Machine Spindle Housing F.R.F. Layout

Table 4.3.1 Impact Location Measurements (inches)										
0.5	1.38	4.25	6.88	10.8	12.0	15.0	16.1	17.3	18.8	20.0

Table 4.3.2 F.R.F. Machine Spindle Housing Natural Frequencies		
Operating Speeds Internal	420 rpm (7 Hz) and 5820 rpm (97 Hz)	
Mode Number	Natural Frequency	Coherence Accuracy
Mode 1	160 ± 8 Hz	73.70 %
Mode 2	336 ± 8 Hz	81.82 %
Mode 3	1216 ± 8 Hz	94.00 %
Mode 4	1640 ± 8 Hz	95.33 %
Operational Mode	Rigid	

4.5 F.R.F. Motor Spindle Housing

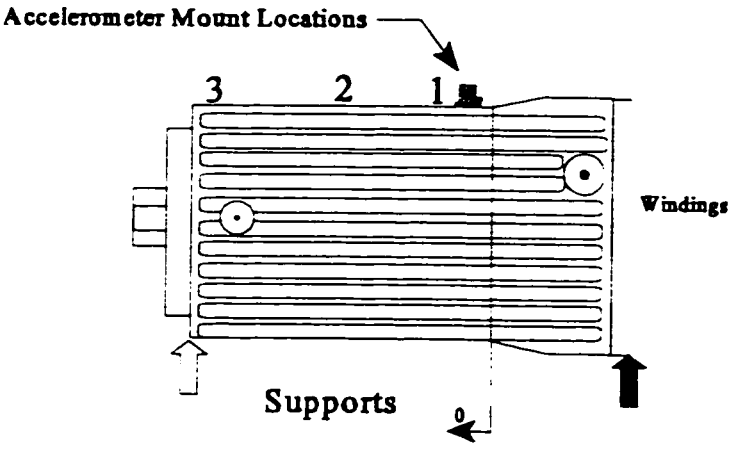

Figure 4.4 Motor Spindle Housing F.R.F. Layout

Table 4.4.1 Impact Location Measurements (inches)			
0.00	2.33	6.00	8.50

Table 4.4.2 F.R.F. Motor Housing Natural Frequencies		
Operating Speeds Internal	1800 rpm (30 Hz)	
Mode Number	Natural Frequency	Coherence Accuracy
Mode 1	272 ± 8 Hz	91.23 %
Mode 2	440 ± 8 Hz	89.43 %
Mode 3	1280 ± 8 Hz	94.53 %
Operational Mode	Rigid	

4.6 F.R.F. Barrel Spindle

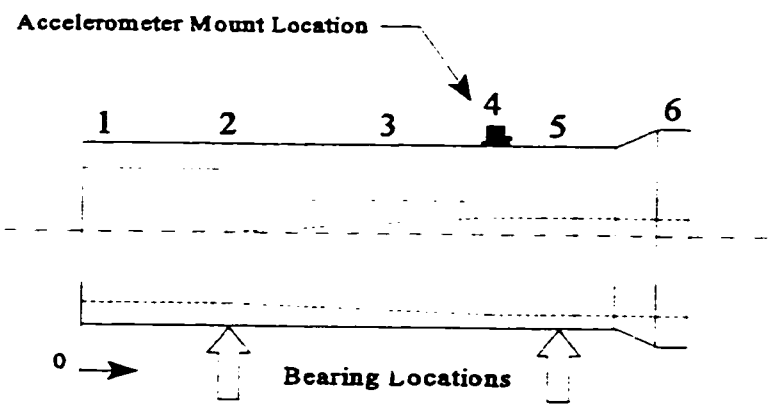

Figure 4.5 Barrel Spindle F.R.F. Layout

Table 4.5.1 Impact Location Measurements (inches)					
0.0	6.500	9.750	12.75	17.4	18.75

Table 4.5.2 F.R.F. Barrel Spindle Natural Frequencies		
Operating Speed	420 rpm (7 Hz)	
Mode Number	Natural Frequency	Coherence Accuracy
Mode 1	136 ± 8 Hz	93.08 %
Mode 2	256 ± 8 Hz	98.10 %
Mode 3	1650 ± 8 Hz	96.93 %
Operational Mode	Rigid Rotor	

4.7 Modal Procedure and Analysis

The Digital Signal Analyzer was setup to perform impact testing for various components to be tested. A frequency window of 3.2 kHz was used to capture at least the first four natural frequencies of each component. An equipment setup described by some texts [2,21], and described in Table A6, was used to perform the impact testing. Channel 1 and Channel 2 were setup to measure frequency response and coherence, respectively. A number of impact locations are shown in Figures 4.1 through 4.5. Five impacts were made at each of these locations along the longitudinal axis of the component. The impacts performed on the frequency response plots will be denoted as *RMS:5, or root mean squared* for five hits in Appendix A. These tests were repeated if the coherence accuracy of the tests were unsatisfactory. Most of the components were tested on their actual bearings, so a good representation of the actual operating conditions was modeled.

Appendix A contains all of the data collected at each location for each component. Figures A1.1 to A1.10 contain the impact locations for the motor spindle. Figures A2 through A5 are labeled for each component and location. The plots produced are frequency response functions. A log scale was employed to lower the extreme amplitudes produced by some of the frequency spikes. The units on the vertical axis are measured in decibels, dB. The frequency response functions are plotted as output divided by input, so the amplitude of this measurement is the only part of interest, regardless of the display unit chosen. The main focus is directed towards the amplitude peaks and the frequency at which they occur. Each natural frequency has been identified on the plot. Some of the plots, for the same

component, do not contain the same natural frequencies along the axis of testing. The most likely reason for this situation is that the measurement point coincides with a node. Another reason is that of inconsistencies in the application of the impact force. Each plot and natural frequency was analyzed and coherence tables were produced, these can be found in Tables A1 to A5. The natural frequencies were determined from these plots by comparison of the mode shape peaks to the coherence plots as well as the real and imaginary plots. By carefully inspecting these plots, an estimate for the first three to four natural frequencies for each component can be obtained and results can be formalized.

The motor spindle (Figure 4.1) operates at 30 Hz and the first natural frequency of the motor spindle was about 116 Hz with a coherence of 82.54 percent. The motor spindle will not operate near its first natural frequency.

The grinder spindle (Figure 4.2), operates at 97 Hz and its first natural frequency was about 40 Hz with a coherence of 73.61 percent. This implies that the spindle will run through its first resonance frequence and operate between its first and second modes (determined experimentally to be 176 Hz), in a flexible rotor mode. Care must be taken when the spindle is in operation so that it does not operate near this frequency, or excessive vibrations will occur. Since the motor spindle operates at 30 Hz, the excitation frequency may enhance the vibration of the grinder spindle, since its third harmonic (90 Hz) is close to the grinder spindle operating frequency. During testing the grinder spindle was supported at the bearing locations.

The hollow machine spindle housing (Figure 4.3), has operating frequencies of 7, 30,

97 Hz internally, and also multiples of these frequencies as well as frequencies generated by gear meshing, etc. Since its first natural frequency lies well above the operating frequencies of all the spindles, this component is satisfactory for internal spindle operation. The supports used for the frequency response testing were of the cantilever type. The shaded arrow in Figure 4.3, denotes the actual mounting location of the machine on the fixture. Since the machine will only be supported by this location, a fixed-free type support would have more accurately portrayed the machine setup.

The motor housing (Figure 4.4), had an internal operating frequency of 30 Hz. Since its first resonance frequency is 272 Hz, this is acceptable because its resonance frequency lies well beyond any spindle operating speed. Like the machine spindle housing, the supports used to test this component did not model the actual support when assembled on the machine.

The barrel spindle (Figure 4.5), was found to operate at 7 Hz. Thus, it would not be expected to exceed its first natural frequency. The barrel was supported at the bearing locations. This was comparable to the actual mounting inside the machine spindle housing.

All the testing in this section of the report was very important to the balancing procedures chosen for the remaining areas of study, which can provide valuable information about detrimental resonance frequencies.

V. STATIC BALANCING PROCEDURES

5.1 Introduction

As with any spindle, balancing is an essential part of optimal machine performance. Without properly balancing a machine, the factors as discussed in the introduction can lead to unwanted vibration and noise during normal operation. This was apparent at the design stage of this particular machine.

The static couple method was used to balance the dual eccentric machine tool spindles. Static balancing is the first step in the Static Couple method of balancing. Static balancing is a procedure by which the cross section of the spindle is examined to determine the heavy side of the spindle and to reduce the out of balance mass. This spindle has a large eccentricity due to the placement of the grinder spindle, and the clearance between the grinder spindle and the barrel spindle, due to the tapered hole.

The first procedure used to correct the void of mass in the grinder spindle, was to drill and tap holes axially about the barrel to counter the excess mass. Through calculations, it was determined that the barrel spindle was still heavy opposite to the grinder spindle. Due to concerns over excess mass removal causing a weakening of the barrel, a collar was designed which would counter the excess mass. A mass balancing with respect to operational speed was calculated keeping the width of the collar as a variable since the thickness of the collar was limited by clearance.

The second part of the static couple method is dynamic balancing. This process consists of the addition of balancing masses radially about the barrel to minimize the out of balance force caused by the dynamically created *rocking couple*. Dynamic balancing can only be accomplished once the rotor is sufficiently balanced statically. A method of two plane balancing can be selected for the dynamic portion. This will be discussed in Chapter VI.

The following Sections 5.2 and 5.3, will provide information concerning the locations of the static balancing holes and dimensions of the static balancing collar weights, respectively.

5.2 Static Balancing Holes

It was evident that the spindles used in the designing of this machine were significantly out of balance with respect to each other. No testing was needed to determine the initial conditions of unbalance. The first trial runs of the machine in operation demonstrated that the void in the grinder spindle as well as the air gaps between the spacer and bearings created a significant unbalance. Holes were drilled and tapped axially and radially about the barrel spindle to reduce this effect, as shown in Figure 5.1 on the following page. Cobra Machine Tool fabricated these holes using 0.500 inch diameter tapped holes which were drilled 1/8 inch smaller to allow for material removal during tapping. These holes were purposely tapped to fit slug bolt weights which could easily be installed if the

holes needed to be refilled. Holes were drilled axially to a depth of 1.75 inches from the outer diameter of the barrel spindle at radial angles of -30, -15, 0, 15 and 30 degrees. Excess material removal in one specific angle was eliminated by tapping holes at different angular locations.

Through calculations the holes tapped did not balance the spindle statically. To correct this problem and prepare the spindle for dynamic balancing, holes were then drilled and tapped radially at the two balance planes as shown in Figure 5.1. These holes were necessary for the addition of dynamic balance weights, as well as the static collar. There was a major problem with drilling radial holes at a greater angle of 120 degrees from the zero degree line. There was an insufficient thickness of material to drill and tap holes past this

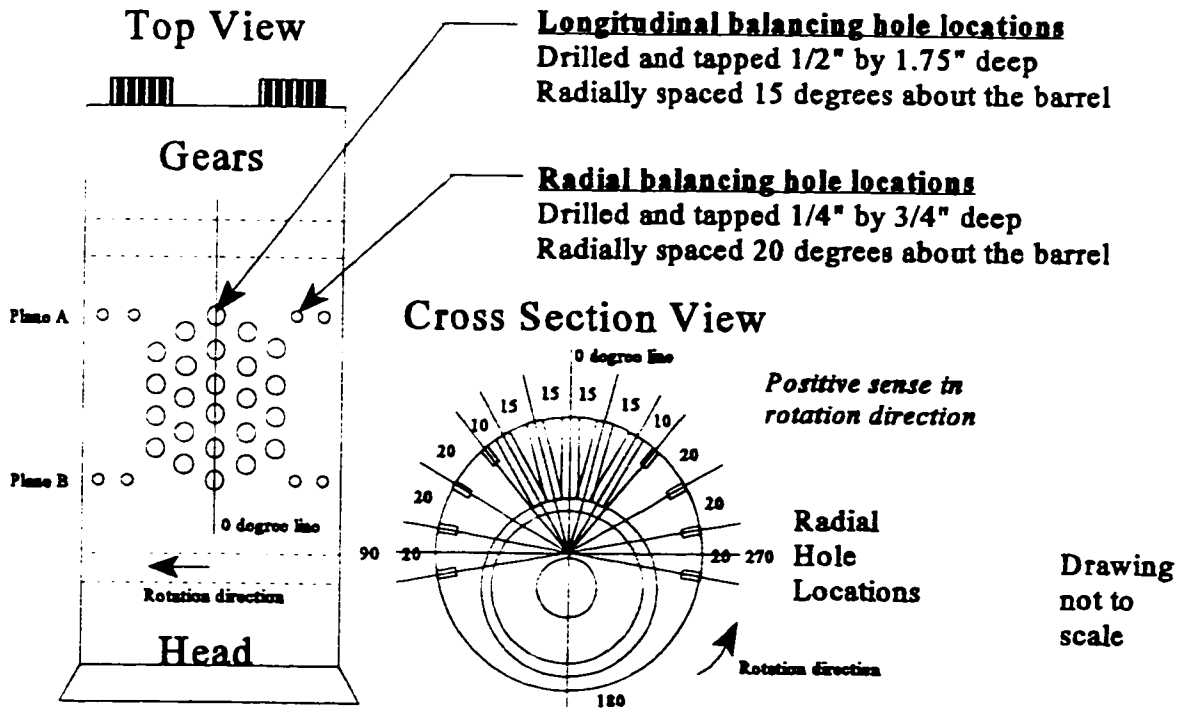

Figure 5.1 Barrel Spindle Hole Specifications

angular position. The collar mass designed would have to be fitted about the barrel and fixed at only two points. These points are located at the ±100 degree angular positions. Only the two ends would have to be sufficient for fastening the collar in place. The calculations required to determine the collar mass will be discussed in the next section.

5.3 Static Balancing Collar

Many factors must be considered for the collar mass calculation. The calculation involves the mass center of the barrel spindle, the mass of the grinder spindle, the mass of the material removed from the barrel holes and the mass of the balancing collar. The calculation was made during experiments, and is an approximation for statically balancing

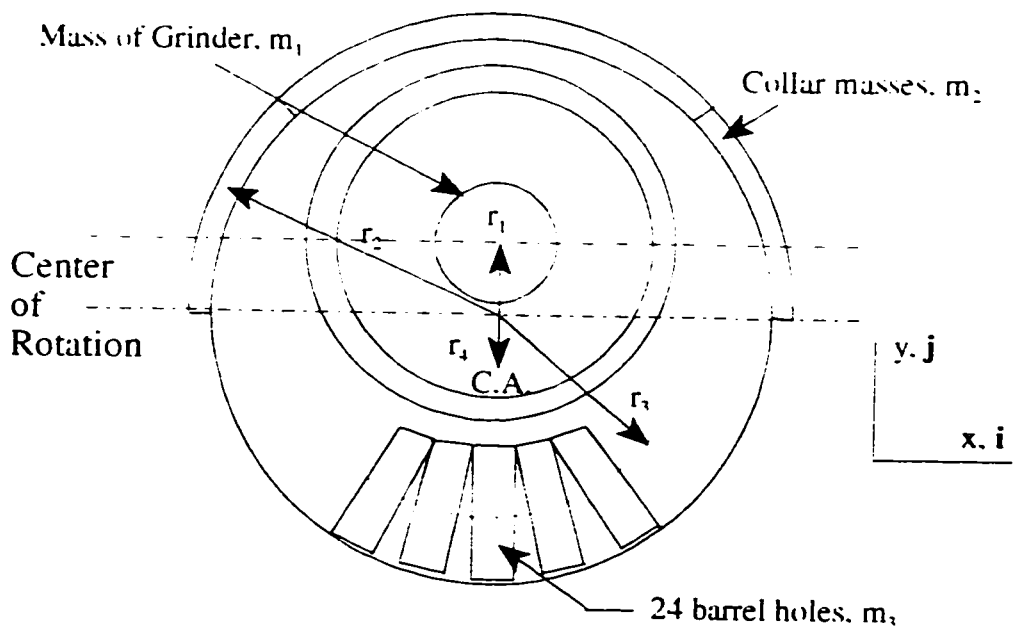

Figure 5.2 Static Collar Calculation Variables

the remaining static void in the barrel spindle. The numbers 1,2,3 and 4, in Figure 5.2 will denote the radial vectors for the grinder spindle, the collar masses, the barrel holes, and the center of gravity of the barrel spindle, respectively. Bold characters represent vectors in the calculations.

5.3.1 Barrel Collar Calculation Assumptions

Assumptions were made when designing the collar. These include:

1) Neglecting the location of the gears, but including them in the mass of the barrel.
2) Neglecting the machine tool heads and using only the two spindles for calculation.
3) Neglecting the material removed from the radial 0.75 by 0.25 inch holes.
4) Assuming that the collar weight and holes are uniform throughout the plane.
5) The calculations for the center of area for the barrel spindle are an accurate depiction of the approximate center of mass at the two cross section planes.
6) The density of machine steel: ρ was assumed to be 0.284 lb/in^3.
7) Assuming semi-uniform axial cross section and mass.

5.3.2 Static Balancing Collar Calculations

These are the static calculations with respect to Figure 5.2:

The mass of the grinder spindle, bearings and spacer are known to be approximately: $m_1 = 41.6$ lbs, where the radial distance $r_1 = 1$ inch.

The mass of the collar attached 180 degrees about the barrel spindle is:

$m_2 = \frac{1}{2} (\pi / 4 (D_2 + 2 t)^2 - D_2^2) w \rho$, where the radial distance $r_2 = 3.8125$ inches.

$m_2 = (1.276 w)$ lbs, were w, is the variable collar width (5.1)

The mass of one barrel hole is approximately:

$m_3 = (\pi / 4 D_3^2) L_3 \rho = (\pi/4)(0.5)^2 (0.284 \text{ lb/in}^3) = 0.0558$ lbs (5.2)

The center of area for the barrel spindle can be calculated at both planes, separately, to determine r_4. This can be accomplished by using the dimensions of the cross section at each plane separately. The calculations are shown in Table 5.1 and 5.2 for both planes. Figure 5.3 shows the axial section of the barrel. These calculations for the radius r_4, are approximated by using the center of area method.

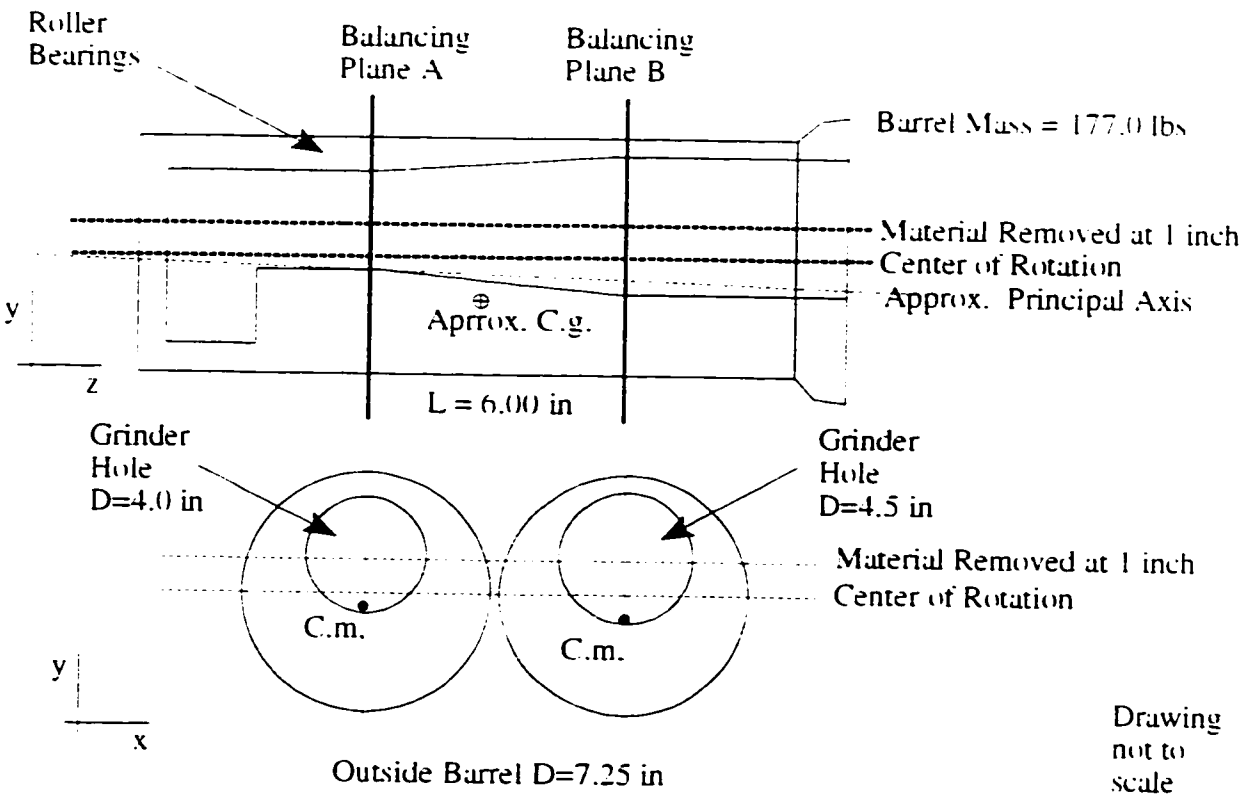

Figure 5.3 Axial and Cross Sectional View of the Barrel Spindle at Plane A and Plane B

Table 5.1 Center of Area Calculation for Plane B					
Description	**Area**	$\bar{x}$	$\bar{y}$	$\bar{x}A$	$\bar{y}A$
Outside Barrel	$\pi / 4 (7.25)^2 = 41.282$ in^2	0	0	0	0
Grinder Hole	$\pi / 4 (4.50)^2 = -15.904$ in^2	0	1	0	-15.904 in^3
Sum	$\sum A = 25.378$ in^2				$\sum \bar{y}A$
	$\bar{y} = \sum \bar{y}A / \sum A = -0.627$ in				=-15.904 in^3

Table 5.2 Center of Area Calculation for Plane A					
Description	**Area**	$\bar{x}$	$\bar{y}$	$\bar{x}A$	$\bar{y}A$
Outside Barrel	$\pi / 4 (7.25)^2 = 41.282$ in^2	0	0	0	0
Grinder Hole	$\pi / 4 (4.0)^2 = -12.566$ in^2	0	1	0	-12.566 in^3
Sum	$\sum A = 28.716$ in^2				$\sum \bar{y}A$
	$\bar{y} = \sum \bar{y} A / \sum A = -0.4375$ in				=-12.566 in^3

The center of area must be estimated for the barrel spindle. Taking the average of the $\bar{y}$ values in Table 5.1 and 5.2 yields $\bar{y} = \mathbf{r}_4 = -0.532\ \mathbf{j}$ inches from the center of rotation. Since all of the components of the barrel are connected and are rotating about the same center of rotation, the equation relating force is $F = m\ r\ \omega^2$. The value of **r** and **j** are radius and unit vectors in the y-direction, respectively.

$\sum \mathbf{F} = \mathbf{F}_e \approx \mathbf{0}$ where F_e is any residual unbalance and is approximately zero vector.

$$\mathbf{F}_1 + \mathbf{F}_2 + \mathbf{F}_3 + \mathbf{F}_4 = \mathbf{F}_e \approx \mathbf{0} \qquad (5.3)$$

$$\mathbf{F}_1 + \mathbf{F}_2 + \mathbf{F}_3 + \mathbf{F}_4 = \mathbf{F}_e = \mathbf{0} \qquad (5.3)$$

$$m_1 \mathbf{r}_1 \omega^2 + m_2 \mathbf{r}_2 \omega^2 + m_3 \mathbf{r}_3 \omega^2 + m_4 \mathbf{r}_4 \omega^2 = 0 \qquad (5.4)$$

All the components of the barrel spindle rotate at ω = constant statically, therefore

$$m_1 \mathbf{r}_1 + m_2 \mathbf{r}_2 + m_3 \mathbf{r}_3 + m_4 \mathbf{r}_4 = 0 \qquad (5.5)$$

Removed mass is designated as negative, therefore

$$[(m_1)\{\ \mathbf{r}_1\ \}] + [(m_2)\{\ \mathbf{r}_2\ \}] + [(-m_3)\{\ \mathbf{r}_3\ \}] + [(m_4)\{\ \mathbf{r}_4\ \}] = 0 \qquad (5.6)$$

$$\begin{aligned}
&[\ (41.6\ \text{lbs})\ (1.0\ \text{in}\ \mathbf{j}\ \}\ ] && (\text{Grinder Spindle}) \\
&\quad + [\ (\ 1.276\ (\ w\ )\ [\text{lbs}]\ )\ \{\ 2\ (\ 3.625\ \text{in} + 3/16\ \text{in})\ \mathbf{j} \cos 22.5 \\
&\qquad\qquad + 2\ (\ 3.625\ \text{in} + 3/16\ \text{in})\ \mathbf{j} \cos 67.5\ \}\ ] && (\text{4 Collar Weights}) \\
&\quad + [\ (\ -0.0558\ \text{lbs})\ \{\ 6\ (-2.75\ \text{inch}\ \mathbf{j}\ ) && (\text{24 Barrel Holes}) \\
&\qquad\qquad + 10\ (-2.75\ \text{inch}\ \mathbf{j}\ ) \cos 15\ + 8\ (-2.75\ \text{inch}\ \mathbf{j}\ ) \cos 30\}\ ] \\
&\quad + [\ (177\ \text{lbs})\ \{\ -0.532\ \text{inch}\ \mathbf{j}\ \}\ ] = 0 && (\text{Barrel Spindle}) \qquad (5.7)
\end{aligned}$$

All x-direction force components cancel, and solving for the variable w = 3.857 inches wide.

From the calculation it was evident that the machine spindle was still heavy on the barrel spindle 0-degree line, or opposite to the center of mass for the barrel spindle. The barrel collar weight was designed as shown in Figure 5.4. The width was divided by two, one collar for each plane. This gives an approximate value of 1.9 inches wide for both planes. The fabricated collar was designed with a width of 1.5 inches per side. If the collar was sufficient in shifting the heavy side of the spindles to its own side, slug bolt weights could be added to counter any excess collar weight.

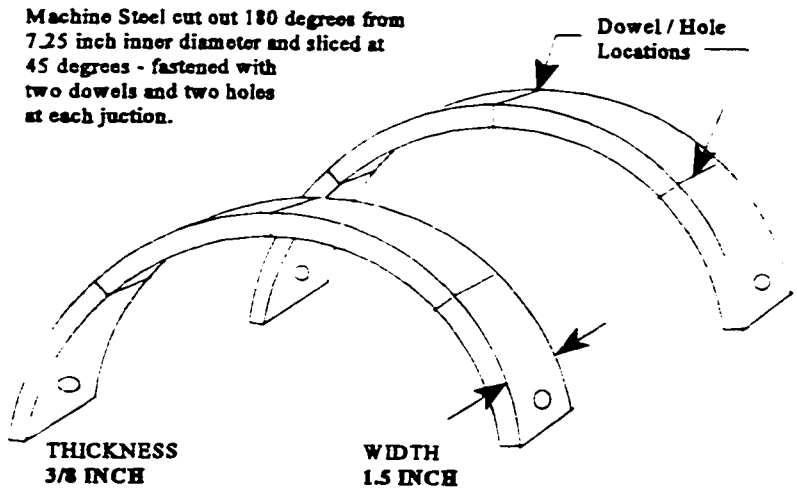

Figure 5.4 Barrel Collar Specifications

5.3.3 Comments on Barrel Collar Calculations

The actual calculations for the collar at two separate planes should not have been the same width at both ends. Since the center of mass of plane B was larger than the center of mass for plane A, the collar should have been calculated accordingly, instead of dividing the width by two. This results in a collar width at plane A of 1.585 inches and plane B of 2.272 inches, for static balancing.

These approximations were made with the knowledge that the barrel spindle will balance the residual static unbalance, dynamically. The static balancing collar was applied to the barrel spindle and taken as the new initial spindle condition for the dynamic balancing section. Part one of the static couple method has been completed by installing the static collar. Part two of the analysis will consist of choosing the appropriate two plane balancing method for dynamically balancing the spindle.

VI. DYNAMIC BALANCING PROCEDURES

6.1 Introduction

Dynamic balancing is simply the addition of correction masses placed on a rotor at a specific radial and angular positions, to correct the out of balance force produced when a rotor is in rotation. The rotation of a rotor produces forces and moments, both axially and radially. A rotor which is perfectly balanced statically may not be balanced when it is in rotation. The *rocking couple*, or moment, about the longitudinal axis of the rotor must be controlled or detrimental excess forces will result.

The previous chapter outlined the method for approximately balancing the rotor statically. The following sections deal with the second part of the static couple method. This involves employing a two plane balancing method which will best fit the process. Three different methods of balancing the rotor were investigated to determine which would best describe the positions of the correction masses and their magnitudes. These include: single plane balancing with phase response, two plane balancing with phase response, and two plane balancing without phase response.

With any balancing, magnitude and phase are the most important areas of interest for measuring unbalance. When performing dynamic balancing, experimental setup and the understanding of the signals being captured, demands considerable experience. DSA setup, accelerometer placement, amplifier setup, balancing speed, trial mass size, and many more

aspects must be understood before experimentation. These aspects will be explained in the following sections.

6.2 Experimental Procedures

As shown in many engineering texts [3.6.27.32. et al.] an experimental setup as shown in Figure 6.1 can be setup to perform measurements at two planes. Shown in Figure 6.1. the measurement axis for acceleration measurement must be in the same radial position.

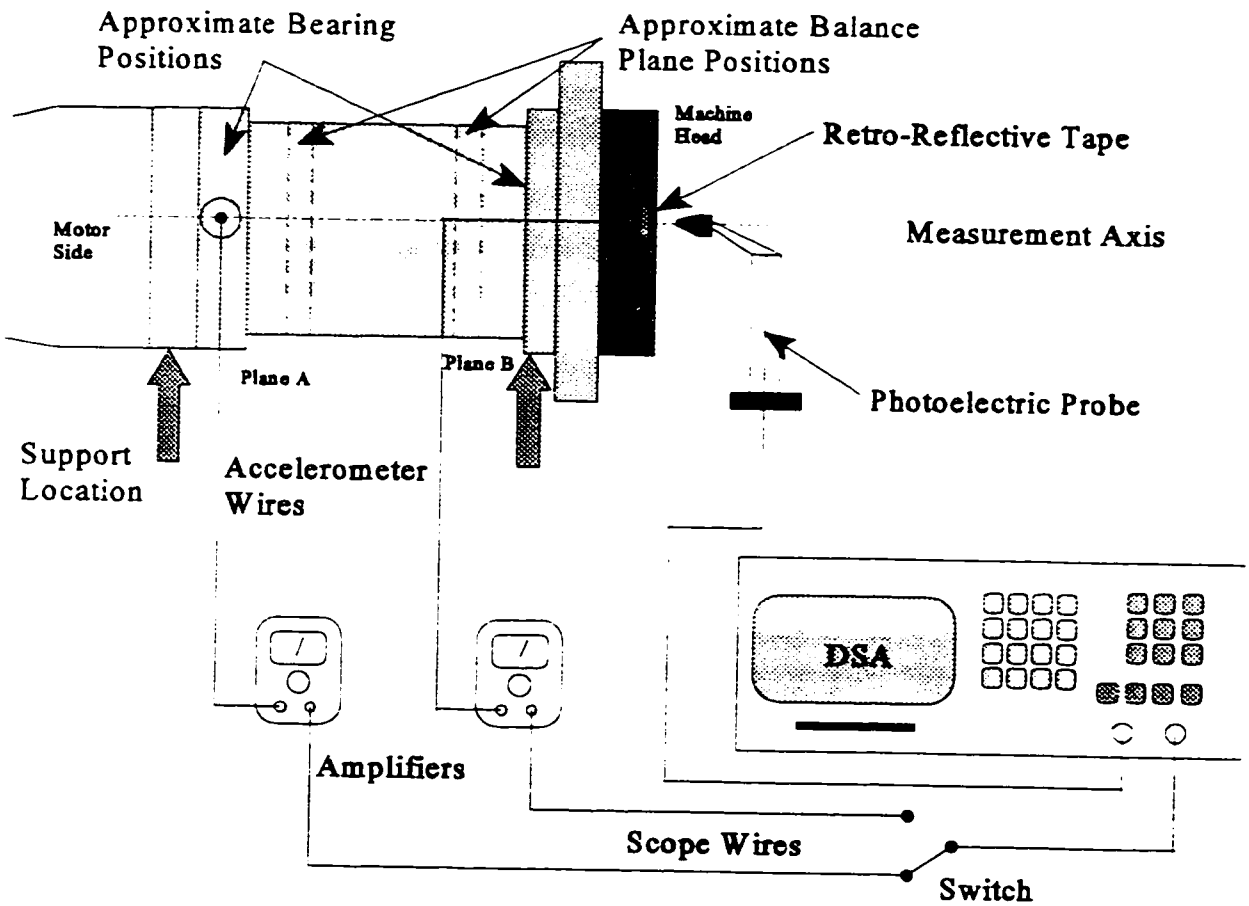

Figure 6.1 Experimental Setup for Dynamic Balancing Procedures

The accelerometers and the photoelectric probe must lie in this axis for both planes when taking accelerometer measurements. Measurements which determine displacement and velocity can be measured in the same manner but, a phase difference of ± 90 degrees will result. The measured values for acceleration are taken at the bearing locations, or as close as possible to the correction mass planes. These locations must have a smoothly machined surface where the accelerometers can be anchored securely. The accelerometers are attached to signal amplifiers to enhance the vibration amplitude at a multiple of 1, 10 or 100 times the input amplitude. These amplifiers are connected directly to the DSA at a corresponding channel. Since the DSA has only two channels, it was necessary to install a switch to toggle between the two planes. The second channel was used for phase measurements. The equipment used, and their specifications, were given in Chapter three of this study.

Data acquisition techniques must be studied and understood before any testing can take place. These include: frequency window sizing, operation and balancing speed, filtering, signal conditioning, alias frequencies, signal analysis, phase measurement, sensor strip length, mechanical timing lag, trial mass selection, plane transposition, the cross effect, axial runout and many other areas of interest. Most of these areas depend on rotor characteristics and can only be determined during testing. Specific areas are discussed in the following sections.

6.2.1 Trial Mass Selection

The initial determination of trial mass size is determined using the rotor weight, speed and radius. This must be determined before measurements are made, because balancing will be futile if too small of a mass is used to change the characteristics of the out of balance force. Wowk [32] suggests using the following equation:

$$W_t = 56375 \frac{W_R}{N^2 r} \qquad (6.1)$$

$$W_t = 0.004 \frac{W_R}{r} \qquad \text{for } (1200 < N < 3600) \qquad (6.2)$$

Where: W_t = trial mass (oz)
W_R = static rotor weight (lb_f)
N = rotor speed (rpm)
r = radius of the trial mass (in)

The specific variables for this machine are:

$W_R = 220\ lb_f$ N = 420 rpm r = 3.625 in

From equation (6.1), solving for W_t = 19.4 oz.

The most common criteria is to select a mass which produces a force of 10 percent of the rotor weight. Therefore, the solution to equation (6.1), shows that a mass selection of up to 19.4 ounces can safely be selected to perform tests on the rotor. The trial mass will obviously decrease for higher speed rotors.

6.2.2 Sensor Strip Length

Retro-reflective tape is used to perform phase measurements. The length of the tape

along the radial axis must be determined for the photoelectric sensor to properly pick up the phase of unbalance. This is determined by:

$$T = \frac{1}{60}\frac{l}{D\ \pi} > t_{os} \qquad (6.3)$$

Where: T = time (s)
l = length of the strip (in)
D = diameter of rotation (in)
t_{os} = optical sensor time (s)

For this machine the variables are:

D = 10 in t_{os} = 200 µs (for the sensor)

Therefore the length of the strip $l > 0.376$ inches or 3/8 inches for the sensor to be on for at least 200 µs.

6.2.3 Mechanical Timing Lag

The timing lag of the rotor is the time for the force to travel through a length l, of a steel shaft. If the frequency of the measurement is too small, this will effect the DSA measurements for phase and magnitude.

$$T = \frac{l}{16600} \qquad (6.4)$$

Where l = length of the shaft (1.75 ft)
16600 ft/s = velocity of force in steel

and

$$\frac{N}{60}\ 360\,T = \varphi \quad \textit{mechanical lag} \qquad (6.5)$$

Solving for $\varphi = 0.265$ degrees, assuming a rigid rotor. As long as the instruments lie on the measurement axis, the phase lag for this machine is negligible.

6.2.4 Signal Measurement

The measurement signal for a force produced by acceleration is found as the 1X rpm value. This means that the out of balance force peak is measured at the frequency of operation for a particular rotor. From numerous texts [30,32], the signal being measured must have a frequency window of at least 2 X the measured value to eliminate any alias frequencies. For this particular application, a signal of 420 rpm, corresponds to a frequency of 7 Hz. Therefore, the frequency e greater than 14 Hz. The captured signal was windowed consistently from 3 to 53 Hz. This gave a capturing signal interval of 8 seconds for this particular frequency window. If the window is increased the recording interval increases. This window was adequate to perform the experiment.

6.2.5 Signal-to-Noise Ratio

The signal-to-noise ratio, or S/N ratio, is a deterministic measurement in which the measured signal is benchmarked against a known noise signal. Errors are introduced in the measurements from bearing noise, electrical interference or line frequencies, ground vibration, gear noise, and possible external repeatable ambient noise. One way to measure the signal-to-noise ratio is to compare the level of the test signal to the amplifiers wide-band noise. Wide band noise is usually defined as the total *rms* noise within the amplifiers 3 dB bandwidth. For audio measurements standard bandwidth of 20 Hz to 20 kHz is often used [13,15]. For the machine in this study the noise floor for the measured values was about 20

mV. The wide band noise study in Appendix C, shows a noise level of about 86.4 dB. The equation for eliminating the noise measurement from the signal, is simply the total measured amplitude at the frequency of interest, is equal to the actual signal added to the noise floor signal. Obtaining the actual signal is simply found as the difference between the noise floor measurement and the measured value.

6.2.6 Cross-Effect

Cross-effect is the term used in two plane balancing. It is the transmission of unbalanced forces to the two bearings. Therefore, the force at plane one, is a combination of the primary force from the out of balance at plane one, and a secondary force from the out of balance at plane two. This is the fundamental principle behind influence coefficient balancing. The cross-effect becomes more severe as the rotor length to diameter ratio decreases, and the distance from the correction planes to the nearest bearing increases [32]. An illustration of the cross-effect is shown in Figure 6.2. The major contribution of the cross-effect on balancing, is the influence of the correction masses on both forces. Plane one can be balanced first and then plane two is balanced. Once plane two is balanced, plane one may show an increase.

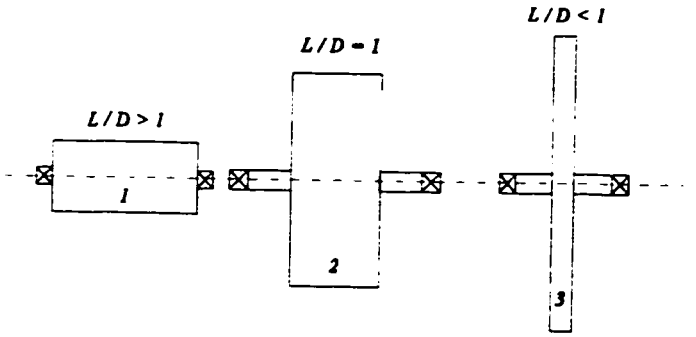

Figure 6.2 The Cross Effects for Different Rotor Styles

It is then re-balanced and measurements at plane two may have increased. This constant increase / decrease is repeated until a desired balance condition is reached, but this can be extremely tedious.

The primary force influence coefficient is defined as α_{11}, or the force measured at plane one due to the force at plane one. The secondary force influence coefficient is the value α_{12}, is the force measured at plane two due to the force at plane one. The value α_{21} is the force measured at plane one due to the force at plane two, and the other primary force α_{22} is the force measured at plane two due to the force at plane two. These are the fundamental basis for the influence coefficient balancing matrix known as

$$[\alpha] = \begin{bmatrix} \alpha_{11} & \alpha_{12} \\ \alpha_{21} & \alpha_{22} \end{bmatrix} \qquad (6.6)$$

6.3 Two Plane Balancing Techniques

Many balancing methods exist for multi-plane balancing of rotors. The two types of dynamic balancing methods used in this study are: Two plane balancing with phase response, and two plane balancing without phase response. The methods used for experimentation will be explained in the next two sections.

6.3.1 Two Plane Balancing With Phase Response

The two plane procedure is similar to single plane balancing with the exception of an increase in the number of measurements, and equipment used for two planes. The method used for two plane balancing with phase is as follows:

1) Two planes are selected close to the bearing locations. The bearings must be flexible or semi-flexible, but not resonant.

2) An equipment setup as in Figure 6.1 is used with the photoelectric probe and the accelerometers are calibrated.

3) The DSA is setup to appropriate measuring characteristics noting frequency window, filters, the gain value, calibration factor, channel setup, scale, and averaging value.

4) The rotor is revolved at a constant speed, and the 1X rpm measurement is taken for the original unbalance condition magnitude and phase at that speed.

5) The rotor is stopped, and a safe trial mass is installed at plane one noting the trial mass size, the radius of plane one, and the phase orientation of the mass. This establishes plane one or the first correction plane.

6) The rotor is then brought to the same speed as the original run, and the amplitude and phase measurements are again taken at both planes.

7) The rotor is stopped, the trial mass for plane one is removed, and a safe trial mass is installed at plane two noting the trial mass size, the radius of plane one, and the phase orientation of the mass. These may not be the same as step 5. This establishes plane two or the second correction plane.

8) The rotor is then brought to the same speed as the original run, and the amplitude and phase measurements are again taken at both planes.

9) The rotor is stopped, and the trial mass is removed.

10) A calculation for the correction masses can now be made using the program found in Appendix B for "Two Plane Balancing With Phase Response".

11) The correction masses are than added to the rotor at both planes.

12) The rotor is then brought to the same speed as the original run, and the amplitude and phase measurements at both planes are verified for improvement. For further improvement, use the correction masses as the new original unbalance condition and re-test the rotor with additional mass trials.

The two plane balancing with phase response program, found in Appendix B, was verified using calculations found in Darlow [3], Wowk [32] and Bruel and Kjaer [30]. It was found to be an adequate method to perform two plane balancing calculations with phase response. A second method of testing was also performed using a similar technique as above but without phase response measurements.

6.3.2 Two Plane Balancing Without Phase Response

Two plane balancing without phase response method is almost identical to the afore mentioned program, with the exception of additional trial runs, and does not require phase measurements. Everett [6], has investigated this technique with considerable success, and it has also been tested and accredited by Wowk [32].

The method of two plane balancing without phase response is as follows:

1) Two planes are selected close to the bearing locations. The bearings must be flexible or semi-flexible, but not resonant.

2) An equipment setup as in Figure 6.1 is used with the photoelectric probe and the accelerometers are calibrated.

3) The DSA is setup to appropriate measuring characteristics noting frequency window, filters, the gain value, calibration factor, channel setup, scale, and averaging value.

4) The rotor is revolved at a constant speed, and the 1X rpm measurement is taken for the original unbalance condition magnitude at that speed.

5) The rotor is stopped, and a safe trial mass is installed at plane one noting the trial mass size, the radius of plane one, and the phase orientation of the mass. This establishes plane one or the first correction plane.

6) The rotor is then brought to the same speed as the original run, and an amplitude measurement is again taken at both planes.

7) The rotor is stopped, the trial mass is removed and re-installed at plane one at the same radius, the same axial plane, but at a different phase first.

8) The rotor is then brought to the same speed as the original run, and an amplitude measurement is again taken at both planes.

9) The rotor is stopped, the trial mass removed and re-installed at plane one at the same radius but at a different phase orientation from the first and second.

10) The rotor is then brought to the same speed as the original run, and an amplitude measurement is again taken at both planes.

11) Steps 5 through 10 are repeated using the same trial mass, the same three phase orientations as before, but installed and removed at plane two.

12) A calculation for the correction masses can now be made using the program found in Appendix B for "Two Plane Balancing Without Phase Response [6]".

13) The correction masses are than added to the rotor at both planes.

14) The rotor is then brought to the same speed as the original run, and the amplitude measurement at both planes are verified for improvement. For further improvement, use the correction masses as the new original unbalance condition and re-test the rotor with additional mass trials.

When the accuracy of the phase response for a rotor is hard to measure, two plane balancing without phase is a very favorable method of balancing. Difficult rotors to balance will include the type of machine in this study. Numerous tests were conducted using both methods. The balance runs with phase response produced inconclusive data for balancing the barrel spindle. This was primarily due to the low frequency operating speed of the barrel spindle. All of the critical balancing data can be found in Appendix B.

6.4 Experimental Analysis

The main focus of the experiment was to capture the 1X rpm amplitude for the spindle to be balanced. Using one of the methods described in section 6.3, two plane balancing can be performed dynamically. A graphic representation of the balancing signal is shown in Figure 6.3. The basic concept is measuring the out of balance force at the bearings. The specific force at the bearings for a rotor rotating about its centerline is $F=me\omega^2$. Where m, is the total mass in rotation, e, is the eccentricity distance of the mass in rotation measured from the center of rotation to the principle axis, and ω is the constant frequency of operation. This is the basis for rotor balancing techniques. When measuring the direct out of balance force of a rotor, the frequency of the constant rotating force at any plane is rotating at one times the rotation per minute. This means if a rotor is spinning at a constant angular velocity of 600 rpm, the balancing signal of 1X rpm would be 10 Hz.

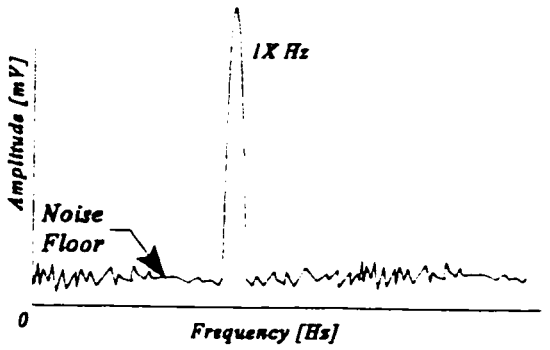

Figure 6.3 The 1X rpm Signal Measurement

6.4.1 Experimental Trials

Balancing runs were performed for four separate conditions. These conditions are outlined in Table 6.1. Both two plane balancing methods were used to perform the balancing

starting with phase, and than without phase. The balancing progression chart will describe the different conditions that were tested to calculate the relative force magnitudes in terms of accelerance [or g-force].

The initial barrel condition zero is engaging both spindles without any balance corrections. This magnitude was not tested at 420 rpm because of excessive vibrations which lead to unsafe conditions. Condition one has both spindles in operation after the 24 barrel holes were tapped radially and axially. Condition two has only the barrel spindle in operation and the grinder spindle disengaged and not turning, again including the 24 barrel holes. Condition three is the result of static balancing, in which the collar is attached to the barrel spindle at both planes. The final condition four has both spindles in operation with the static collar and 24 barrel holes, and the dynamic masses attached to the barrel spindle.

Figure 6.4 graphically depicts the tabulated values listed in Table 6.1. It shows the balancing progression through the project and how specific conditions (one through four), influence the vibration magnitudes. Specific vibration specifications for General Motors is also shown as a chart in Figure 6.5. This was a necessary point for determining the maximum levels a customer will tolerate in the factory. Two measurement variables were charted in Figure 6.5 for the final grinder spindle [5823 rpm, 0.510 g], and barrel spindle [420 rpm, 0.066 g] unbalance magnitudes.

Table 6.1 Balancing Progression Chart			
Condition Description		Plane A (motor side) Balance Speed 7 Hz [g's]	Plane B (head side) Balance Speed 7 Hz [g's]
Barrel spindle engaged Grinder spindle engaged 1) 24 barrel holes tapped	❶	0.617	0.596
Barrel spindle engaged Grinder spindle disengaged 1) 24 barrel holes tapped	❷	0.277	0.329
Barrel spindle engaged Grinder spindle engaged 1) 24 barrel holes tapped 2) Static barrel collar attached	❸	0.164	0.148
Barrel spindle engaged Grinder spindle engaged 1) 24 barrel holes tapped 2) Static barrel collar attached 3) Dynamic balancing masses attached	❹	0.133 *to noise floor*	0.105 *to noise floor*

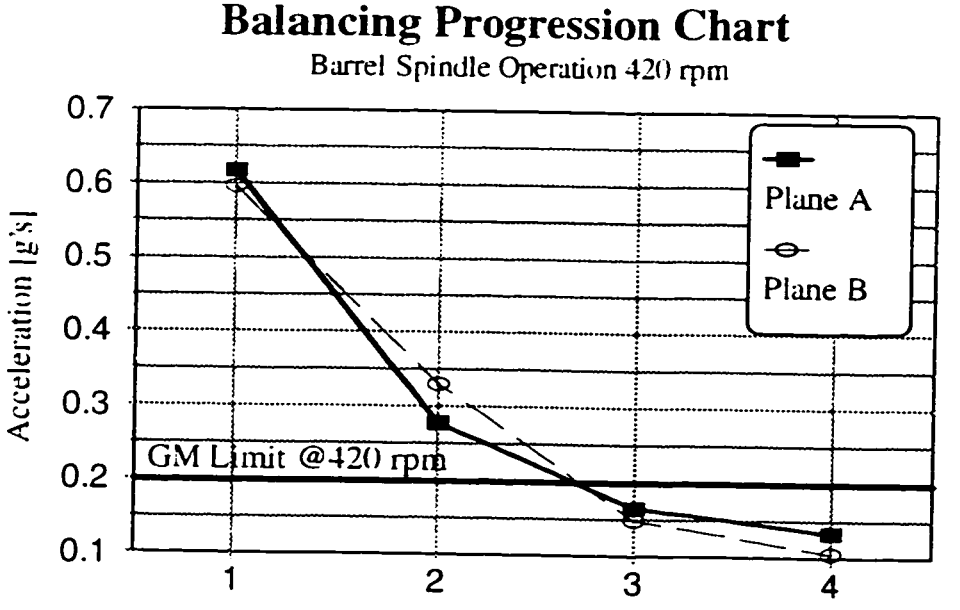

Figure 6.4 Balancing Progression Chart

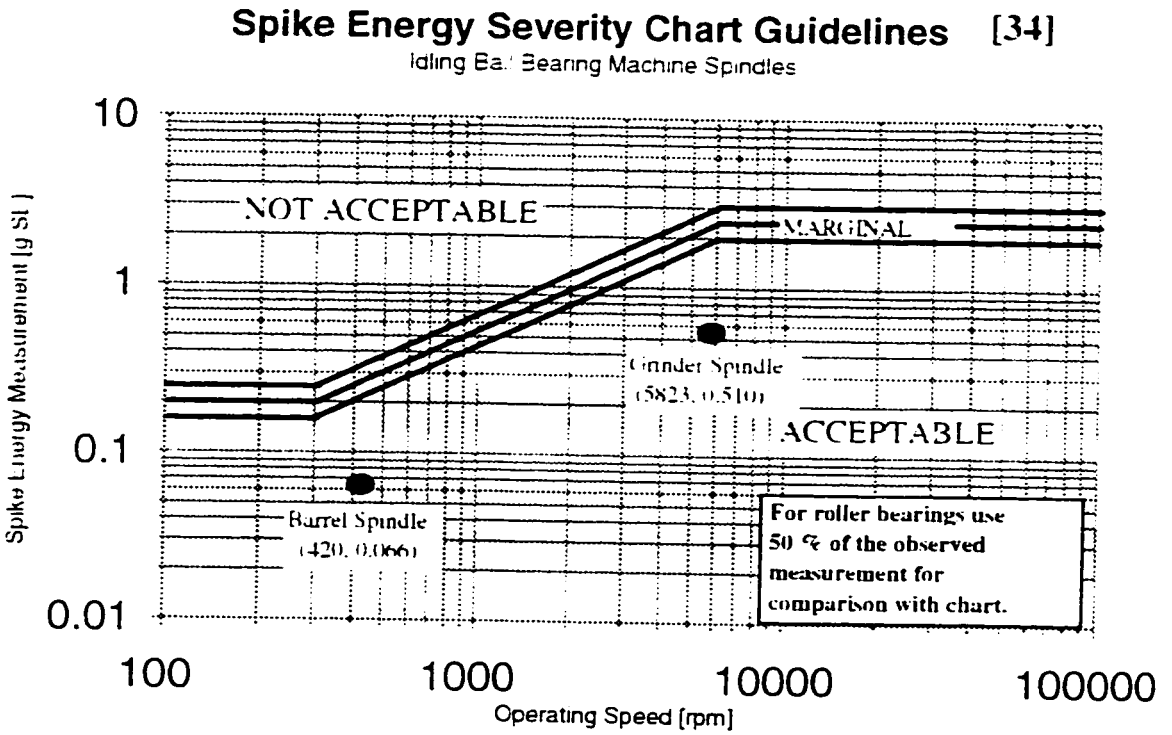

Figure 6.5 Spike Energy Severity Chart

The vibration magnitudes for the barrel spindle were divided by two because of the roller bearings. This was necessary for comparison to the chart in Figure 6.5. The actual vibration values were used for the grindle spindle in Figure 6.5.

6.4.2 Final Mass Positions

The final balance mass locations are detailed in this section for all masses placed about the barrel spindle. Figures 6.6 and 6.7 show the locations of the correction masses about the cross section of the barrel spindle at both planes.

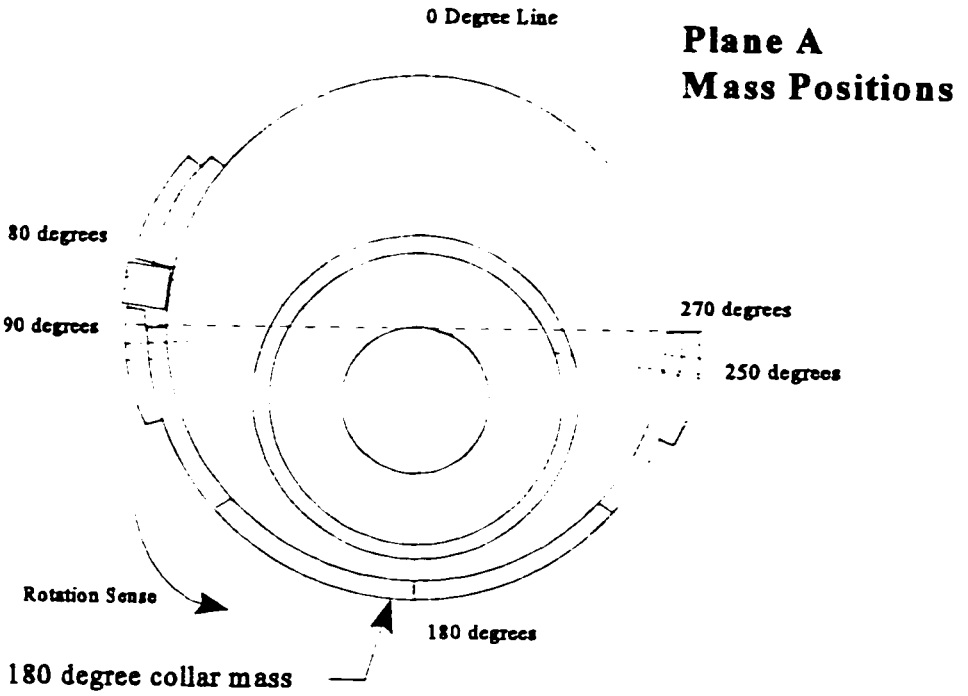

Figure 6.6 Plane A Final Mass Positions

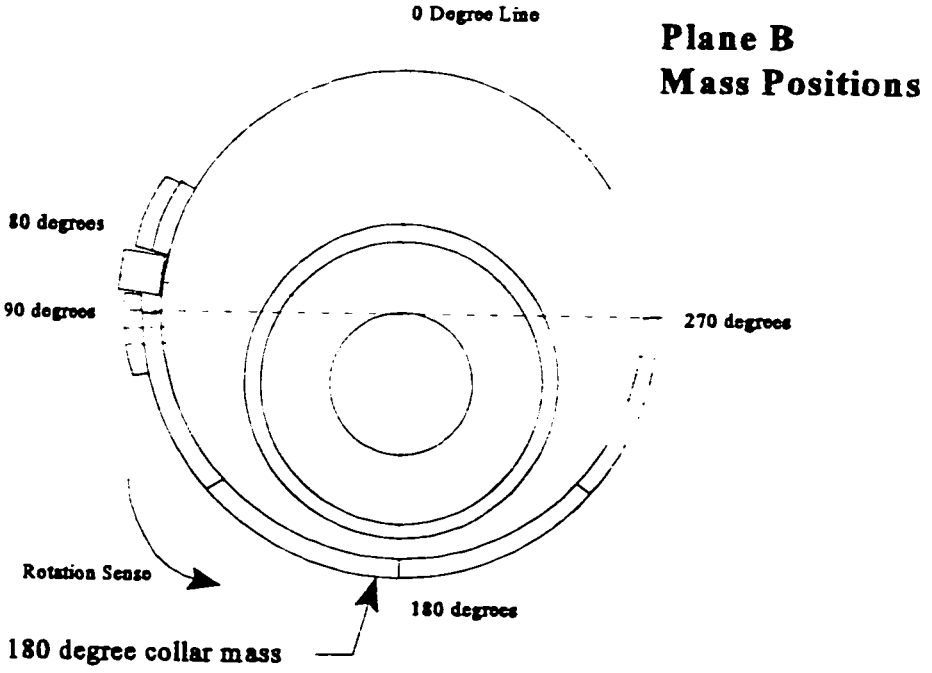

Figure 6.7 Plane B Final Mass Positions

The following Table 6.2, is a summary of the correction masses and their orientations.

Table 6.2 Balance Mass Summary Chart				
Side	**Mass**	**Position**	**Radius (inch)**	**Comments**
Plane A	Collar Mass ~0.375 lbs	180 degrees about the barrel	3.625	4 masses per collar joined with two dowels and fastened to the barrel spindle at the ±100 degree marks *3 x 3/2 x 3/8 inch
Plane B	Collar Mass ~0.375 lbs	180 degrees about the barrel	3.625	
Plane A/B	Steel Bar Mass ~0.123 lbs	80 degrees	3.625	Bar joins Plane A and B with dimensions ** 6 x ½ x 3/4"
Plane A	Full Mass 0.034 lbs	One each at 60, **60, 100** degrees	3.625 **4.00**	One center cut hole *2 x 1 x 3/8"
Plane A	Full Mass 0.032 lbs	250 degrees	4.00	Two end cut holes *2 x 1 x 3/8"
Plane B	2/3 Mass 0.023 lbs	One each at 60, **60, 100** degrees	3.625 **4.00**	One center cut hole *5/4 x 1 x 3/8"

* Masses were machined to fit about an inner diameter of 7.25 inches and holes fastened to the 1/4 inch bolt holes tapped radially about the barrel spindle

** The bar joins across Plane A and Plane B and a slight cavity was milled at the bottom to fit along the barrel spindle axially. It was fastened at the 80 degree radial holes at both planes.

Since the primary focus of the balancing routines was to balance the machine to General Motors machine tool specifications, the graph in Figure 6.5 is compared with the final vibration data, or condition four. Other balance grade charts are also provided in Appendix B.

VII. OPERATING CHARACTERISTICS

7.1 Run Up and Run Down Analysis

This chapter will provide an outline of the operating conditions that the spindles will encounter during cutting and free running. As with any machine tool head, the operating speeds will change during cutting. This is due to cutting load friction which creates a resistance torque decelerating the head lowering rotational speeds throughout the milling operation. Once the head clears the part, it accelerates back to its set operating speed when it experiences a zero external resistance torque.

The operating range studied for the run up and run down analysis was determined through criteria found in engineering manuals. Usually, measurements are made for a 20 percent decrease and 20 percent increase on the operating speed. The design operating speed for the *Super Finish* head is 420 rpm. This corresponds to a motor speed of 1800 rpm and a grinder speed of 5823 rpm. To apply a 20 percent increase and decrease, defines a range from 1440 to 2160 rpm motor speed. Figure 7.1 shows the machine on the actual machine stand where the measurements were taken. Figures 7.2 through 7.5, depict the run up and run down analysis for the barrel spindle and the grinder spindle, respectively. Table 7.1 depicts the frequencies of interest for Figures 7.2 through 7.5. The bold characters in Table 7.1, represent the design speeds in which the spindles operate in the machine.

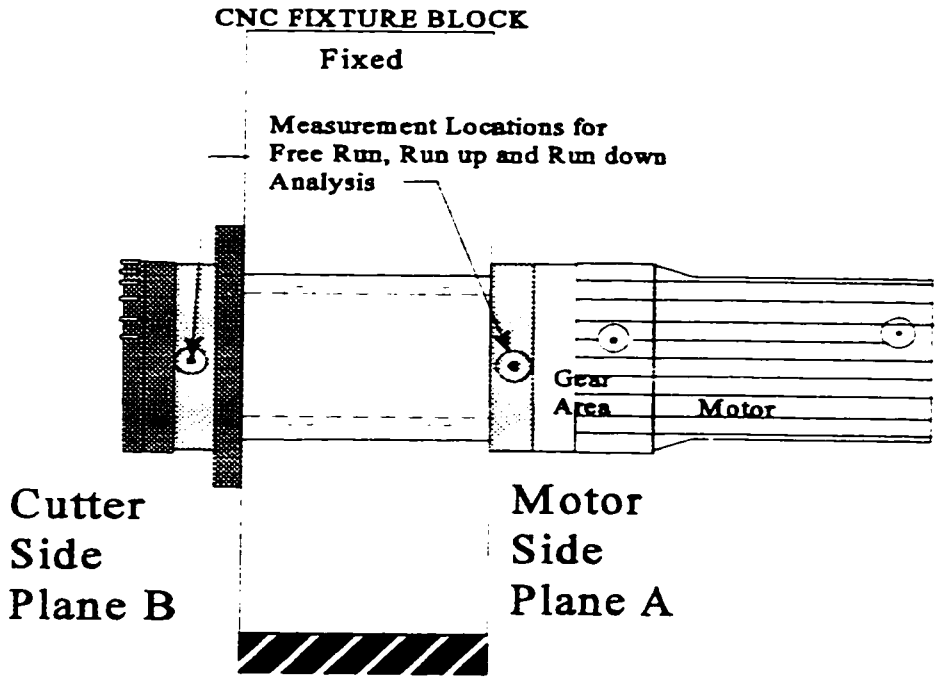

Figure 7.1 Fixture Block Diagram for Operation Analysis

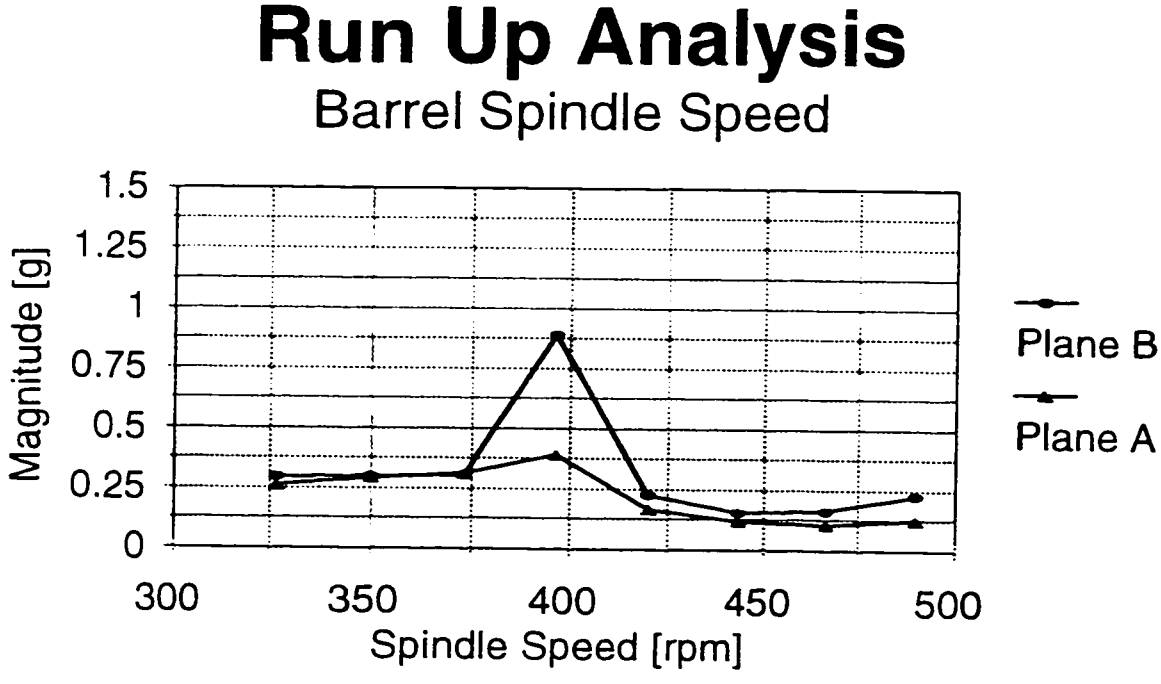

Figure 7.2 Run Up Analysis for Barrel Spindle

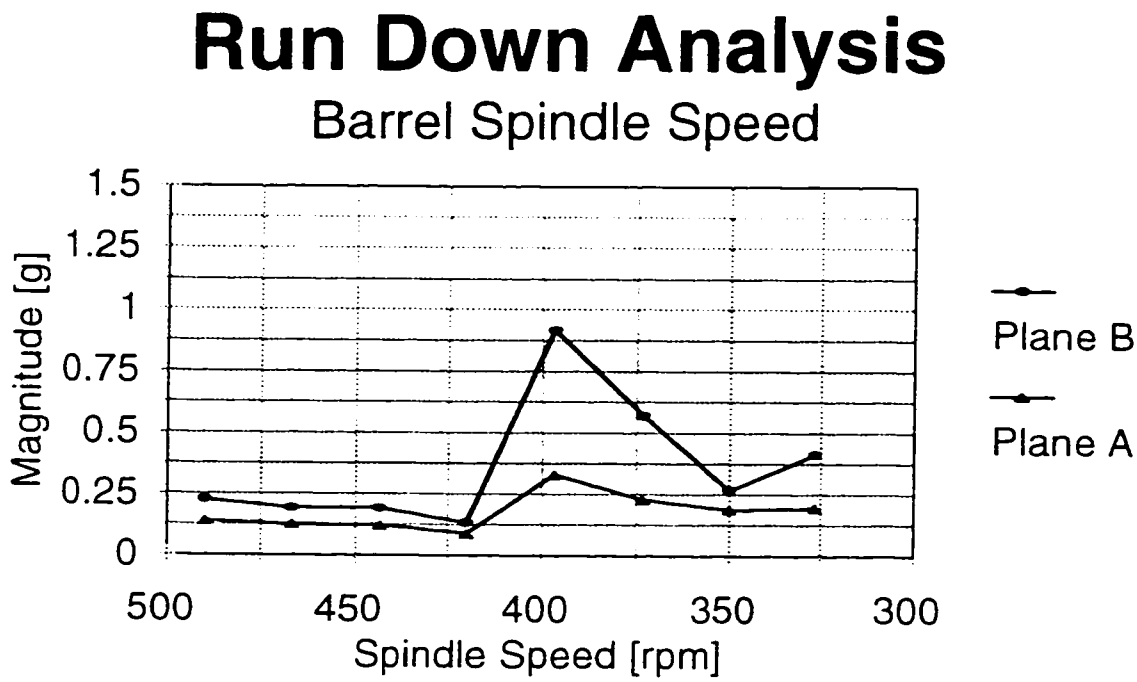

Figure 7.3 Run Down Analysis for Barrel Spindle

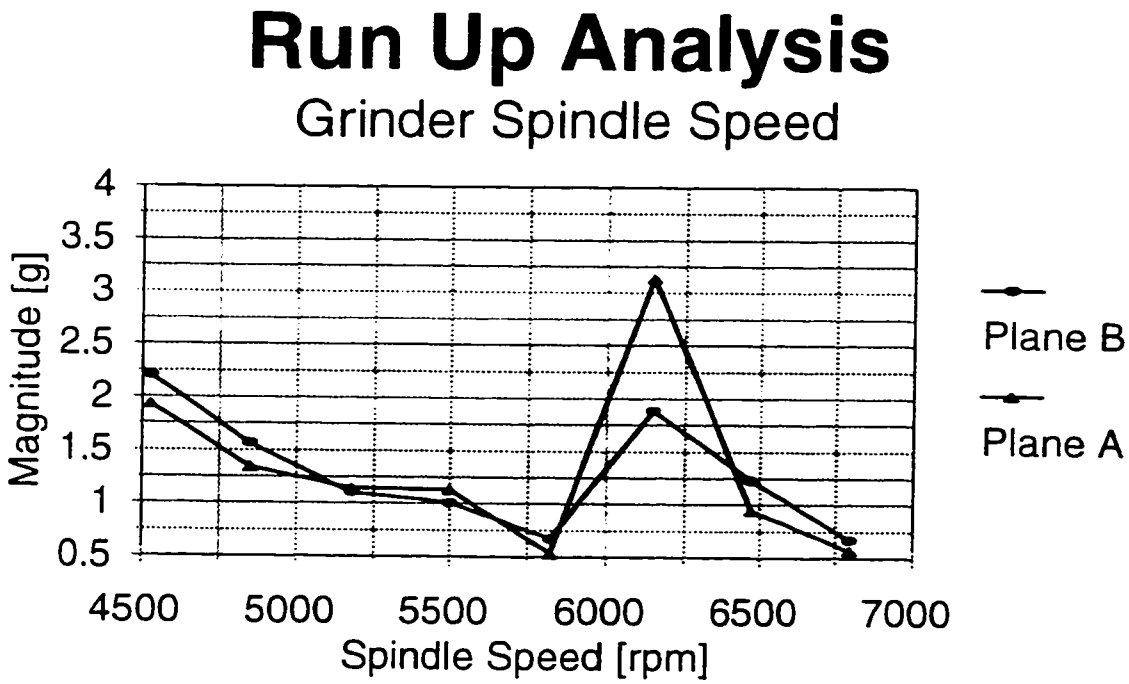

Figure 7.4 Run Up Analysis for Grinder Spindle

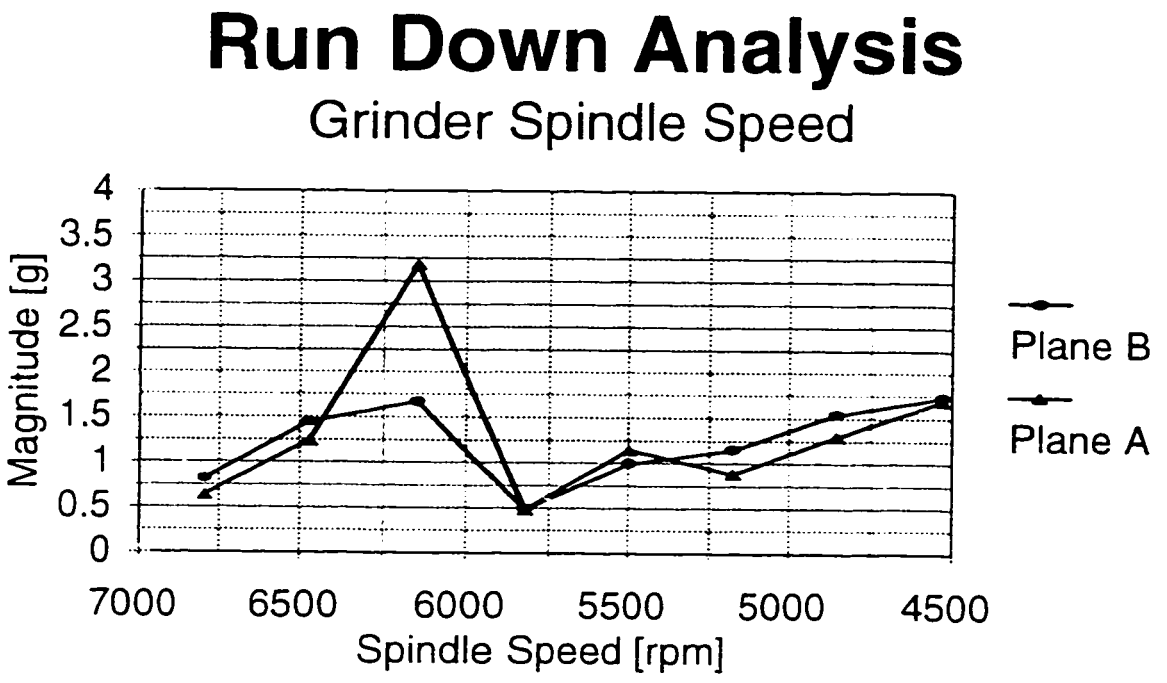

Figure 7.5 Run Down Analysis for Grinder Spindle

Table 7.1.1 Run Up Analysis								
					Plane B		Plane A	
Motor	**Barrel**	**Barrel**	**Grinder**	**Grinder**	**Barrel**	**Grinder**	**Barrel**	**Grinder**
[rpm]	[rpm]	[Hz]	[rpm]	[Hz]	[g's]	[g's]	[g's]	[g's]
1400	326.67	5.44	4529.00	75.48	0.296	2.208	0.262	1.933
1500	350.00	5.83	4852.50	80.88	0.299	1.566	0.292	1.343
1600	373.33	6.22	5176.00	86.27	0.307	1.107	0.312	1.147
1700	396.67	6.61	5499.50	91.66	0.893	1.016	0.393	1.140
1800	**420.00**	**7.00**	**5823.00**	**97.05**	**0.227**	**0.675**	**0.169**	**0.537**
1900	443.33	7.39	6146.50	102.44	0.157	1.887	0.119	3.145
2000	466.67	7.78	6470.00	107.83	0.164	1.232	0.107	0.950
2100	490.00	8.17	6793.50	113.22	0.226	0.675	0.126	0.577

Table 7.1.2 Run Down Analysis								
					Plane B		Plane A	
Motor	Barrel	Barrel	Grinder	Grinder	Barrel	Grinder	Barrel	Grinder
[rpm]	[rpm]	[Hz]	[rpm]	[Hz]	[g's]	[g's]	[g's]	[g's]
2100	490.00	8.17	6793.50	113.22	0.228	0.819	0.141	0.642
2000	466.67	7.78	6470.00	107.83	0.194	1.448	0.128	1.239
1900	443.33	7.39	6146.50	102.44	0.193	1.678	0.123	3.191
1800	**420.00**	**7.00**	**5823.00**	**97.05**	**0.134**	**0.491**	**0.090**	**0.485**
1700	396.67	6.61	5499.50	91.66	0.919	0.996	0.332	1.147
1600	373.33	6.22	5176.00	86.27	0.572	1.153	0.230	0.885
1500	350.00	5.83	4852.50	80.88	0.266	1.547	0.191	1.298
1400	326.67	5.44	4529.00	75.48	0.414	1.737	0.199	1.697

7.2 Discussion of Operating Characteristics

Figures 7.2 through 7.5 depict the operating characteristics of both spindles and the relative speeds which will be encountered throughout the expected range of operating conditions. Since all the graphs show low values at the 1800 rpm motor speed, it can be concluded that the spindles will be relatively stable for operation at this speed. Some of the values in the table are lower than the noise floor for the Dynamic Signal Analyzer. For this reason, inaccuracies in values around the noise floor will occur. Also, at lower operating speeds the accelerometer pick-ups will contribute to the problem since the signals being monitored are proportional to the square of the speed.

The graphs in Figure 7.2 and 7.3 depicting the barrel spindle run up and run down, show an increase in vibration magnitude around the 397 rpm

barrel operating speed. This can be detrimental to the process if the spindles slow to this value during a typical cutting operation. This situation should be investigated further when cutting components with the machine head. If in fact, larger vibrations do occur during cutting at this speed, the rotor cutting speed may have to be increased to a stable speed.

The grinder spindle shows a significant increase in vibration around the 6200 rpm, or 103 Hz operating speed. This could be the result of the speed being too close to the motor line frequency. The motor line frequency is about 120 Hz for the 2X line frequency. Since the line frequency exhibits side bands about this frequency, the result is a falsely amplified signal around 104 Hz which may or may not be a result of excess vibrations of over 3 g's. This result is clearly shown in Figures D2 and D3. There exists a frequency spike at 106 Hz which causes a false increase in vibration magnitude due to electrical interference.

From the GM spike energy severity chart, Figure 6.5, the maximum spike energy for a machine spindle operating at 420 rpm is 0.20 g. The maximum spike energy for a spindle operating at 5823 rpm is 2.5 g. From Table 7.1 most of the values for the specified frequencies are below or meet, the acceptable limits. The barrel spindle spike energy is divided by two for a value of 0.113 g maximum, and the grinder spindle value is 0.675 g maximum. These values are very acceptable and provide a good factor of safety in the balancing.

VIII. DISCUSSION

8.1 Frequency Response Testing

The main focus of the frequency response testing is to determine natural frequencies of the machine components. From the experiments performed on the five major machine components, a good representation of the actual resonance frequencies can be estimated reasonably well depending on the support configuration used for the experimental measurements.

The motor spindle was the most accurate portrayal of the bearing support environment during actual operating conditions. The grinder spindle shows a very low first natural frequency with respect to the other two components. This may be attributed to the support configuration as only two bearings were supported by v-blocks. A more appropriate test using three supports to be representative of the actual load carrying conditions is expected to have yielded different results. The machine spindle housing measurements were the most difficult to achieve a consistent impact force with little noise interference because of its hollow center. The motor housing was very difficult to achieve repeatable results, again because it is hollow. The barrel spindle measurement results were satisfactory for its application in the experiment because the first resonance frequency is well above the operation frequency.

The overall frequency response plots show natural frequencies well below all of the

first rigid mode of all the components, with the exception of the grinder spindle. All of the spindles operate smoothly with little or no axial vibration. The operating speed of the grinder spindle is 97 Hz. This value is near the first natural frequency of the motor spindle (112 Hz) and the barrel spindle (136 Hz). During operation, the forced linear excitation of the grinder spindle could affect the behavior of these two spindles by increasing the vibration amplitude. As Gupta [10] et al. have discovered, cross excitation will be present in the rotation of dual spindles. This is the reason that spindle acceleration tests were performed and documented in the previous chapter. It was verified that this phenomenon exists for this machine because it exhibited a decrease in vibration levels when the internal grinder spindle was disengaged and only the barrel spindle was in operation.

8.2 Equipment Considerations

The equipment used for all the experimentation was provided by the University of Windsor. Equipment calibration was performed at Cobra Machine Tool and at the University. The only major consideration for the equipment was that the calibration of the accelerometers was performed before every test and recorded in a log. This value remained constant within ± 6 mV / g. An average value of 152.6 mV / g was used as the constant vibration calibration factor for all the measurements and conversions. For the values stated, this shows an error of only ±4 percent.

8.3 The Static Balancing Collar

The fabricated balancing collar designed for application to the barrel spindle reduced the vibration amplitudes to acceptable levels. The collar alone would have been sufficient for decreasing the vibration amplitude to acceptable levels; however, a finer balance is required for a machine equipped with a diamond face grinder. Finer balancing yields a premium finish for machined components.

Calculations for the collar involved assumptions described in Section 5.3.1. The main purpose of the collar was to offset the void of material removed from the barrel spindle and grinder spindle. In hind sight, other methods have been thought of that are more preferable than the implementation of a barrel collar. One method is the elimination of the barrel holes and collar by removing a sufficient diameter of material 180 degrees opposite to the grinder spindle. This will offset the void as well as eliminate the time spent tapping holes in the barrel spindle and fabricating collars. The calculation for the new hole diameter can be performed using Equation 5.3. Another method considered during the testing was to fill the grinder spindle with a material of higher density. This was dismissed because of the high operating speed and because any non-uniformities of material in the grinder spindle might generate excessive vibration at higher speeds. Furthermore, a solid grinder spindle would increase the inertia properties of the spindle as well as change its natural frequency. At the time, the best method available was thought to be the addition of barrel collars to add mass, thereby no unwanted material can be mistakenly removed from the barrel spindle.

8.4 Dynamic Balancing Conclusions

The primary scope of the project was to indicate the best methods for dynamically balancing the spindle at idle speed. For a speed of 420 rpm (or 7Hz), magnitude and phase measurement inconsistency and repeatability were the major problems. The use of accelerometers to measure low frequency vibration is not the accepted best method of balancing. Velocity and displacement transducers would have captured low frequency signals better than accelerometers. Low frequency measurements were extremely difficult to achieve repeatable values especially in phase measurement. During the initial balancing trials before the application of the balancing collars, the vibration amplitudes remained unaffected by the addition of correction weights. It was later determined that using phase measurements at low frequencies was not sufficient for determining the out of balance phase angle of the rotor at two planes. Using the program provided by Everett [6], the phase angle measurement was eliminated, and the accuracy of the correction weight positions at the two planes became very clear using only magnitude measurements. Once these positions were known, trial and error correction masses were added and subtracted from these locations until the lowest possible vibration levels existed for the spindles. It was determined experimentally that the Everett method of two plane balancing without phase, was the best method of balancing a dual eccentric machine rotor.

The grinder spindle and the motor spindle were both shop balanced at different locations to a desirable balance grade. Therefore no balancing effort was targeted at these two spindles. The minimum desirable balance grade for machine tool spindles is G2.5, (or balance grade 2.5) which is acceptable for a face mill application. The balancing standard

for a concentric grinding wheel is G1.0. Since a combination of two operations is present, the lowest grade is desirable and levels can be compared to Table B5.1.

8.5 Operating Characteristics

Figures 7.2 to 7.5 show a relative increase in vibration when the spindles accelerate and decelerate. This can be detrimental to optimal machine operation since the spindles will slow during a cutting operation. The spindles may be experiencing a internal excitation for one or more components within the machine or coinciding with one or more harmonic frequencies. Since the frequency response data does not support this conclusion, the reasons for increased vibration could be from instrumentation, or simply unexplained.

8.6 Dynamic Machine Model

A basic consideration for the machine modeling is that the variables will change considerably at different cross sections and planes. Modeling at a specific plane will only dictate variables in two directions. Dynamic moments and other considerations for the model are not considered in calculations for the depth of this study, but future work in this area could produce excellent modeling results.

IX. CONCLUSIONS

As stated in the introduction, the objectives of this study were: to develop a routine to benchmark the balancing of a dual face mill eccentric grinder machine head: to access the machine operation using vibration analysis for gear and motor noise: and to perform an experiment for full spectrum sound power level determination.

The machine was balanced according to GM corporation's vibration standards for new and rebuilt machinery and equipment. The best method for achieving minimum vibration magnitudes was to use the static couple method of balancing. This involved statically balancing the barrel spindle by the addition of mass 180 degrees opposite to the grinder spindle, and dynamically balancing the barrel spindle using the Everett [6] two plane balancing without phase response program.

Through additional experiments it was determined that the noise problems were caused by the existing spur gears in the prototype machine. It has been suggested by Dudley [4] that replacing spur gears with helical gears will reduce the sound pressure levels up to 20 dB. This is a very significant decrease in noise and was recommended to Cobra Machine Tool before assembling future machines. The changes outlined above will also decrease the overall sound power levels for this unique machine.

APPENDIX A

Frequency Response Function Data

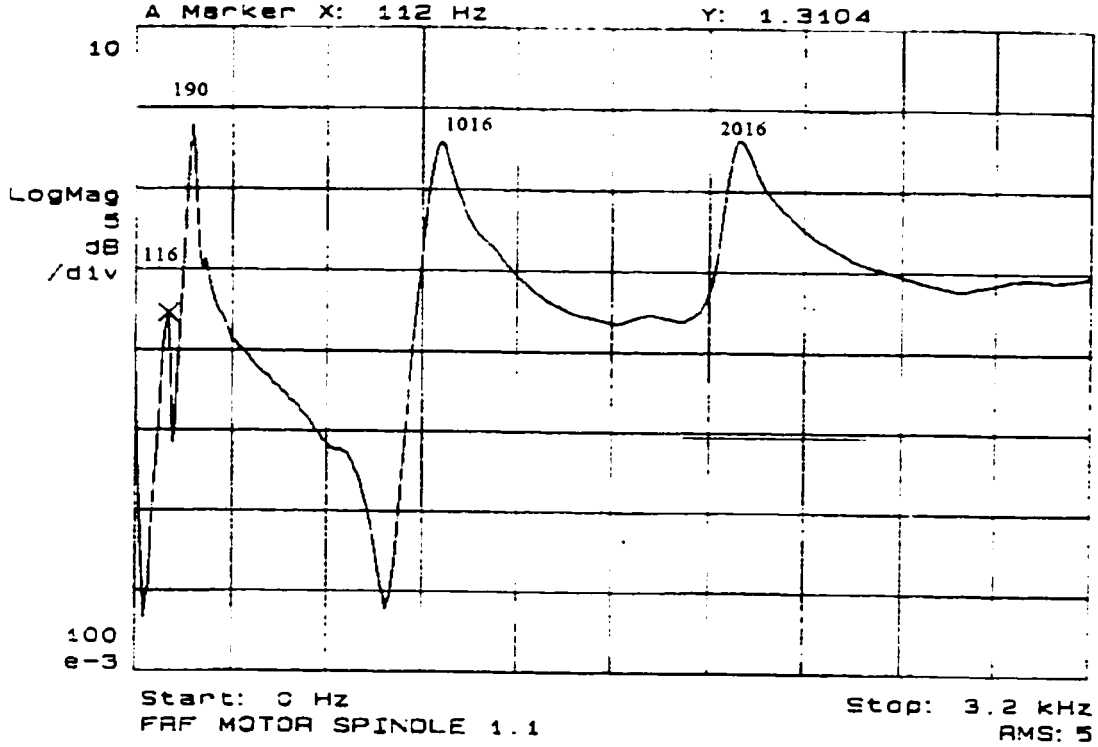

Figure A1.1 Frequency Response of Motor Spindle Location 1

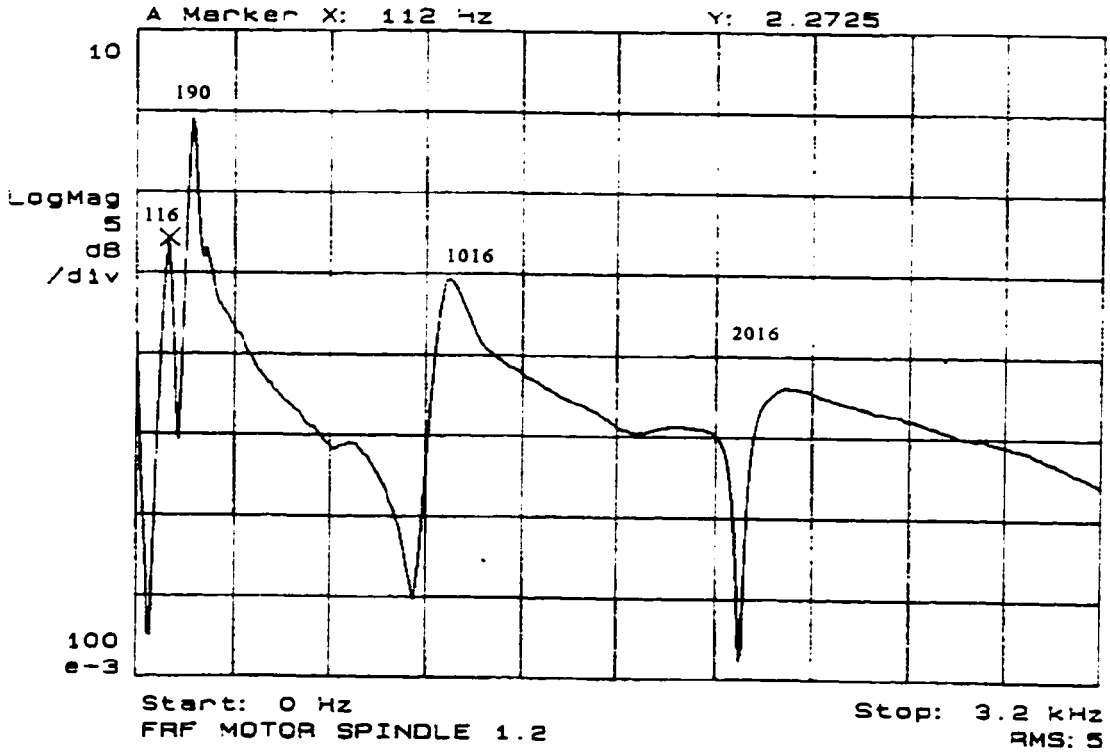

Figure A1.2 Frequency Response of Motor Spindle Location 2

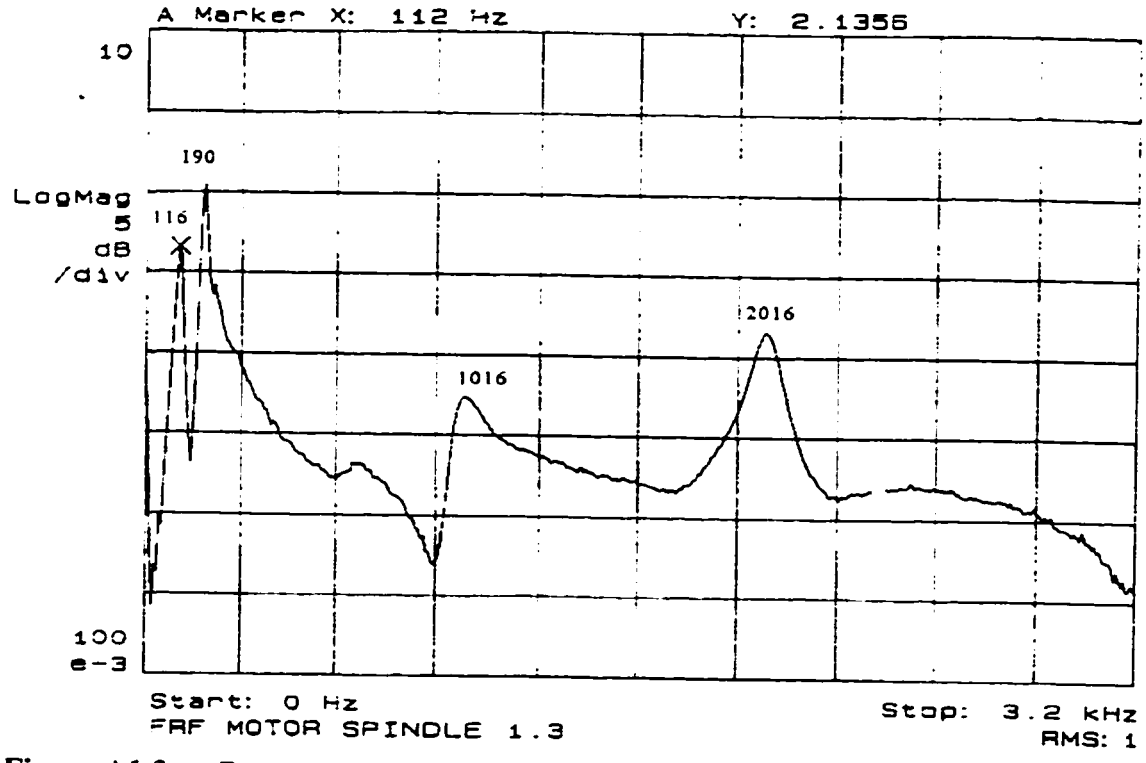

Figure A1.3 Frequency Response of Motor Spindle Location 3

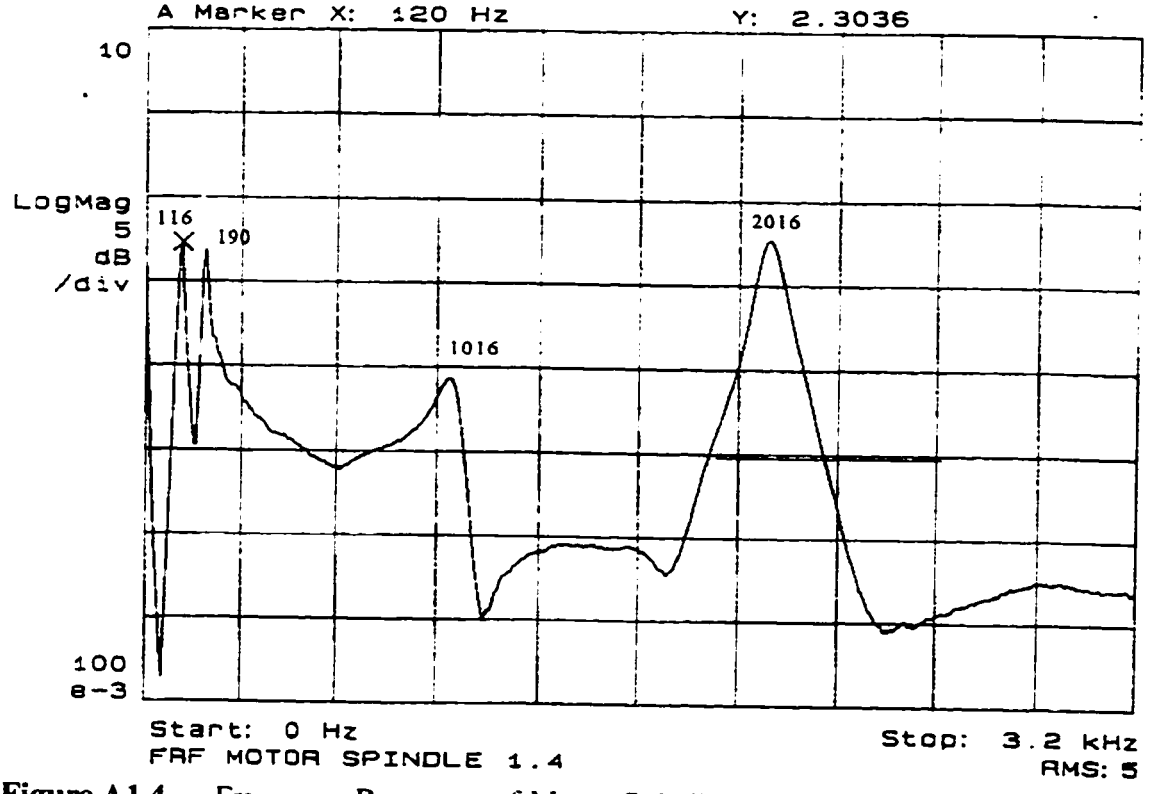

Figure A1.4 Frequency Response of Motor Spindle Location 4

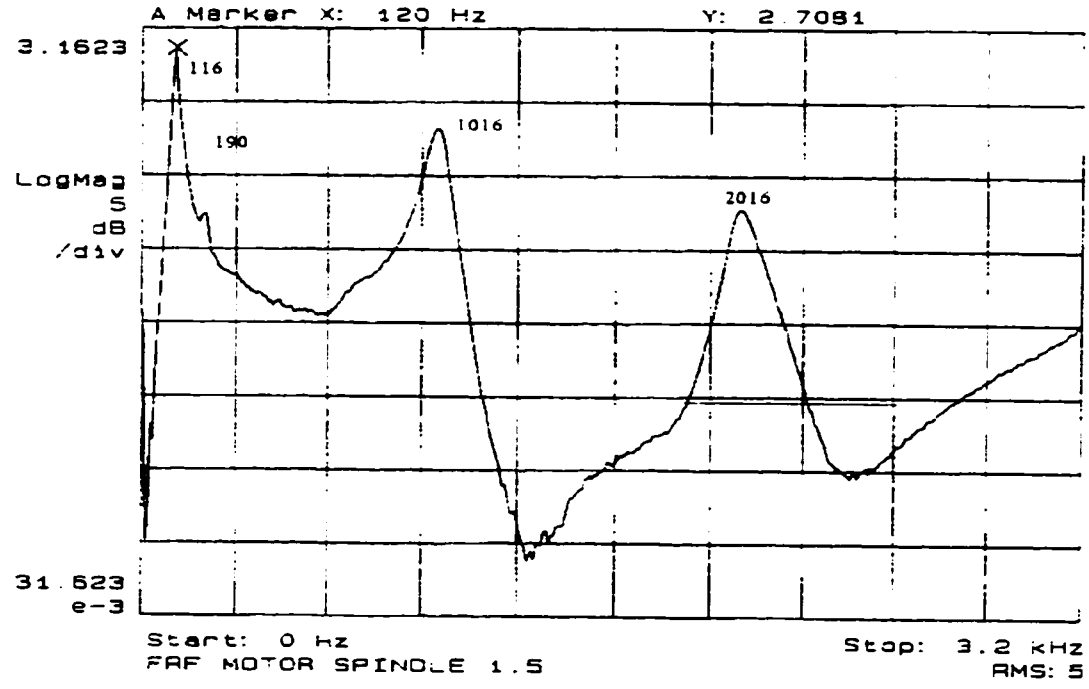

Figure A1.5 Frequency Response of Motor Spindle Location 5

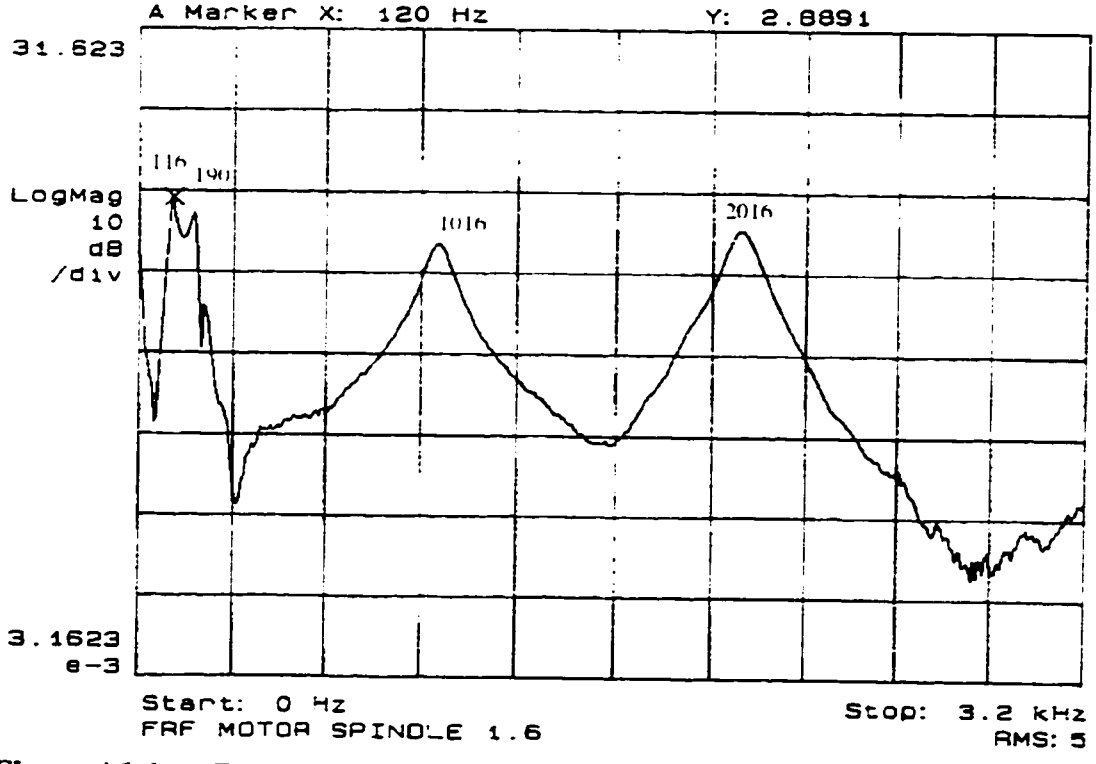

Figure A1.6 Frequency Response of Motor Spindle Location 6

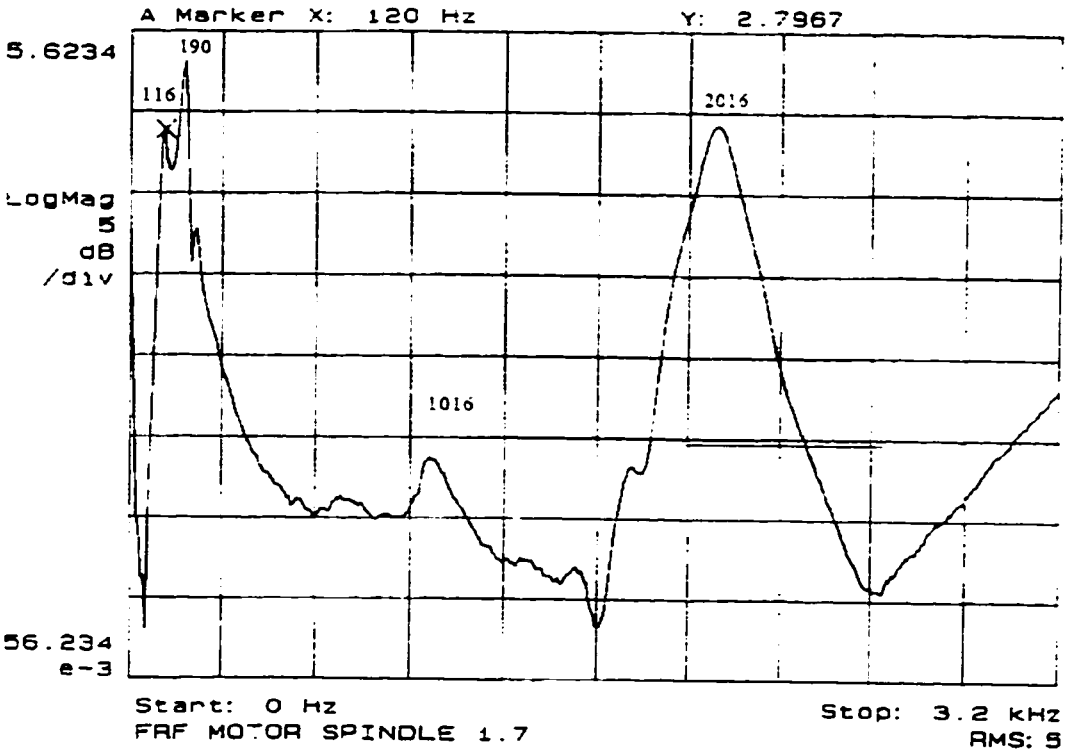

Figure A1.7 Frequency Response of Motor Spindle Location 7

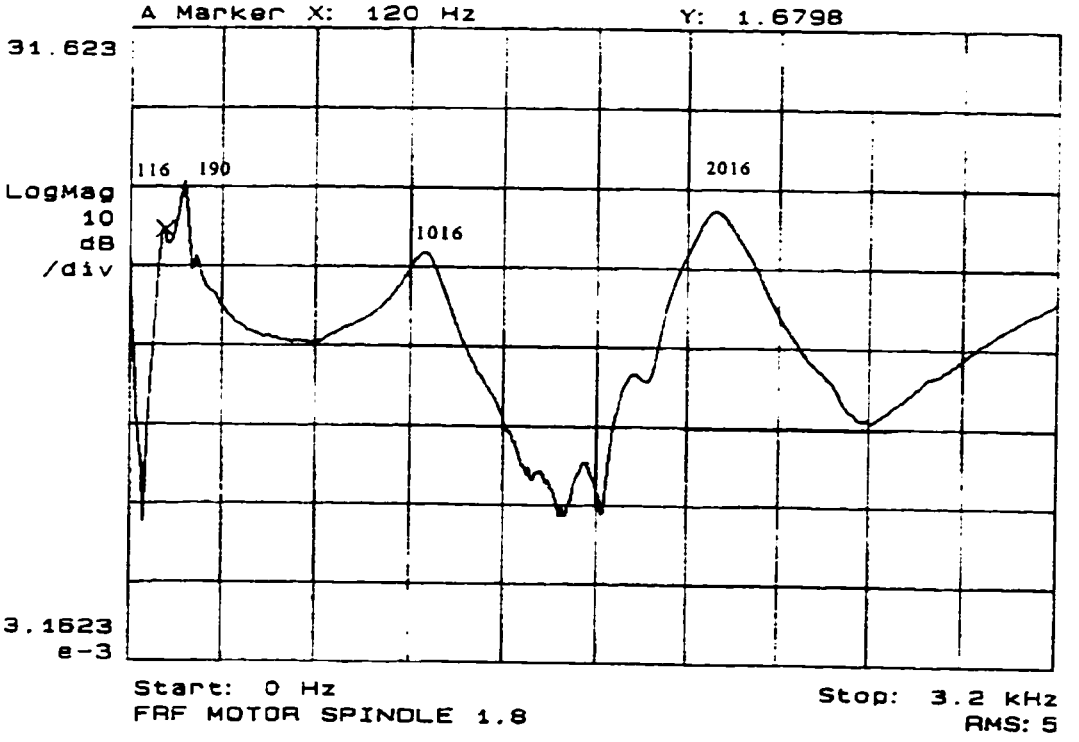

Figure A1.8 Frequency Response of Motor Spindle Location 8

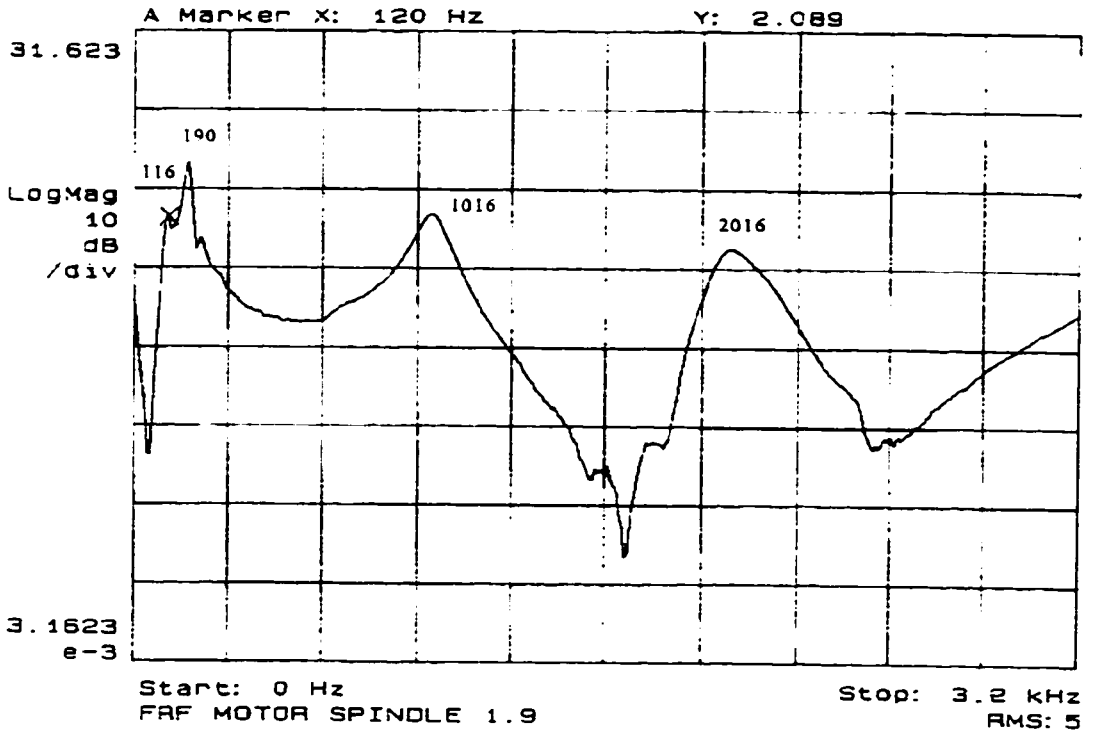

Figure A1.9 Frequency Response of Motor Spindle Location 9

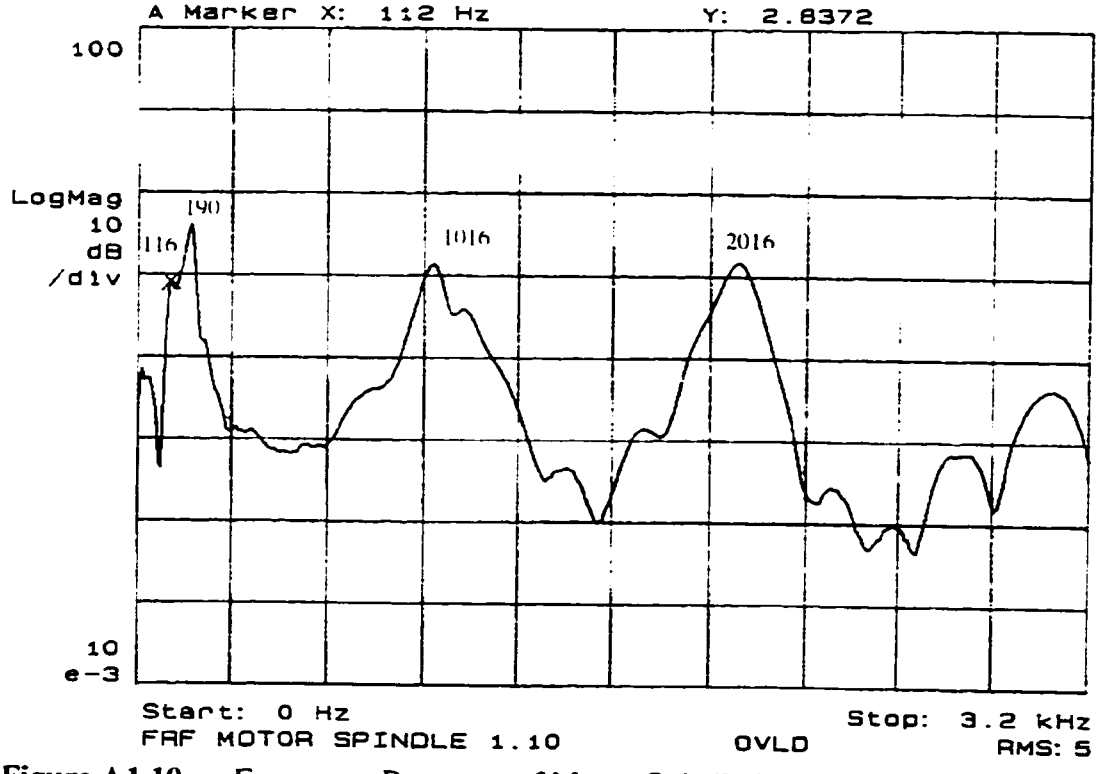

Figure A1.10 Frequency Response of Motor Spindle Location 10

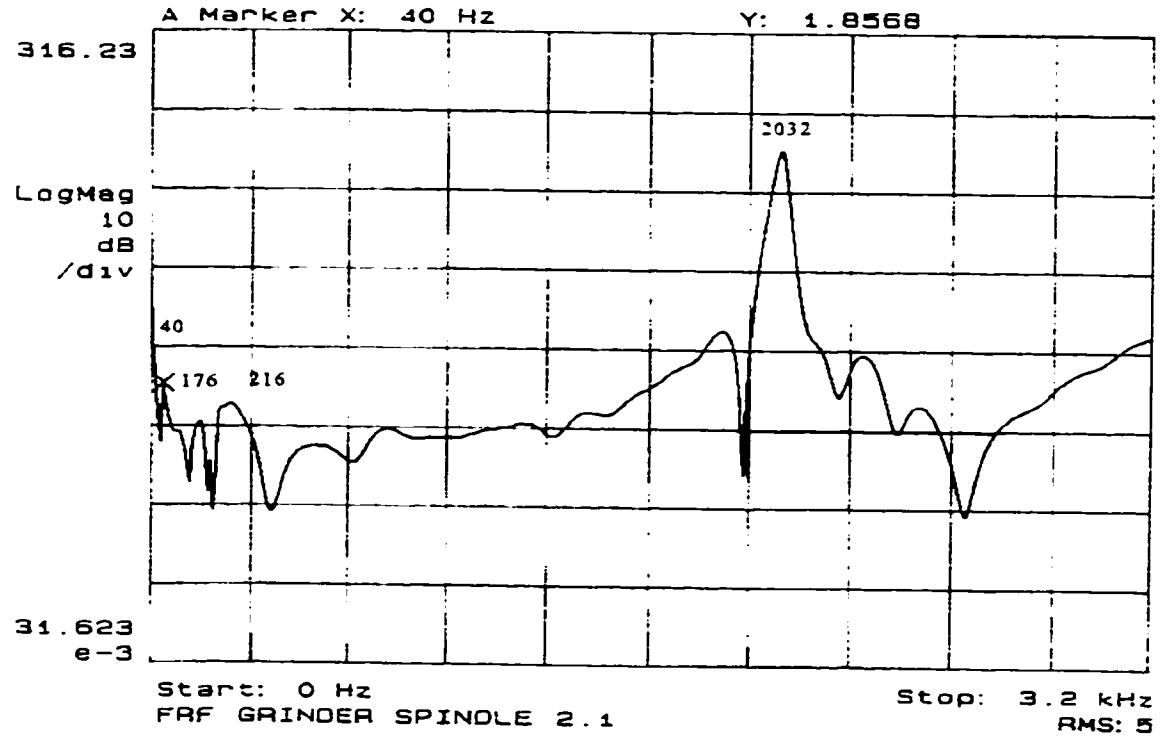

Figure A2.1 Frequency Response of Grinder Spindle Location 1

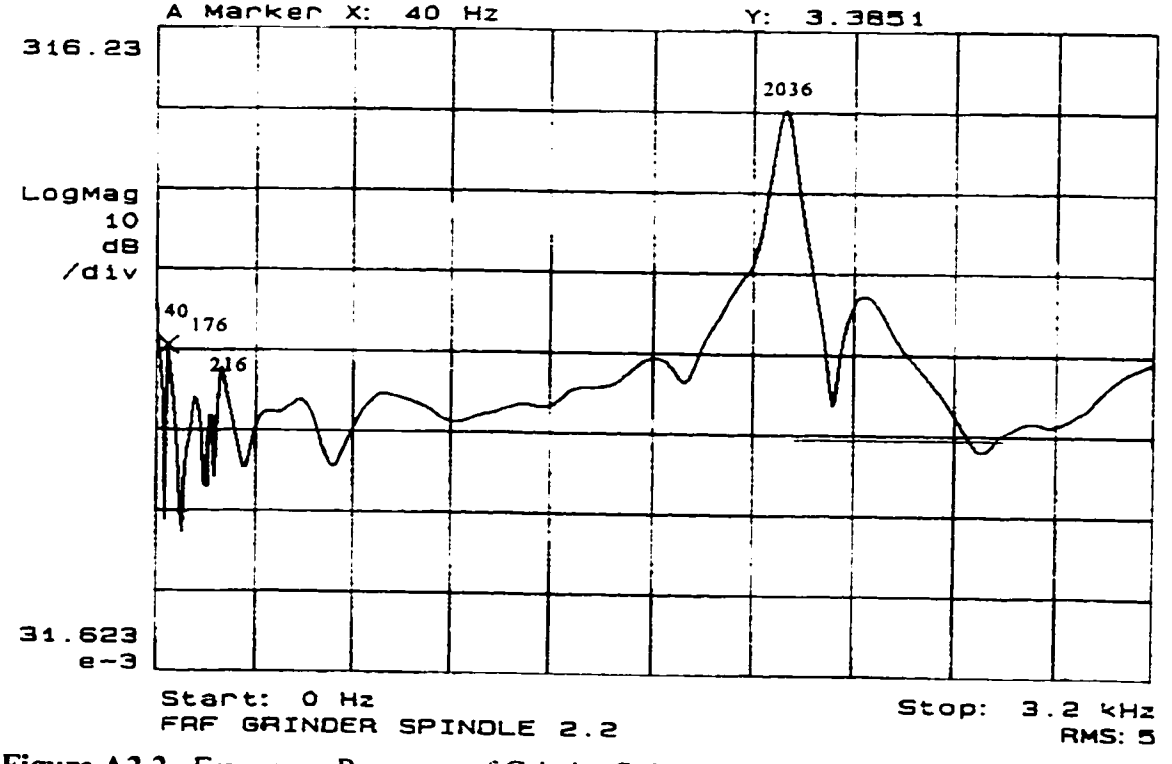

Figure A2.2 Frequency Response of Grinder Spindle Location 2

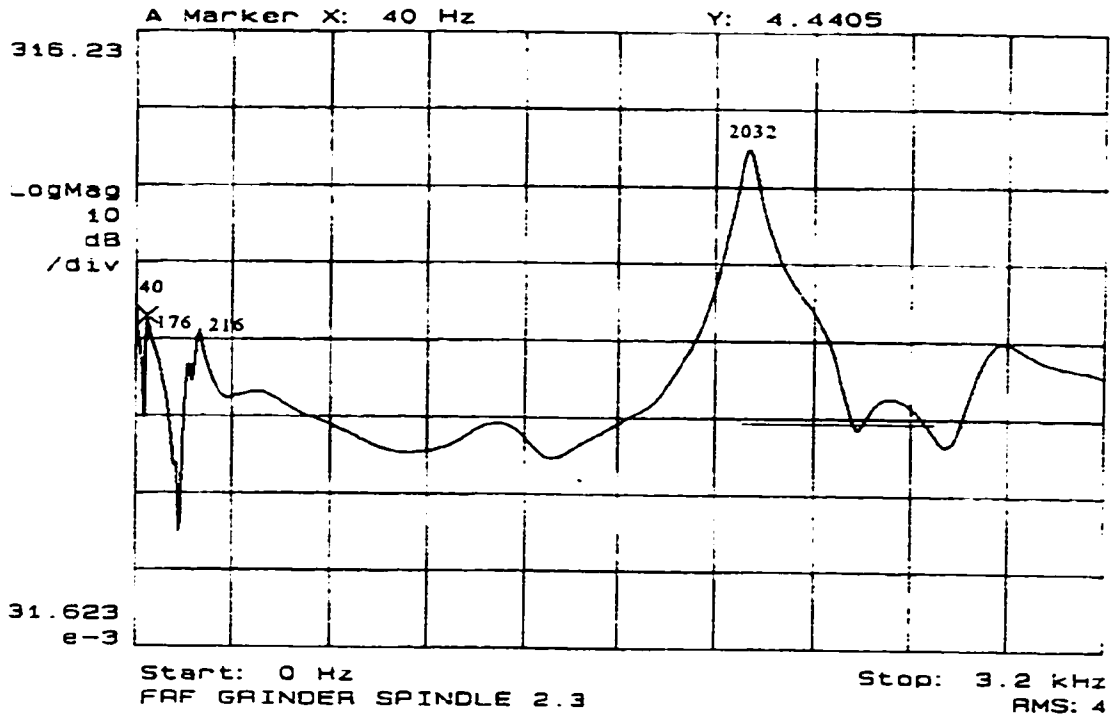

Figure A2.3 Frequency Response of Grinder Spindle Location 3

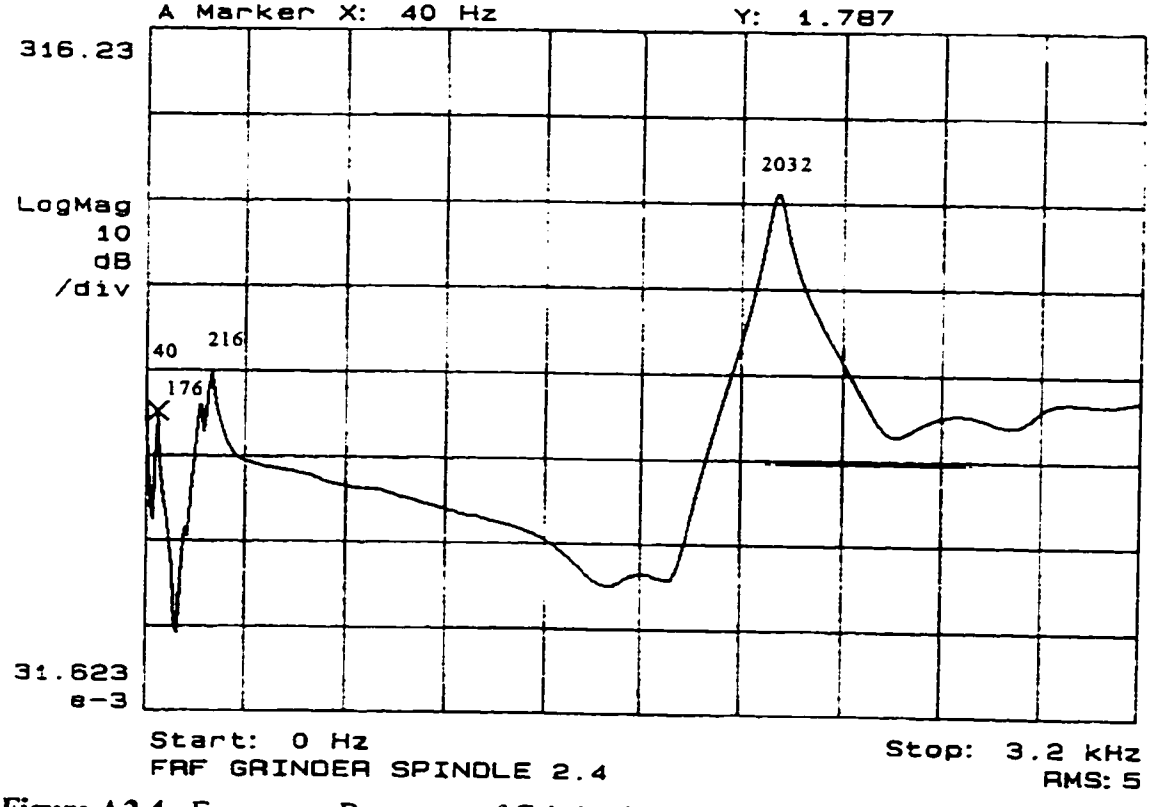

Figure A2.4 Frequency Response of Grinder Spindle Location 4

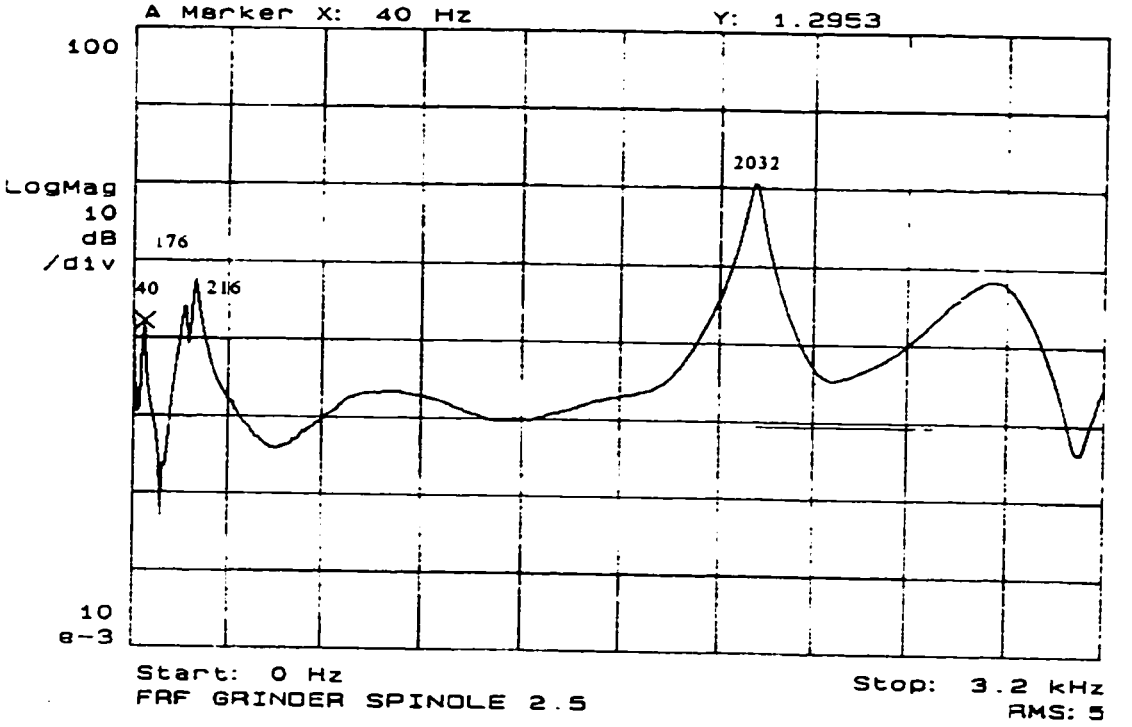

Figure A2.5 Frequency Response of Grinder Spindle Location 5

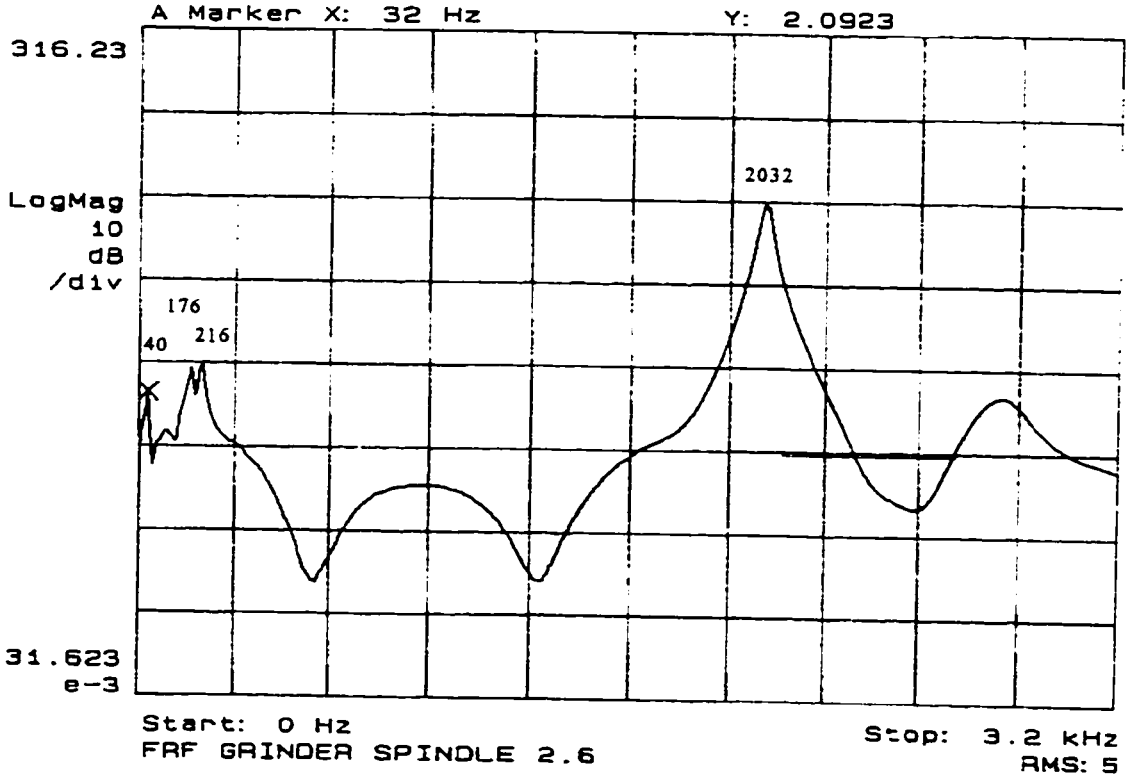

Figure A2.6 Frequency Response of Grinder Spindle Location 6

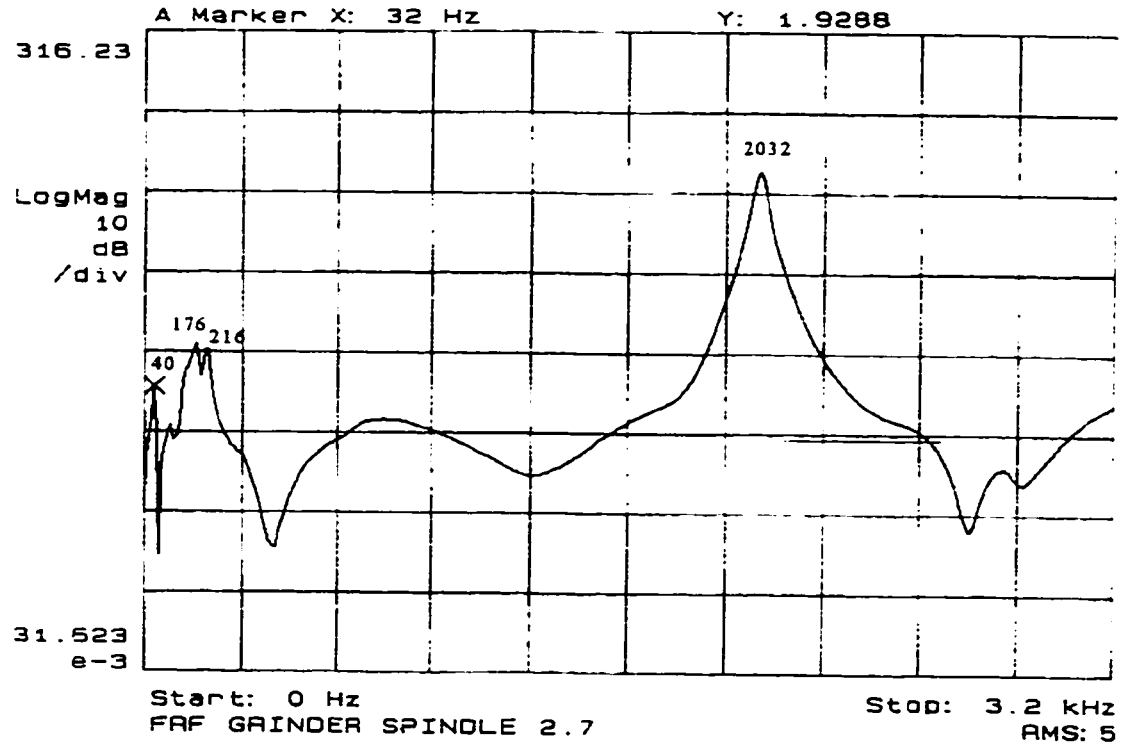

Figure A2.7 Frequency Response of Grinder Spindle Location 7

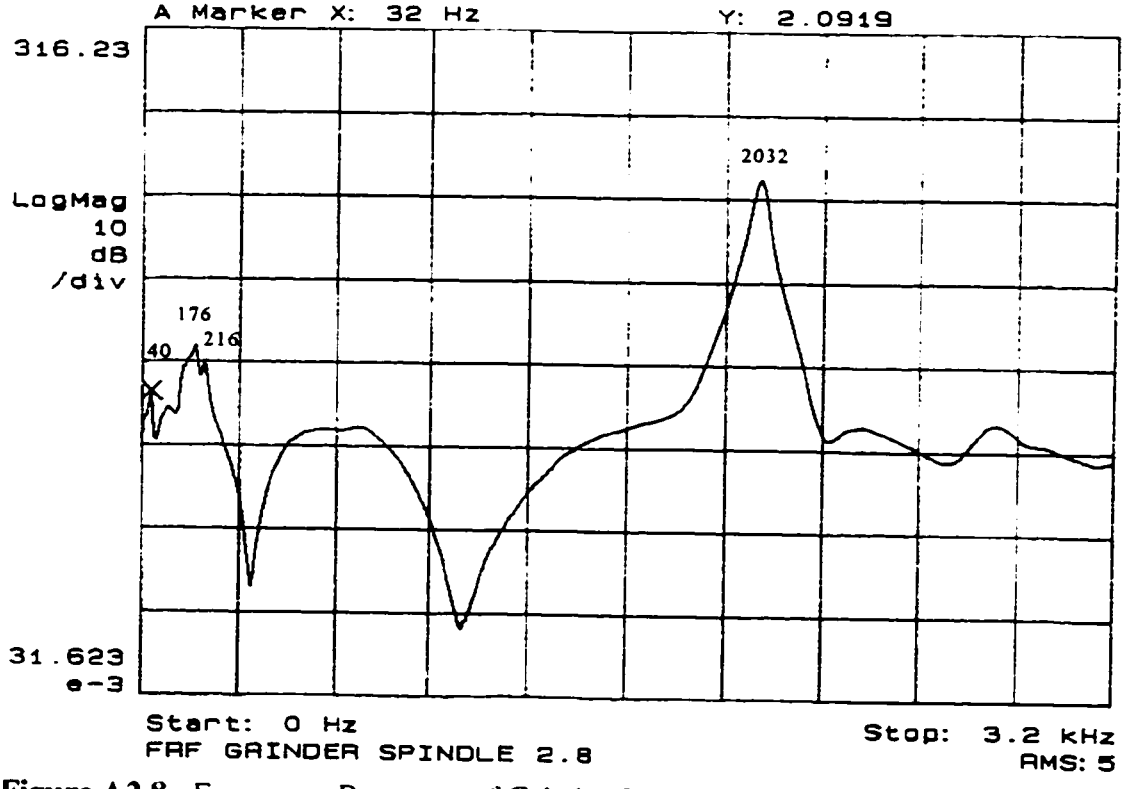

Figure A2.8 Frequency Response of Grinder Spindle Location 8

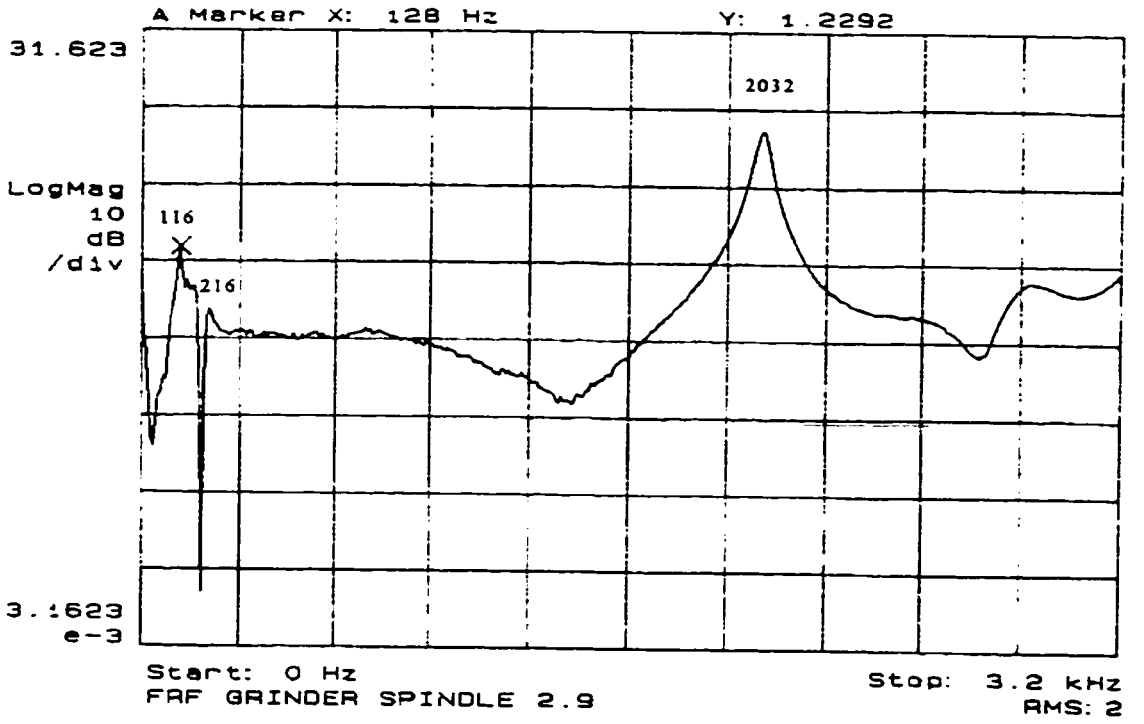

Figure A2.9 Frequency Response of Grinder Spindle Location 9

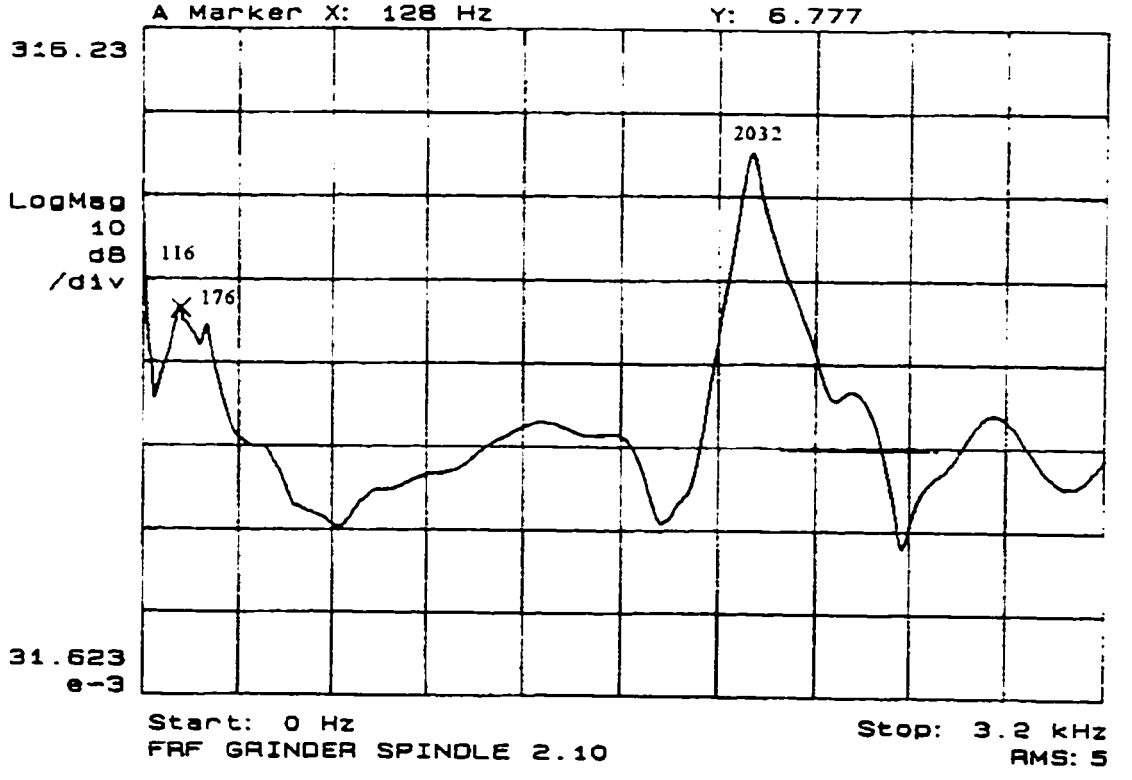

Figure A2.10 Frequency Response of Grinder Spindle Location 10

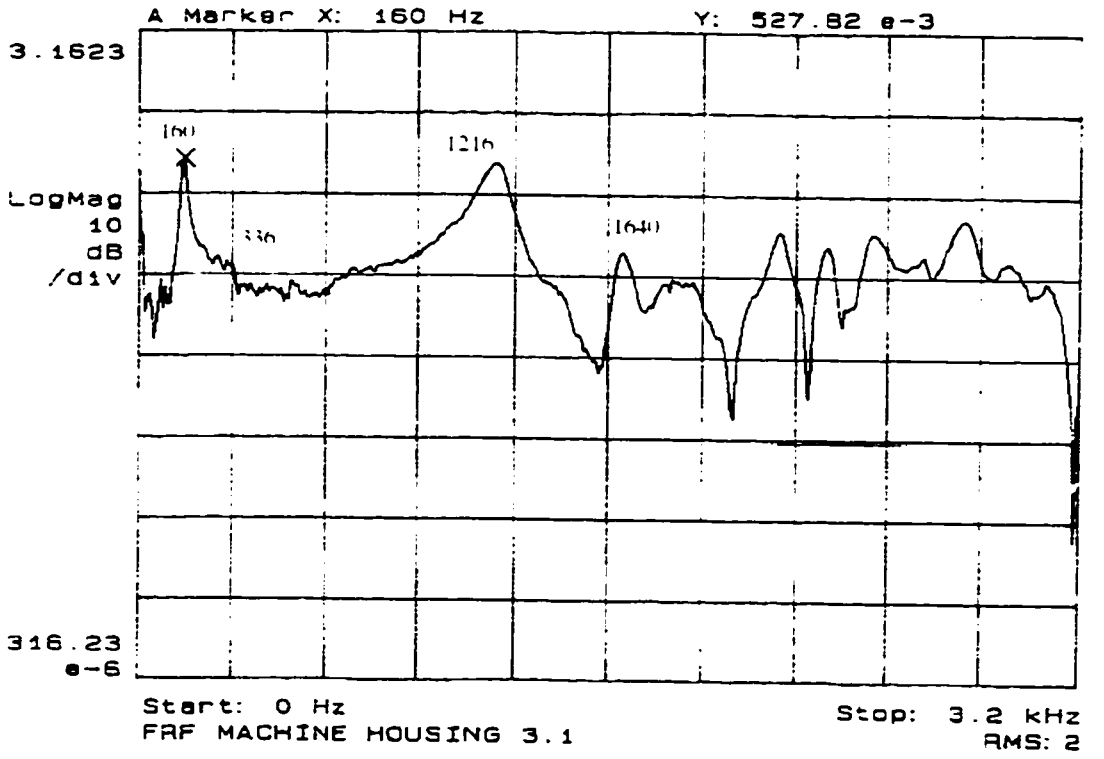

Figure A3.1 Frequency Response of Machine Spindle Housing Location 1

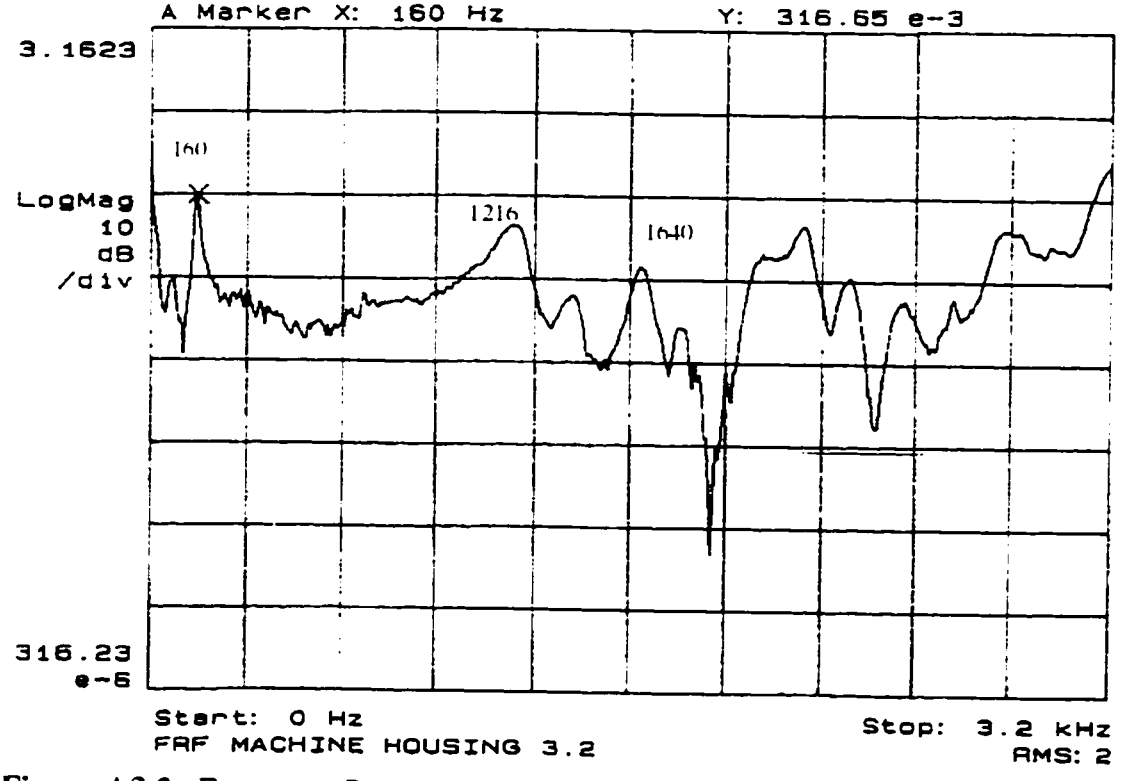

Figure A3.2 Frequency Response of Machine Spindle Housing Location 2

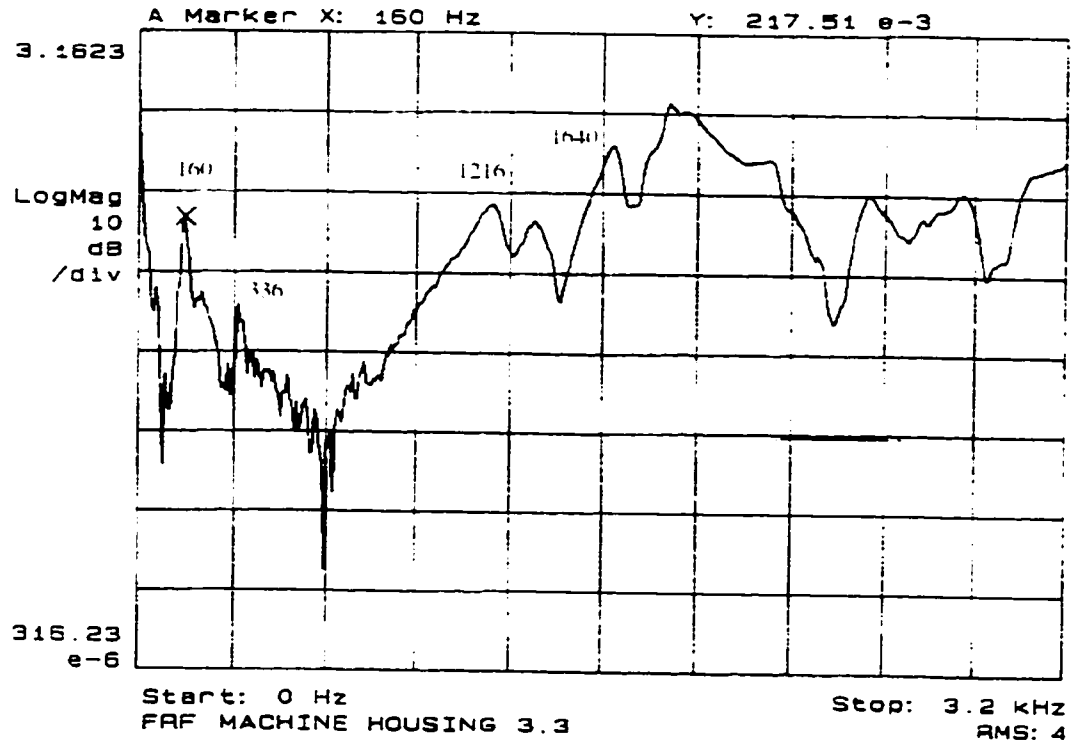

Figure A3.3 Frequency Response of Machine Spindle Housing Location 3

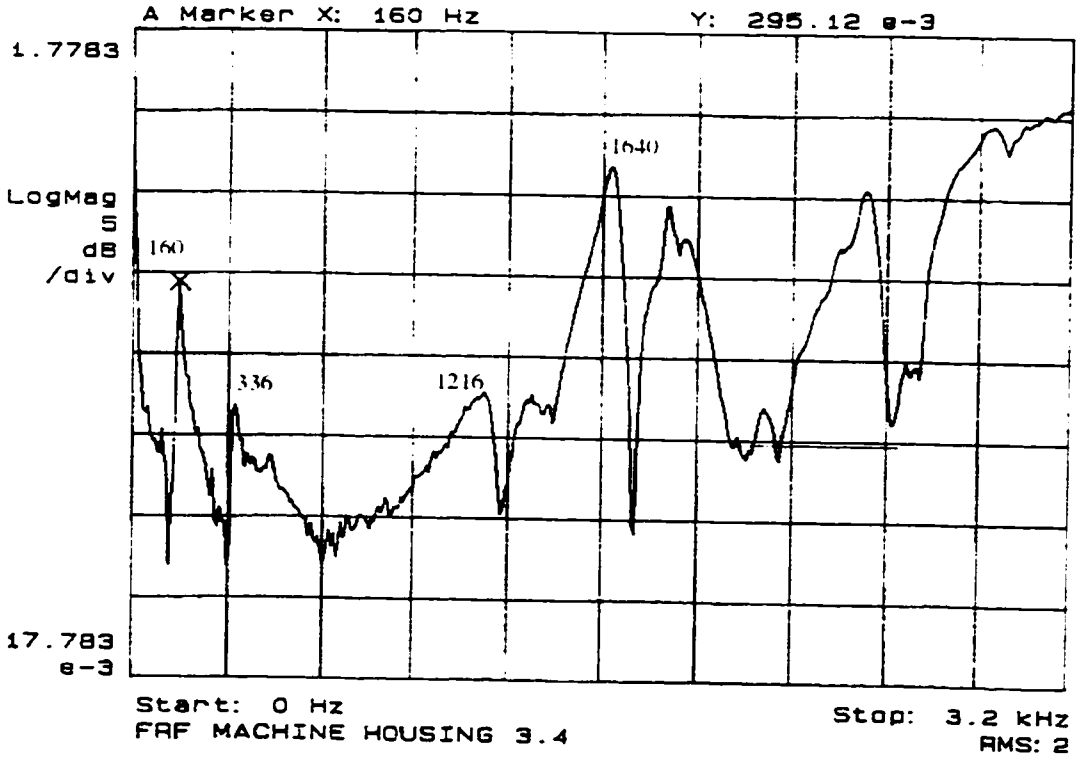

Figure A3.4 Frequency Response of Machine Spindle Housing Location 4

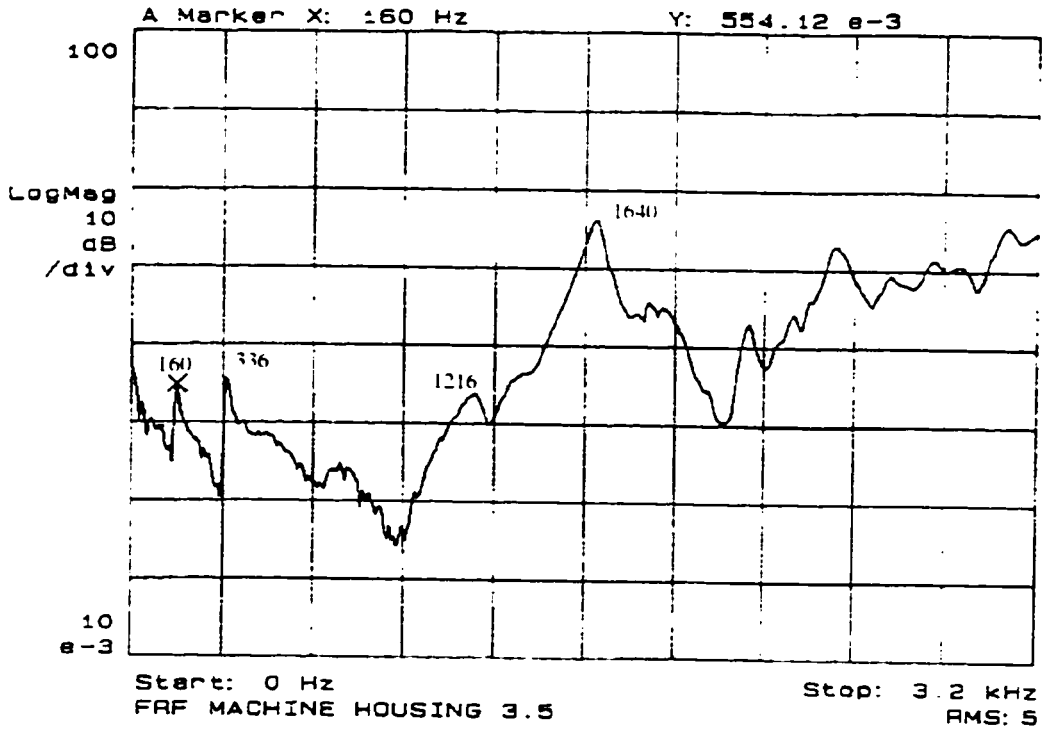

Figure A3.5 Frequency Response of Machine Spindle Housing Location 5

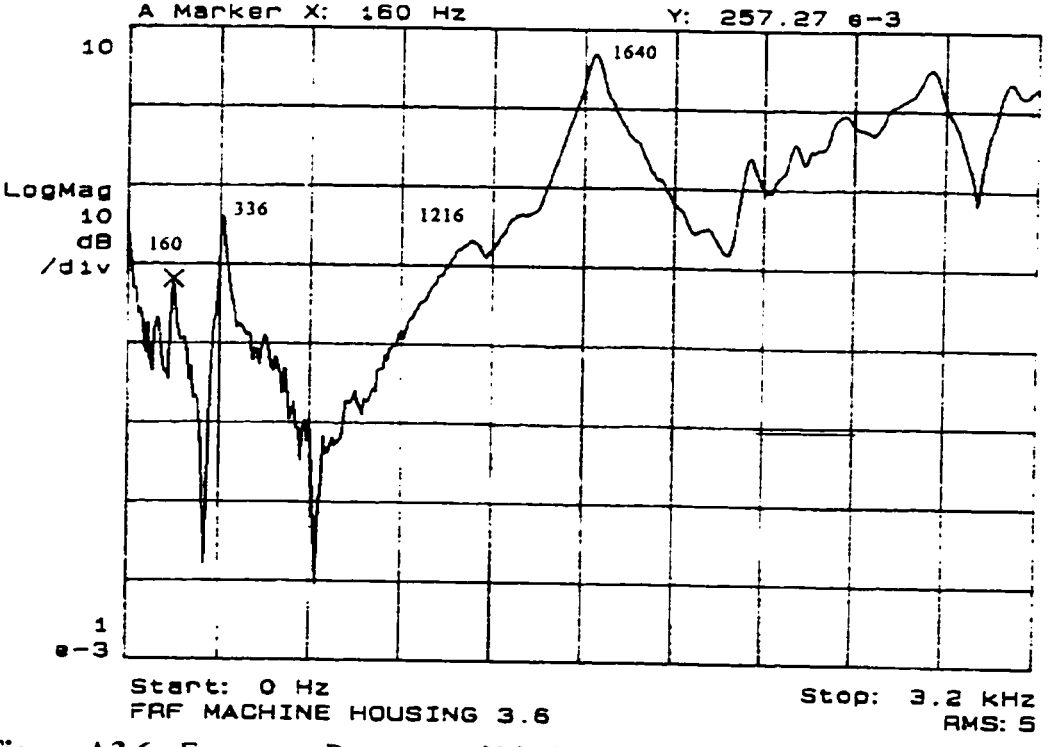

Figure A3.6 Frequency Response of Machine Spindle Housing Location 6

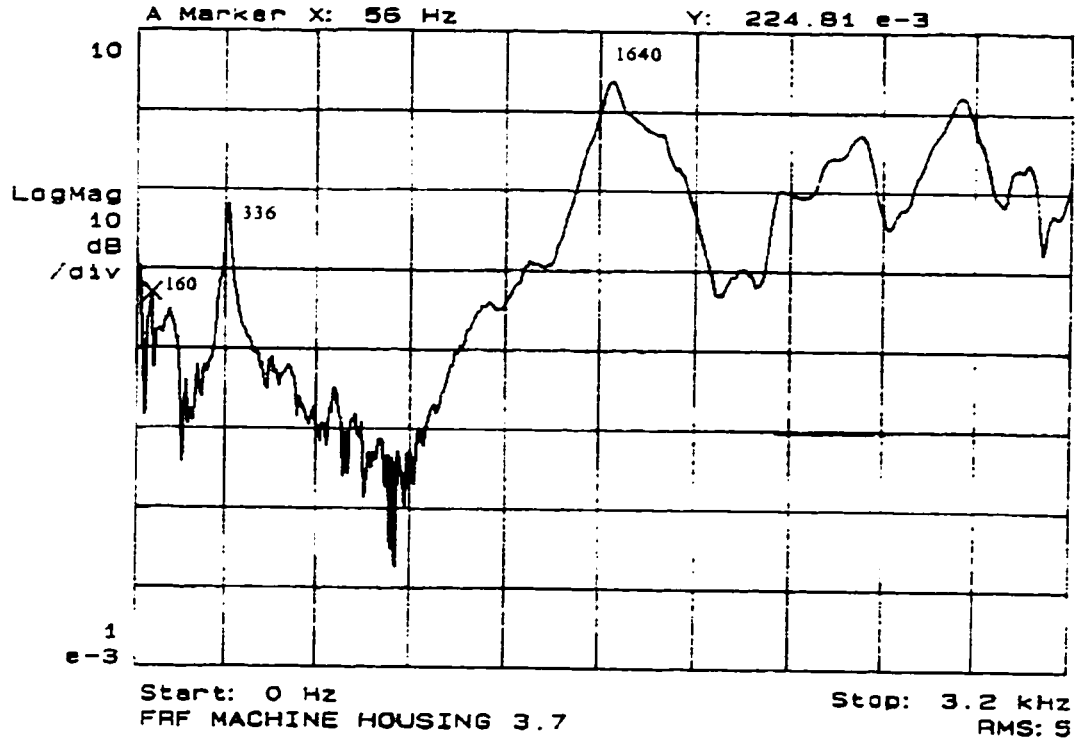

Figure A3.7 Frequency Response of Machine Spindle Housing Location 7

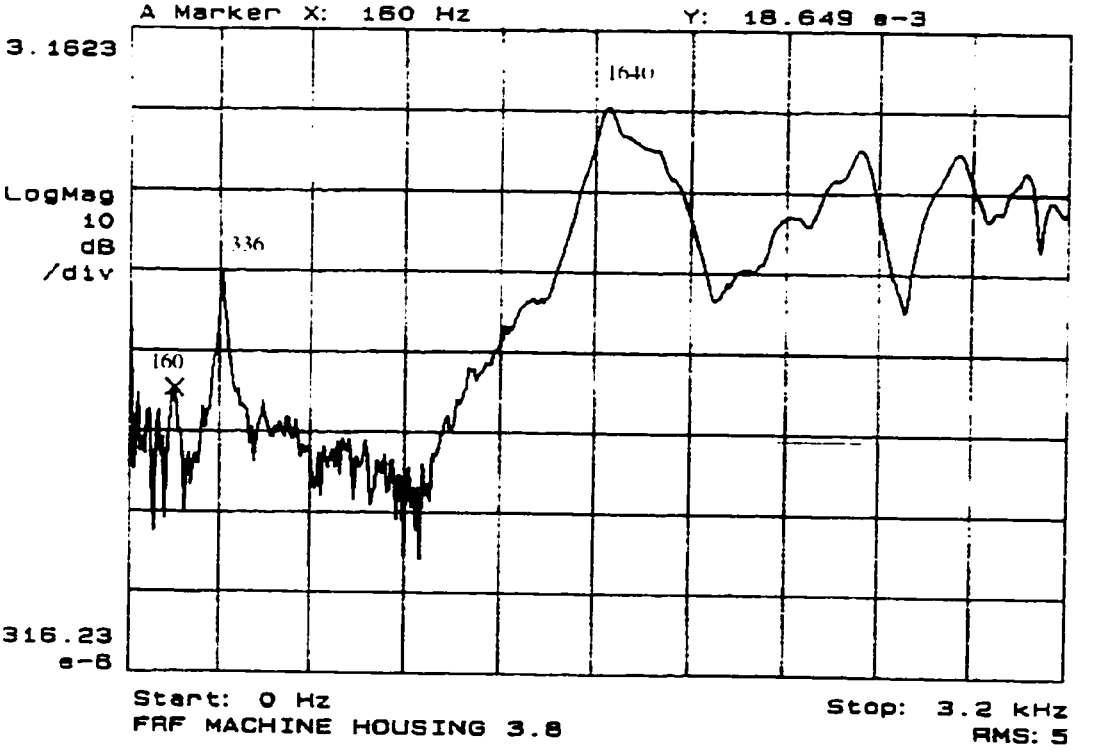

Figure A3.8 Frequency Response of Machine Spindle Housing Location 8

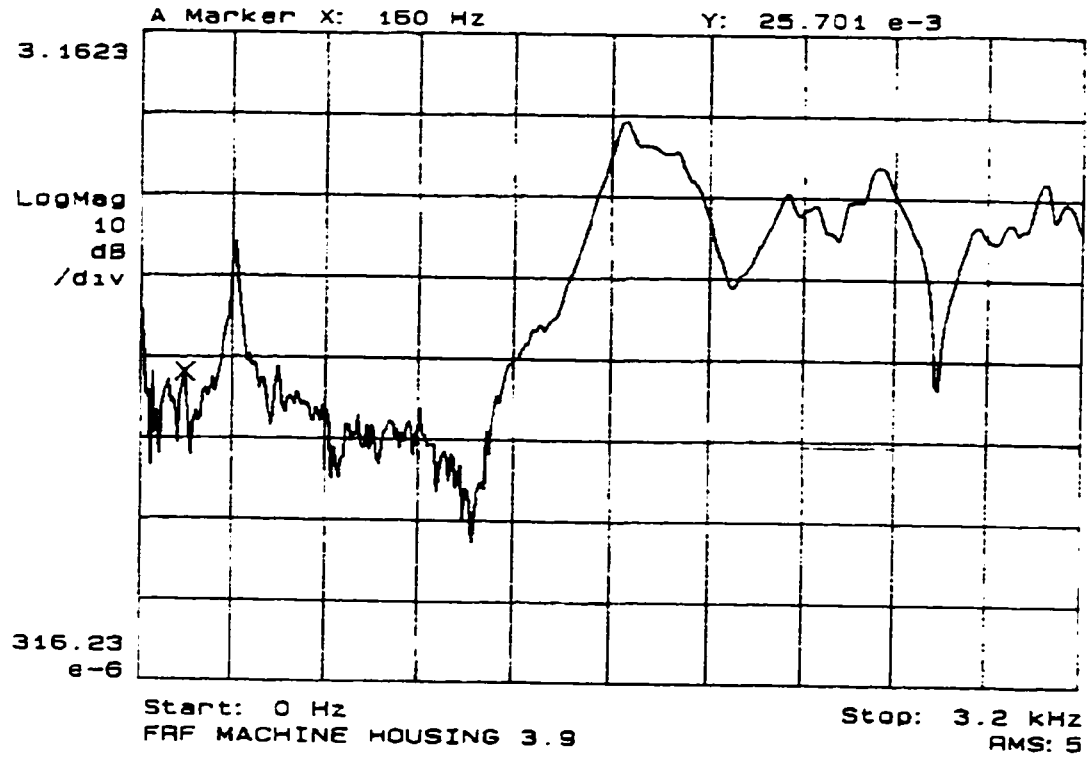

Figure A3.9 Frequency Response of Machine Spindle Housing Location 9

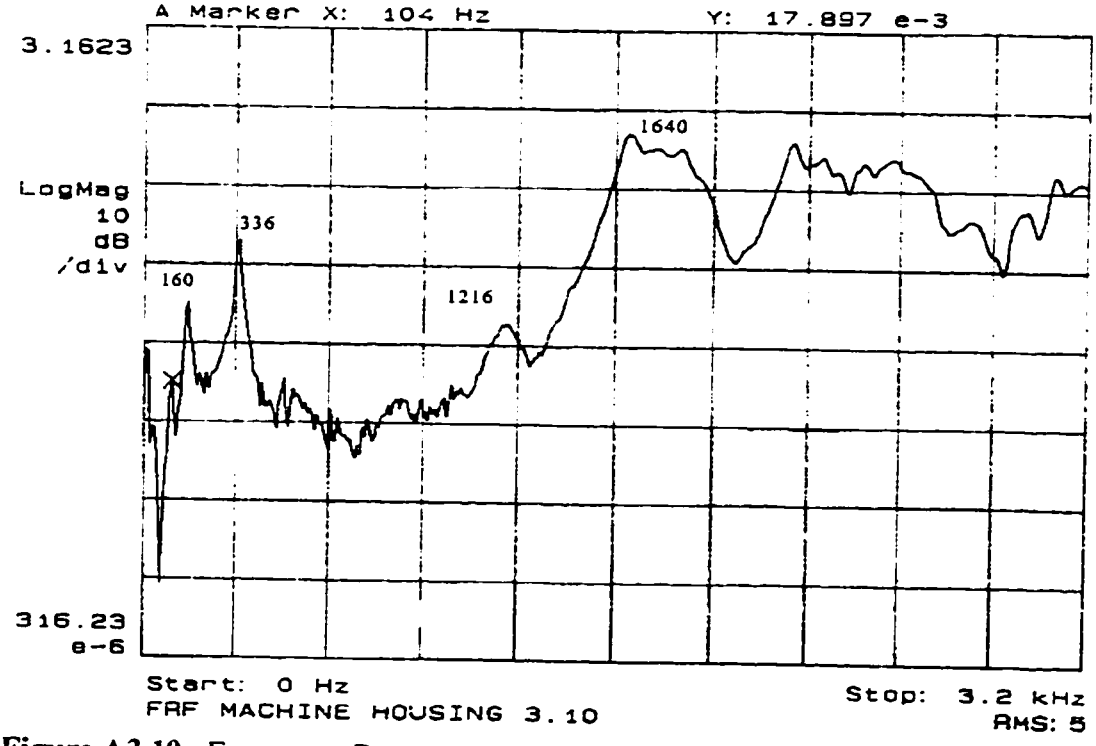

Figure A3.10 Frequency Response of Machine Spindle Housing Location 10

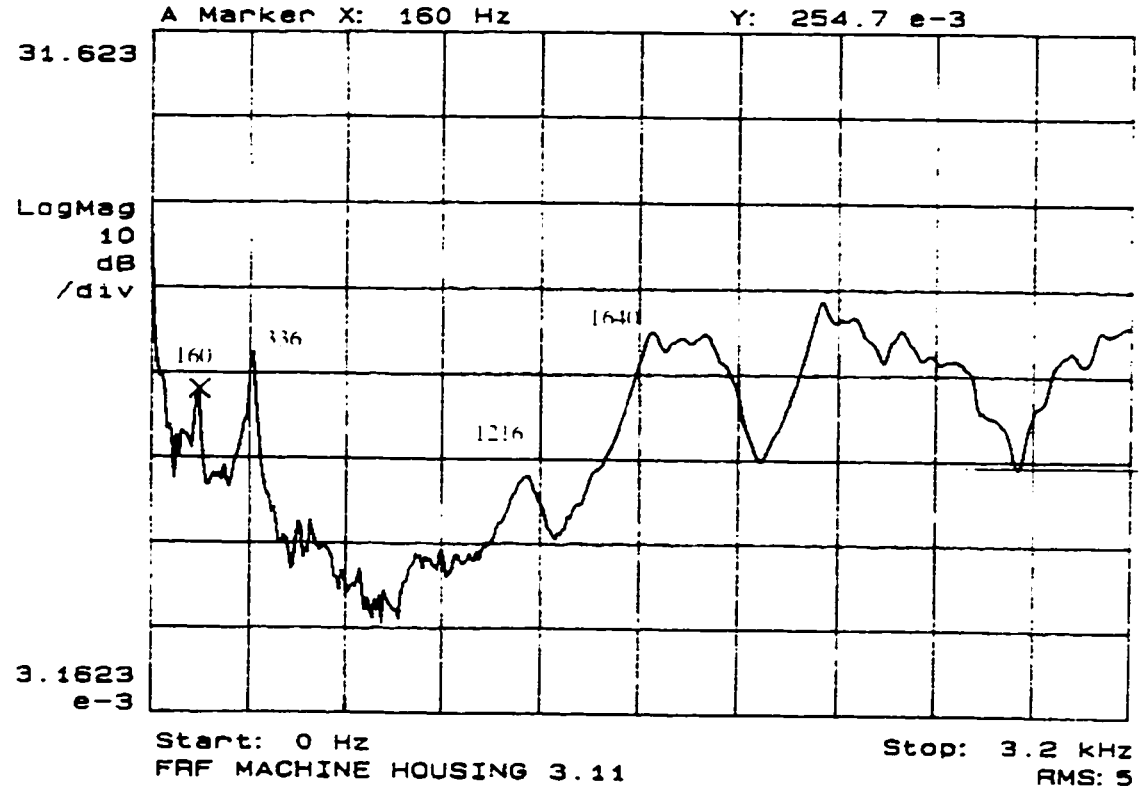

Figure A3.11 Frequency Response of Machine Spindle Housing Location 11

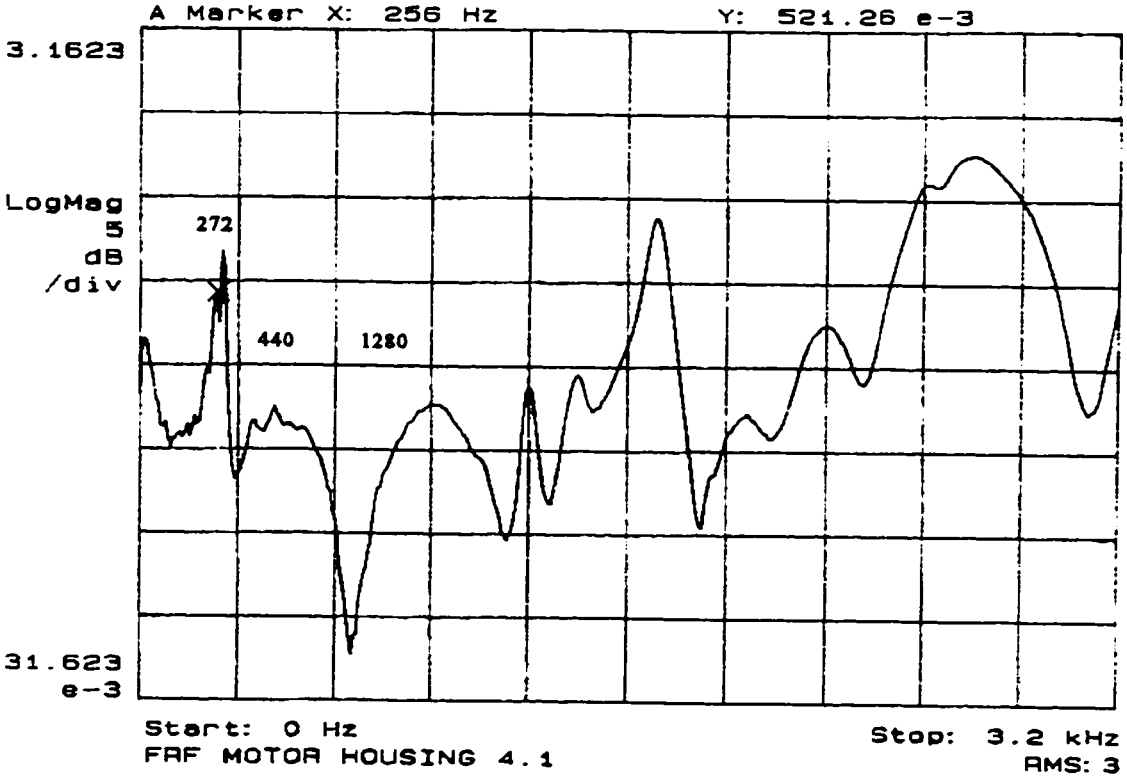

Figure A4.1 Frequency Response of the Motor Spindle Housing Location 1

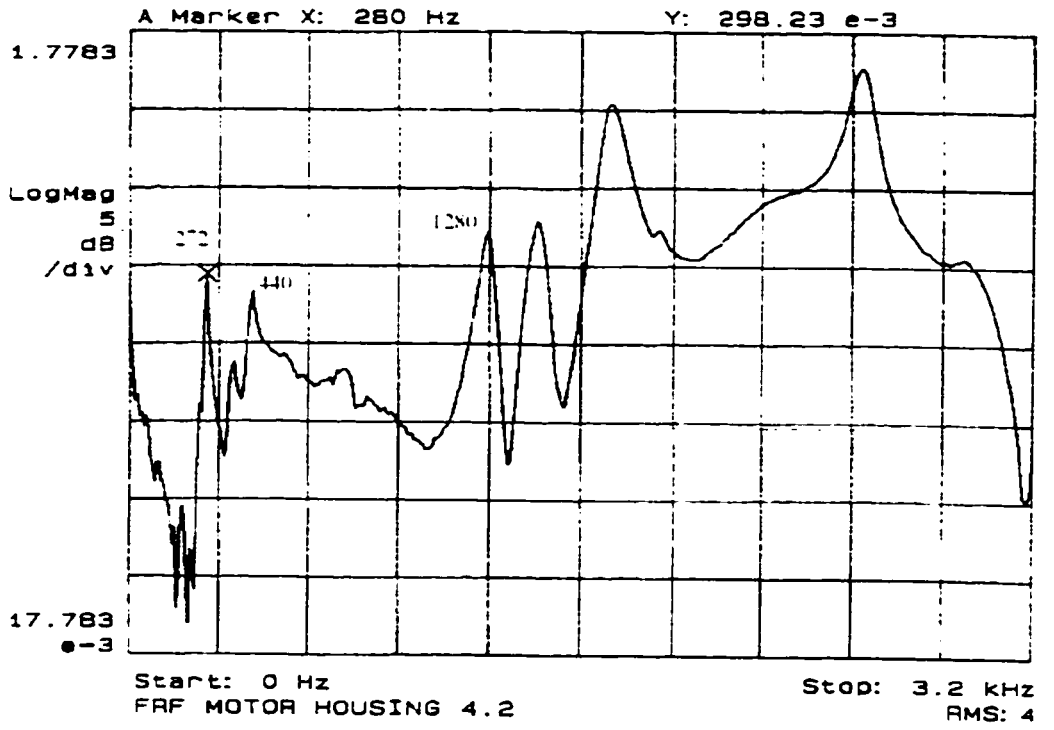

Figure A4.2 Frequency Response of Machine Spindle Housing Location 2

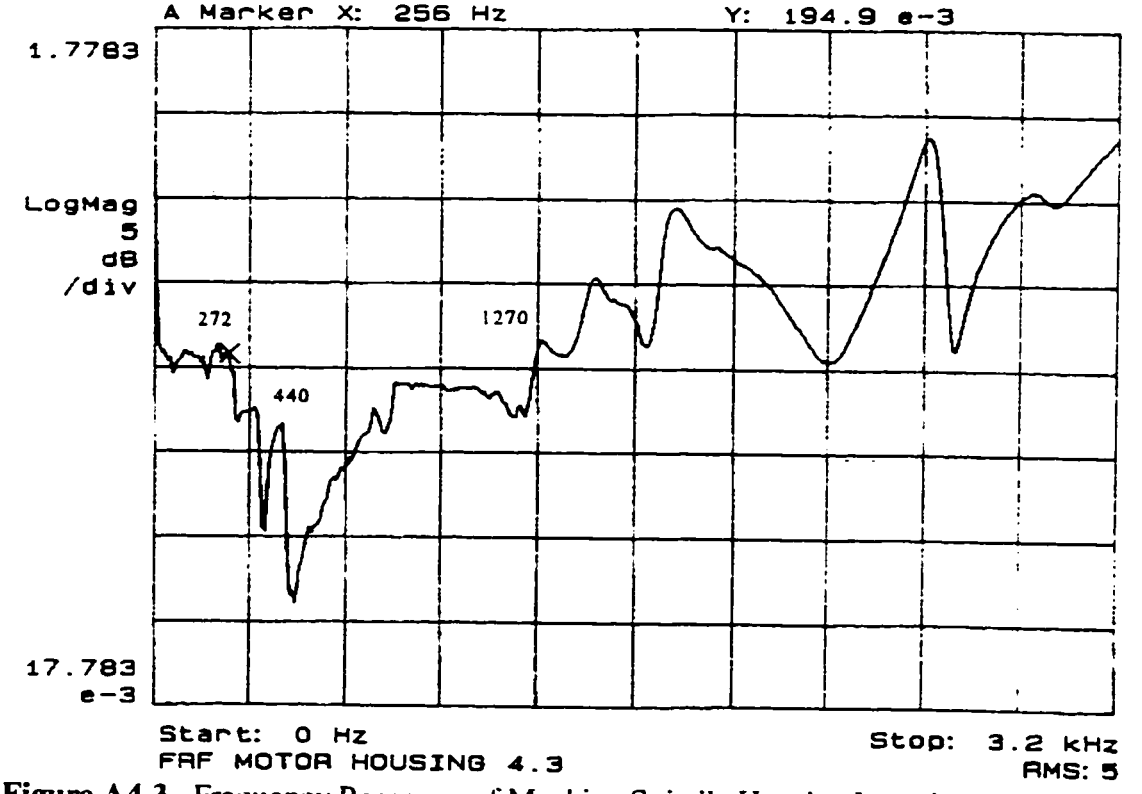

Figure A4.3 Frequency Response of Machine Spindle Housing Location 3

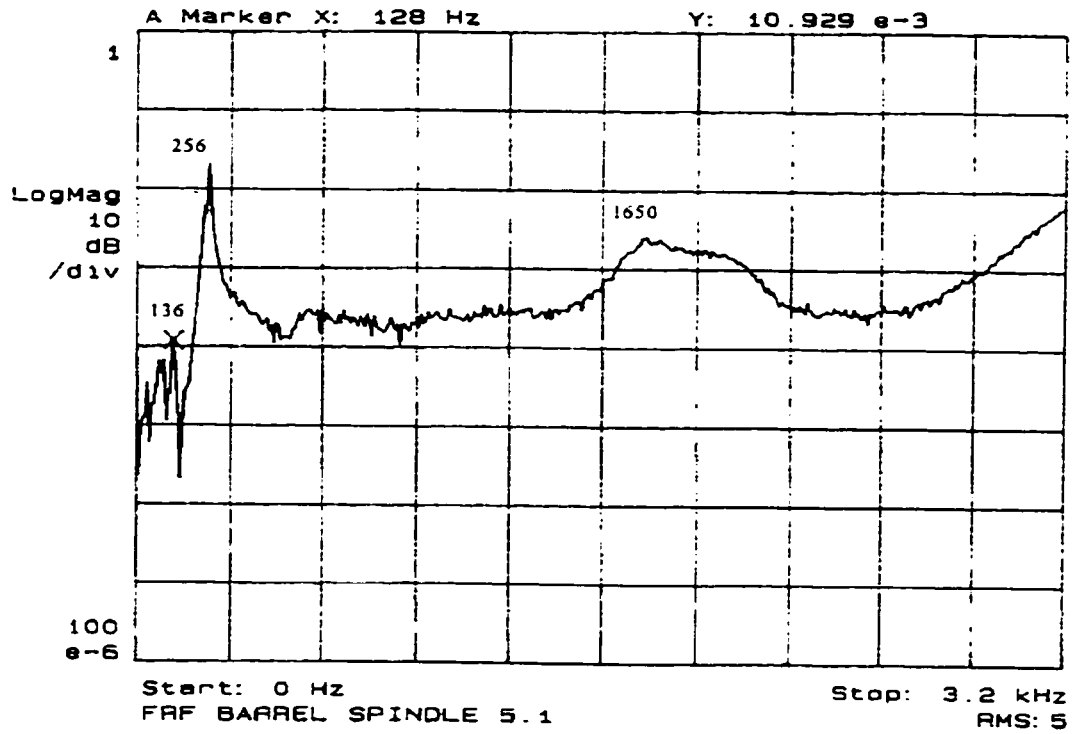

Figure A5.1 Frequency Response of the Barrel Spindle Location 1

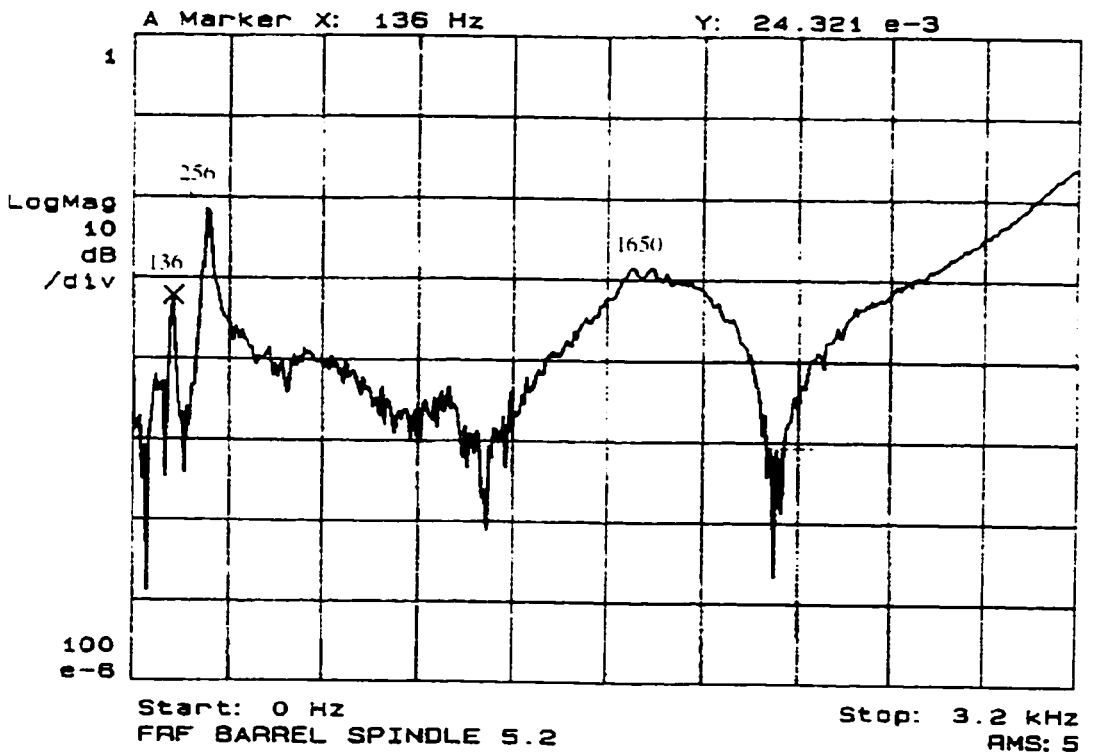

Figure A5.2 Frequency Response of Barrel Spindle Location 2

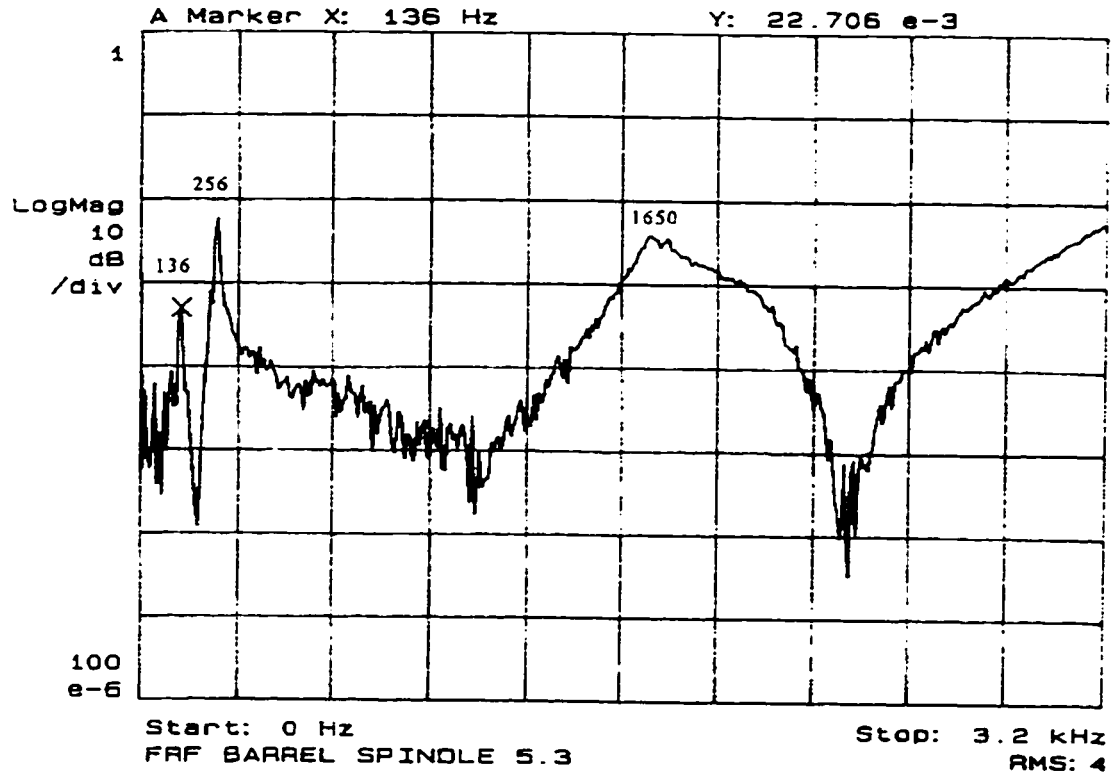

Figure A5.3 Frequency Response of Barrel Spindle Location 3

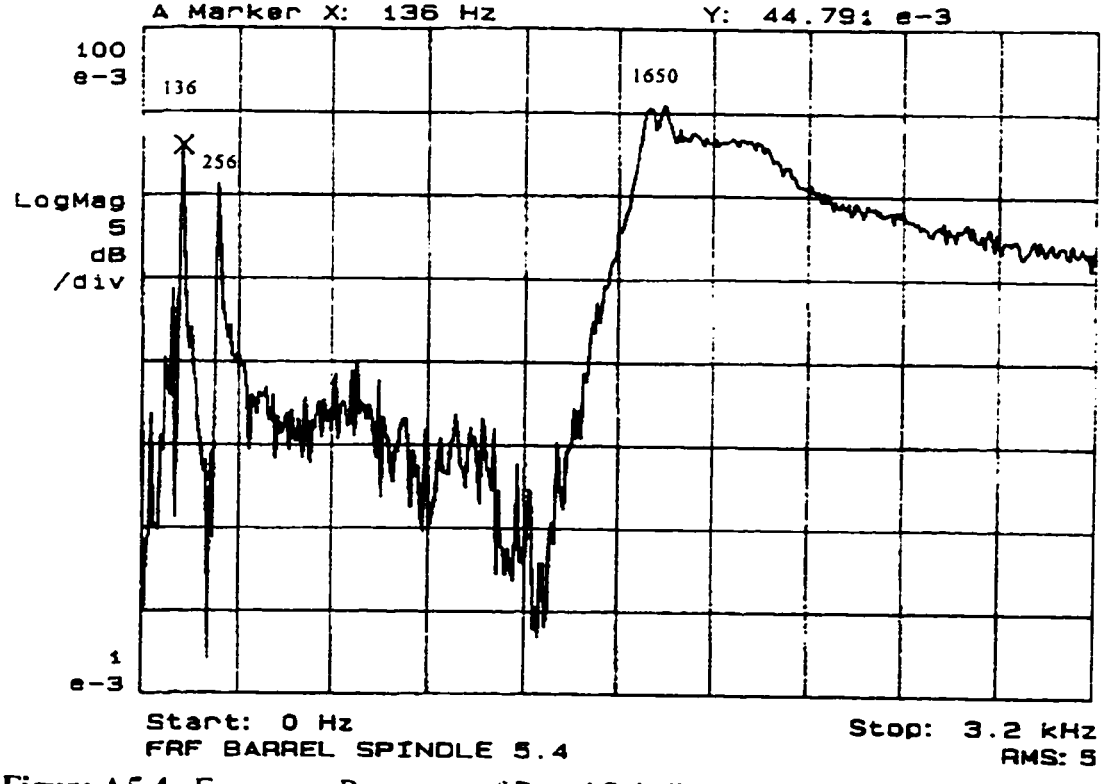

Figure A5.4 Frequency Response of Barrel Spindle Location 4

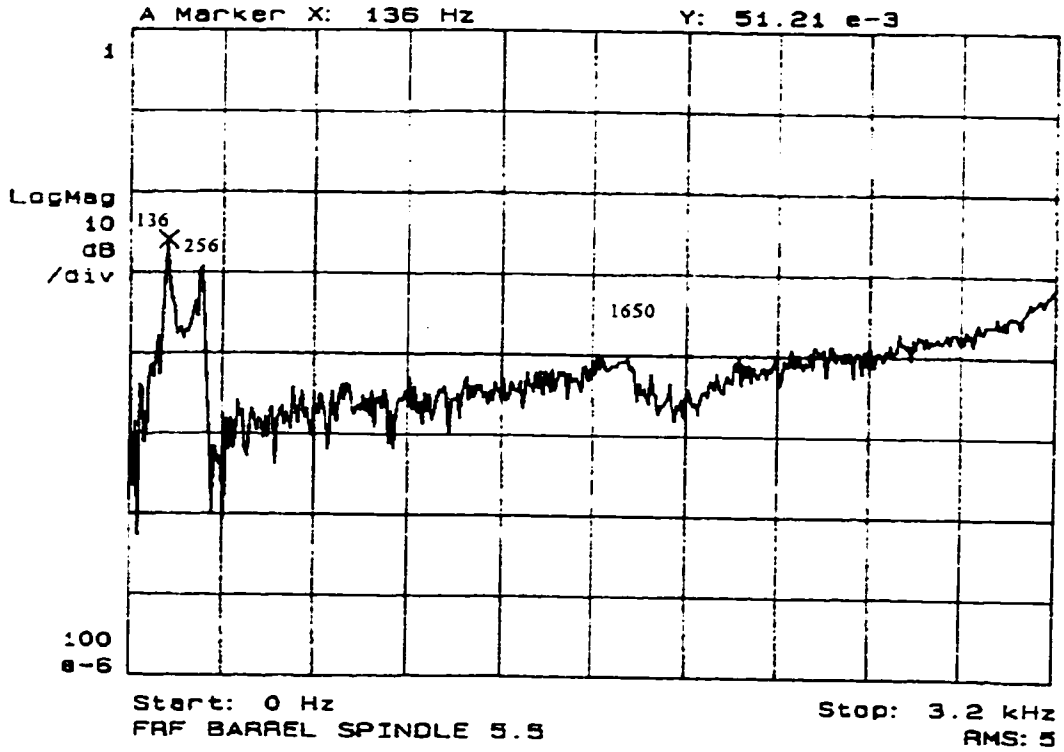

Figure A5.5 Frequency Response of Barrel Spindle Location 5

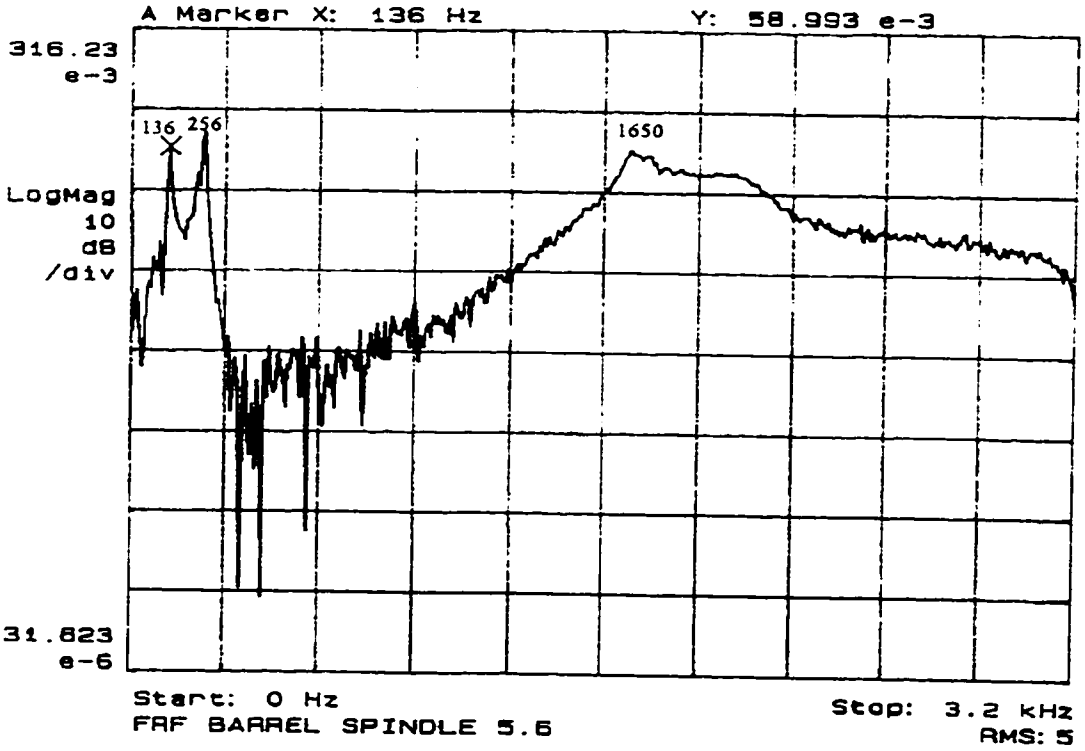

Figure A5.6 Frequency Response of Barrel Spindle Location 6

Table A1 Coherence Accuracy for Motor Spindle				
Figure	116 Hz	190 Hz	1016 Hz	2016 Hz
A1.1	98.6	99.5	99.2	99.45
A1.2	83.2	90.3	94.1	93.4
A1.3	100.0	100.0	100.0	100.0
A1.4	54.3	79.2	96.8	97.4
A1.5	90.0	93.2	95.6	97.0
A1.6	97.4	96.7	98.7	97.4
A1.7	65.1	72.8		97.1
A1.8	59.2	73.2	97.3	98.0
A1.9	85.5	89.9	94.8	96.5
A1.10	92.1	94.5	97.8	98.5
Average	82.54	88.93	97.14	97.48

Table A2 Coherence Accuracy for Grinder Spindle				
Figure	40 Hz	176 Hz	216 Hz	2032 Hz
A2.1	47.0	64.9	85.4	98.8
A2.2	89.5	63.1	87.0	98.2
A2.3	84.9	88.2	91.6	99.3
A2.4	82.3	84.3	86.1	98.5
A2.5	62.5	76.7	75.5	99.6
A2.6	70.1	79.1	78.4	94.3
A2.7	79.0	92.2	94.3	99.3
A2.8		66.8	78.1	96.7
A2.9		98.1	98.0	94.4
A2.10		79.0	84.3	98.6
Average	73.61	79.24	85.87	97.77

Table A3 Coherence Accuracy for Machine Spindle Housing				
Figure	160 Hz	336 Hz	1216 Hz	1640 Hz
A3.1	66.6	88.1	95.5	95.9
A3.2	64.6	67.1	97.1	96.8
A3.3	43.6	68.4	96.4	97.4
A3.4	94.6	85.4	95.6	100.0
A3.5	89.2	86.5	92.6	97.1
A3.6	75.7	93.7	98.2	96.3
A3.7		92.1	95.3	95.3
A3.8	80.8	85.2		90.9
A3.9				91.9
A3.10	55.2	56.7	79.4	88.1
A3.11	93.0	95.0	95.9	98.9
Average	73.70	81.82	94.00	95.33

Table A4 Coherence Accuracy for Motor Spindle Housing			
Figure	272 Hz	440 Hz	1280 Hz
A4.1	97.2	95.4	89.4
A4.2	97.2	97.3	98.8
A4.3	79.3	75.6	95.4
Average	91.23	89.43	94.53

Table A5 Coherence Accuracy for Barrel Spindle			
Figure	**136 Hz**	**256 Hz**	**1650 Hz**
A5.1	76.8	98.2	98.0
A5.2	97.6	97.5	97.0
A5.3	93.5	99.0	99.0
A5.4	95.6	97.3	99.0
A5.5	96.7	97.3	89.0
A5.6	98.3	99.3	99.6
Average	**73.61**	**79.24**	**85.87**

Table A6 Impact Testing Setup

Window	3200 Hz
Interval	± 8 Hz

Channel One Setup

Y-Axis	LogMag [dB]
X-Axis	Frequency Response [Hz]

* Only this setup was used to graph the F.R.F. plots

Channel Two Setup

Y-Axis	Real [0 to 1]
X-Axis	Coherence Accuracy [Hz]

* Coherence values were calculated on these plots

External Trigger

Averages	5 : RMS Max

* Some test locations were less than 5 impacts due to poor results

APPENDIX B

Spindle Balancing Data

Balancing Data Sheet

Balancing Speed	420 rpm	**7 Hz**
Gain	10 X	
Radius of Mass	2.75 inch	
Accelerometer K_a	1 g / 152.6 mV	

* All magnitudes are in the unit of g's
** All phase angles are in degrees

Trial No Mass	**Plane A**		**Plane B**	
	Magnitude	**Phase**	**Magnitude**	**Phase**
	0.622	38.6	0.538	26.4

Trial Masses Added to **Plane A**	5 masses at 205.2 grams at 0 degrees			
	Plane A		**Plane B**	
	Magnitude	**Phase**	**Magnitude**	**Phase**
	0.202	95.9	0.192	111.4

Trial Masses Added to **Plane B**	6 masses at 249.2 grams at 0 degrees			
	Plane A		**Plane B**	
	Magnitude	**Phase**	**Magnitude**	**Phase**
	0.148	218.25	0.186	263.5

Correction Mass and Phase 2 plane with phase		
	Plane A	332.3 grams at 275 degrees
	Plane B	415.3 grams at 19 degrees

Table B1.1 Balancing Data for Barrel Holes Only Condition

Balancing Data Sheet

Balancing Speed	488 rpm	**8.133 Hz**
Gain	10 X	
Radius of Mass	2.75 inch	
Accelerometer K_a	1 g / 152.6 mV	

* All magnitudes are in the unit of g's
** All phase angles are in degrees

Trial No Mass	**Plane A**		**Plane B**	
	Magnitude	**Phase**	**Magnitude**	**Phase**
	1.02	27.8	1.058	235

Trial Masses Added to **Plane A**	5 masses at 205.2 grams at 0 degrees			
	Plane A		**Plane B**	
	Magnitude	**Phase**	**Magnitude**	**Phase**
	0.995	254	0.978	1.74

Trial Masses Added to **Plane B**	6 masses at 249.2 grams at 0 degrees			
	Plane A		**Plane B**	
	Magnitude	**Phase**	**Magnitude**	**Phase**
	0.920	250	0.888	348

Correction Mass and Phase 2 plane with phase		
	Plane A	961.2 grams at 136.8 degrees
	Plane B	970.8 grams at 325.4 degrees

Table B1.2 Balancing Data for Barrel Holes Only Condition

Balancing Data Sheet

Balancing Speed	488 rpm	**8.133 Hz**
Gain	10 X	
Radius of Mass	2.75 inch	
Accelerometer K_a	1 g / 152.6 mV	

* All magnitudes are in the unit of g's
** All phase angles are in degrees

Trial No Mass	**Plane A**		**Plane B**	
	Magnitude	**Phase**	**Magnitude**	**Phase**
	1.001	63.15	0.980	213

Trial Masses Added to **Plane A**	5 masses at 205.2 grams at 0 degrees			
	Plane A		**Plane B**	
	Magnitude	**Phase**	**Magnitude**	**Phase**
	1.027	89.8	1.024	155.8

Trial Masses Added to **Plane B**	6 masses at 249.2 grams at 0 degrees			
	Plane A		**Plane B**	
	Magnitude	**Phase**	**Magnitude**	**Phase**
	1.016	210	1.009	140.2

Correction Mass and Phase 2 plane with phase		
	Plane A	188.1 grams at 323.0 degrees
	Plane B	135.3 grams at 91.0 degrees

Table B1.3 Balancing Data for Barrel Holes Only Condition

Balancing Data Sheet

Balancing Speed	420 rpm	**7 Hz**
Gain	10 X	
Radius of Mass	3.625 inch	
Accelerometer K_a	1 g / 152.6 mV	

* All magnitudes are in the unit of g's
** All phase angles are in degrees

Trial No Mass	**Plane A**		**Plane B**	
	Magnitude	**Phase**	**Magnitude**	**Phase**
	0.606	224.9	0.655	223.7
Trial Masses Added to **Plane A**	152.8 grams at 90 degrees			
	Plane A		**Plane B**	
	Magnitude	**Phase**	**Magnitude**	**Phase**
	0.318	217	0.316	194.8
Trial Masses Added to **Plane B**	152.8 grams at 270 degrees			
	Plane A		**Plane B**	
	Magnitude	**Phase**	**Magnitude**	**Phase**
	0.319	222.3	0.542	234
Correction Mass and Phase 2 plane with phase	Plane A	206 grams at 73 degrees		
	Plane B	117 grams at 282 degrees		

Table B1.4 Balancing Data for Barrel Holes Only Condition

Balancing Data Sheet

Balancing Speed	420 rpm	**7 Hz**
Gain	10 X	
Radius of Mass	2.75 inch	
Accelerometer K_a	1 g / 152.6 mV	

* All magnitudes are in the unit of g's
** All phase angles are in degrees

Trial No Mass

Plane A		**Plane B**	
Magnitude	**Phase**	**Magnitude**	**Phase**
0.269	134.8	0.381	143
0.273	130.6	0.427	149
0.227	139.8	0.438	141
0.329	133.3	0.364	145
0.280	155.9	0.393	143

Trial Masses Added to **Plane A**: 205.2 grams at 0 degrees

Plane A		**Plane B**	
Magnitude	**Phase**	**Magnitude**	**Phase**
0.376	148.5	0.318	148.9
0.318	143.3	0.297	136.3
0.231	138.1	0.413	147.1
0.304	149.7	0.409	143.5
0.265	153.7	0.385	148.7

Trial Masses Added to **Plane B**: 249.2 grams at 0 degrees

Plane A		**Plane B**	
Magnitude	**Phase**	**Magnitude**	**Phase**
0.163	102.9	0.106	141
0.212	141.9	0.208	153.3
0.202	120.7	0.202	128.7
0.159	118.8	0.182	127.4
0.136	134.8	0.168	128.3

Table B2.1 Balancing Data for Grinder Disengaged Condition

Balancing Data Sheet

Balancing Speed	420 rpm	**7 Hz**
Gain	10 X	
Radius of Mass	2.75 inch	
Accelerometer K_a	1 g / 152.6 mV	

* All magnitudes are in the unit of g's
** All phase angles are in degrees

Trial No Mass

Plane A		**Plane B**	
Magnitude	**Phase**	**Magnitude**	**Phase**
0.248	158.0	0.259	144.0
0.233	123.0	0.248	167.0
0.286	143.5	0.258	137.8
0.277	156.0	0.241	140.8
0.296	122.3	0.296	136.3

Trial Masses Added to **Plane A**: 205.2 grams at 0 degrees

Plane A		**Plane B**	
Magnitude	**Phase**	**Magnitude**	**Phase**
0.290	141.0	0.284	156.9
0.261	159.0	0.251	137.1
0.268	137.4	0.288	150.7
0.261	168.8	0.291	130.4
0.297	150.4	0.253	128.3

Trial Masses Added to **Plane B**: 249.2 grams at 0 degrees

Plane A		**Plane B**	
Magnitude	**Phase**	**Magnitude**	**Phase**
0.272	163.7	0.266	157.7
0.309	151.4	0.228	228.2
0.258	191.5	0.206	194.0
0.274	168.6	0.248	216.5
0.309	141.5	0.269	201.9

Table B2.2 Balancing Data for Grinder Disengaged Condition

Balancing Data Sheet

Balancing Speed	420 rpm	**7 Hz**
Gain	10 X	
Radius of Mass	2.75 inch	
Accelerometer K_a	1 g / 152.6 mV	

* All magnitudes are in the unit of g's
** All phase angles are in degrees

Trial No Mass	**Plane A**		**Plane B**	
	Magnitude	**Phase**	**Magnitude**	**Phase**
	0.268	140.7	0.254	145.2

Trial Masses Added to **Plane A**	5 masses at 205.2 grams at 0 degrees			
	Plane A		**Plane B**	
	Magnitude	**Phase**	**Magnitude**	**Phase**
	0.275	151.3	0.273	140.7

Trial Masses Added to **Plane B**	6 masses at 249.2 grams at 0 degrees			
	Plane A		**Plane B**	
	Magnitude	**Phase**	**Magnitude**	**Phase**
	0.280	163	0.242	198.0

Correction Mass and Phase 2 plane with phase		
	Plane A	498.4 grams at 106 degrees
	Plane B	319 grams at 73.2 degrees

Table B2.3 Balancing Data for Grinder Disengaged Condition

Balancing Data Sheet

Balancing Speed	558 rpm	**9.3 Hz**
Gain	10 X	
Radius of Mass	3.625 inch	
Accelerometer K_a	1 g / 152.6 mV	

* All magnitudes are in the unit of g's
** All phase angles are in degrees

Trial No Mass	**Plane A**		**Plane B**	
	Magnitude	**Phase**	**Magnitude**	**Phase**
	0.331	256.0	0.347	251.0
Trial Masses Added to **Plane A**	825 grams at 180 degrees			
	Plane A		**Plane B**	
	Magnitude	**Phase**	**Magnitude**	**Phase**
	0.187	208.6	0.146	79.1
Trial Masses Added to **Plane B**	825 grams at 180 degrees			
	Plane A		**Plane B**	
	Magnitude	**Phase**	**Magnitude**	**Phase**
	0.162	161.4	0.152	50.0
Both Collar Masses Added to Planes A and B	**Plane A**		**Plane B**	
	Magnitude	**Phase**	**Magnitude**	**Phase**
	0.164	180	0.144	295.0

Table B3.1 Balancing Data Before the Addition of the Collar Mass - Grinder Engaged

Balancing Data Sheet

Balancing Speed	558 rpm	**9.3 Hz**
Gain	10 X	
Radius of Mass	3.625 inch	
Accelerometer K_a	1 g / 152.6 mV	

* All magnitudes are in the unit of g's
** All phase angles are in degrees

Trial No Mass	**Plane A**		**Plane B**	
	Magnitude	**Phase**	**Magnitude**	**Phase**
	0.145	203.0	0.178	168.7
Trial Masses Added to **Plane A**	194 grams at 65 degrees			
	Plane A		**Plane B**	
	Magnitude	**Phase**	**Magnitude**	**Phase**
	0.351	246.0	0.229	126.0
Trial Masses Added to **Plane B**	194 grams at 295 degrees			
	Plane A		**Plane B**	
	Magnitude	**Phase**	**Magnitude**	**Phase**
	0.714	224.0	0.806	219.0
Correction Mass and Phase 2 plane with phase	Plane A	44.6 grams at 257 degrees		
	Plane B	48.2 grams at 65 degrees		

Phase from 2 Plane system is good but mass will not improve conditions.

Table B3.2 Balancing Data After the Addition of the Collar Mass - Grinder Engaged

Balancing Data Sheet

Balancing Speed	420 rpm	**7 Hz**
Gain	10 X	
Radius of Mass	3.625 inch	
Accelerometer K_a	1 g / 152.6 mV	
Trial Mass	**112 grams**	

* All magnitudes are in the unit of g's
** All phase angles are in degrees

Trial No Mass	**Plane A Magnitude**	**Plane B Magnitude**
	0.183	0.178
80 degrees at Plane A	0.402	0.213
0 degrees at Plane A	0.390	0.176
280 degrees at Plane A	0.406	0.193
80 degrees at Plane B	0.239	0.143
0 degrees at Plane B	0.488	0.241
280 degrees at Plane B	0.518	0.341

Trial 1 Corrections	Plane A	78.5 grams at 295 degrees
	Plane B	117.7 grams at 110 degrees
Trial 2 Corrections	Plane A	106 grams at 233 degrees
	Plane B	76 grams at 75 degrees
Actual Placement	Plane A	75 grams at 250 degrees
	Plane B	225 grams at 80 degrees
Results	Plane A	0.159 g
2 plane without phase	Plane B	0.153 g

Table B4.1 Balancing Data for Final Balance Mass Conditions

Balancing Data Sheet

Balancing Speed	420 rpm	**7 Hz**
Gain	10 X	
Radius of Mass	3.625 inch	
Accelerometer K_a	1 g / 152.6 mV	
Trial Mass	**112 grams**	

* All magnitudes are in the unit of g's
** All phase angles are in degrees

Trial No Mass	**Plane A Magnitude**	**Plane B Magnitude**
	0.159	0.153

Trial 1 Corrections	Plane A	Add 225 grams at 80 degrees Add 70 grams at 250 degrees
	Plane B	Add 140 grams at 80 degrees
	Plane A to Plane B	Add 270 grams at 80 degrees
Total Placements	Plane A	70 grams at 250 degrees 225 grams at 80 degrees 825 grams at 180 degrees (4 masses total)
	Plane B	140 grams at 80 degrees 825 grams at 180 degrees (4 masses total)
	Plane A to Plane B	270 grams at 80 degrees (machined bar)

Final Vibration Results	**Plane A**	**0.133 g**
	Plane B	**0.105 g**

These values are balanced to the noise floor (about 0.130 g) and are the minimal vibration amplitudes possible for the given conditions.

Table B4.2 Balancing Data for Final Balance Mass Corrections

```
// balandoc.cpp : implementation of the CBalanceDoc class//
#include "stdafx.h"
#include "balance.h"
#include "speed.h"
#include "mdata.h"
#include "trialmas.h"
#include "linear.h"
#include "nrutilw.h"
#include "balandoc.h"
#include "balanvw.h"
#include <math.h>
#ifdef _DEBUG
#undef THIS_FILE
static char BASED_CODE THIS_FILE[] = __FILE__;
#endif
// CBalanceDoc
IMPLEMENT_DYNCREATE(CBalanceDoc, CDocument)
BEGIN_MESSAGE_MAP(CBalanceDoc, CDocument)
        //{{AFX_MSG_MAP(CBalanceDoc)
        ON_COMMAND(ID_BALANCE_SPEED, OnBalanceSpeed)
        ON_COMMAND(ID_DATA, OnMData)
        ON_COMMAND(ID_MASS, OnMass)
        ON_COMMAND(ID_RUN, OnRun)
        ON_UPDATE_COMMAND_UI(ID_RUN, OnUpdateRun)
        //}}AFX_MSG_MAP
END_MESSAGE_MAP()
// CBalanceDoc construction/destruction
/***************************/
CBalanceDoc::CBalanceDoc()
/***************************/
{
        // TODO: add one-time construction code here
        m_textLine  = 50;
        m_massYes   = 0;
        m_MdataYes  = 0;
        m_speedYes  = 0;
        // input data
        m_speedUnit  = 0;
        m_omega     = 0.f;
```

```
        // analyzer data
        m_a01    = 0.f;
        m_a02    = 0.f;
        m_a11    = 0.f;
        m_a12    = 0.f;
        m_a21    = 0.f;
        m_a22    = 0.f;
        m_ang01  = 0.f;
        m_ang02  = 0.f;
        m_ang11  = 0.f;
        m_ang12  = 0.f;
        m_ang21  = 0.f;
        m_ang22  = 0.f;
        m_T1     = 0.f;
        m_T2     = 0.f;
        // trial mass data
        m_angle1  = 0.f;
        m_angle2  = 0.f;
        m_units   = 0;
        m_mass1   = 0.f;
        m_mass2   = 0.f;
        m_radii1  = 0.f;
        m_radii2  = 0.f;
        m_accel   = 1.f;

        m_a = NULL;
        int m_NoPrint = 1;
}
CBalanceDoc::~CBalanceDoc()
{
        if( m_a != NULL )
                free_matrix(m_a, 1, 4, 1, 4 );
}
/*************************************************************/
void CBalanceDoc::ErrorMessage(CString caption, CString message )
/*************************************************************/
{
        ::MessageBeep( MB_ICONEXCLAMATION );
        ::MessageBox( NULL, message, caption,
            MB_OK | MB_SYSTEMMODAL | MB_ICONEXCLAMATION );
}
BOOL CBalanceDoc::OnNewDocument()
{
```

```
        if (!CDocument::OnNewDocument())
                return FALSE;
        // TODO: add reinitialization code here
        // (SDI documents will reuse this document)
        return TRUE;
}
// CBalanceDoc serialization
void CBalanceDoc::Serialize(CArchive& ar)
{
        WORD a;
        if (ar.IsStoring())
        {
                a = (WORD) m_speedUnit;
                ar << a << m_omega;
                ar << m_a01 << m_ang01 << m_a02 << m_ang02;
                ar << m_a11 << m_ang11 << m_a12 << m_ang12;
                ar << m_a21 << m_ang21 << m_a22 << m_ang22;
                a = (WORD)m_units;
                ar << a << m_accel;
                ar << m_mass1 << m_angle1 << m_radii1;
                ar << m_mass2 << m_angle2 << m_radii2;
        }
        else
        {
                a = (WORD)m_speedUnit;
                ar >> a >> m_omega;
                ar >> m_a01 >> m_ang01 >> m_a02 >> m_ang02;
                ar >> m_a11 >> m_ang11 >> m_a12 >> m_ang12;
                ar >> m_a21 >> m_ang21 >> m_a22 >> m_ang22;
                a = (WORD)m_units;
                ar >> a >> m_accel;
                ar >> m_mass1 >> m_angle1 >> m_radii1;
                ar >> m_mass2 >> m_angle2 >> m_radii2;
                m_massYes  = 1;
                m_MdataYes = 1;
                m_speedYes = 1;
        }
}
/////////////////////////////////////////////////////////////////////////////
// CBalanceDoc diagnostics
#ifdef _DEBUG
void CBalanceDoc::AssertValid() const
{
```

```
        CDocument::AssertValid();
}
void CBalanceDoc::Dump(CDumpContext& dc) const
{
        CDocument::Dump(dc);
}
#endif //_DEBUG
////////////////////////////////////////////////////////////////////////////
// CBalanceDoc commands
/*********************************/
void CBalanceDoc::OnBalanceSpeed()
/*********************************/
{
        CSpeed dlg;
        dlg.m_speedUnits = m_speedUnit;
        dlg.m_speed      = m_omega;
        if( dlg.DoModal() != IDOK )
                return ;
        m_speedUnit = dlg.m_speedUnits;
        if( m_speedUnit ) // rpm -> convert to radinas / sec
        {
                m_omega = (float)(2.f*PI * dlg.m_speed / 60.f);
        }
        else
                m_omega = dlg.m_speed;
        if( m_omega <= 0.f )
        {
                ErrorMessage("Speed", "The Balancing speed is invalid");
                return;
        }
        m_speedYes = 1;
}
/*********************************/
void CBalanceDoc::OnMData()
/*********************************/
{
  CMData dlg;
  dlg.m_a01    = m_a01;
       dlg.m_a02    = m_a02;
       dlg.m_a11    = m_a11;
       dlg.m_a12    = m_a12;
       dlg.m_a21    = m_a21;
       dlg.m_a22    = m_a22;
```

```
        dlg.m_ang01   = m_ang01;
        dlg.m_ang02   = m_ang02;
        dlg.m_ang11   = m_ang11;
        dlg.m_ang12   = m_ang12;
        dlg.m_ang21   = m_ang21;
        dlg.m_ang22   = m_ang22;
        if( dlg.DoModal() != IDOK )
                return ;
        m_a01    = dlg.m_a01;
        m_a02    = dlg.m_a02;
        m_a11    = dlg.m_a11;
        m_a12    = dlg.m_a12;
        m_a21    = dlg.m_a21;
        m_a22    = dlg.m_a22;
        m_ang01   = dlg.m_ang01;
        m_ang02   = dlg.m_ang02;
        m_ang11   = dlg.m_ang11;
        m_ang12   = dlg.m_ang12;
        m_ang21   = dlg.m_ang21;
        m_ang22   = dlg.m_ang22;
        m_MdataYes = 1;
}
/**********************************/
void CBalanceDoc::OnMass()
/**********************************/
{
        CTrialMass dlg;
        dlg.m_angle1   = m_angle1;
        dlg.m_angle2   = m_angle2;
        dlg.m_units    = m_units;
        dlg.m_mass1    = m_mass1;
        dlg.m_mass2    = m_mass2;
        dlg.m_radii1   = m_radii1;
        dlg.m_radii2   = m_radii2;
        dlg.m_accel    = m_accel;
        if( dlg.DoModal() != IDOK )
                return ;
        if( dlg.m_units )
        {
                if( dlg.m_accel <= 0.0f )
                {
                        ErrorMessage("Trial Mass Data", "Invalid Acceleration Input.");
                        return;
```

```
                }
                else
                        m_accel = dlg.m_accel;
        }
        else
        m_accel = 1.f;
        m_angle1   = dlg.m_angle1;
        m_angle2   = dlg.m_angle2;
        m_units    = dlg.m_units;
        m_mass1    = dlg.m_mass1;
        m_mass2    = dlg.m_mass2;
        m_radii1   = dlg.m_radii1;
        m_radii2   = dlg.m_radii2;
        m_massYes = 1;
}
/*********************************/
void CBalanceDoc::OnRun()
/*********************************/
{
        if( !Calculate() )
        {
                m_NoPrint = 1;
                return;
        }

        m_NoPrint = 0;
        POSITION pos = GetFirstViewPosition();
        while( pos != NULL )
        {
                CView* pView = GetNextView(pos);
                if( pView->IsKindOf(RUNTIME_CLASS(CBalanceView)))
                {
                        pView->Invalidate();
                        break;
                }
        }
}

/*********************************************/
void CBalanceDoc::OnUpdateRun(CCmdUI* pCmdUI)
/*********************************************/
{
        if( !m_massYes || !m_MdataYes || !m_speedYes )
```

```
        {
                pCmdUI->Enable(FALSE);
        }
        else
                pCmdUI->Enable(TRUE);
}
/****************************/
int CBalanceDoc::Calculate()
/****************************/
{
   int i, j;
        float omega2, xita1, xita2, ang01, ang02, ang11, ang12, ang21, ang22;
        float a11r, a11i,a21r, a21i, a12r, a12i, a22r, a22i, sum;
        m_a = matrix(1,4,1,4);
        if( m_a == NULL )
        {
                ErrorMessage("Memory", "Insufficient memory.");
                return 0;
        }
        omega2 = m_omega*m_omega;
        xita1 = DegToRad(m_angle1);
        xita2 = DegToRad(m_angle2);
        ang01 = DegToRad(m_ang01);
        ang02 = DegToRad(m_ang02);
        ang11 = DegToRad(m_ang11);
        ang12 = DegToRad(m_ang12);
        ang21 = DegToRad(m_ang21);
        ang22 = DegToRad(m_ang22);
        m_T1 = (m_mass1*m_radii1*omega2)/m_accel;
        m_T2 = (m_mass2*m_radii2*omega2)/m_accel;
        // computation of influance coefficients
        a11r = m_a11/m_T1*(float)cos(ang11-xita1) - m_a01/m_T1*(float)cos(ang01 - xita1 );
        a11i = m_a11/m_T1*(float)sin(ang11-xita1) - m_a01/m_T1*(float)sin(ang01 - xita1 );
        a21r = m_a12/m_T1*(float)cos(ang12-xita1) - m_a02/m_T1*(float)cos(ang02 - xita1 );
        a21i = m_a12/m_T1*(float)sin(ang12-xita1) - m_a02/m_T1*(float)sin(ang02 - xita1 );
        a12r = m_a21/m_T2*(float)cos(ang21-xita2) - m_a01/m_T2*(float)cos(ang01 - xita2 );
        a12i = m_a21/m_T2*(float)sin(ang21-xita2) - m_a01/m_T2*(float)sin(ang01 - xita2 );
        a22r = m_a22/m_T2*(float)cos(ang22-xita2) - m_a02/m_T2*(float)cos(ang02 - xita2 );
        a22i = m_a22/m_T2*(float)sin(ang22-xita2) - m_a02/m_T2*(float)sin(ang02 - xita2 );
        // form the influance coefficinet matrix
        m_a[1][1] = a11r;  m_a[1][2] = -a11i;  m_a[1][3] = a12r;  m_a[1][4] = -a12i;
        m_a[2][1] = a11i;  m_a[2][2] =  a11r;  m_a[2][3] = a12i;  m_a[2][4] =  a12r;
        m_a[3][1] = a21r;  m_a[3][2] = -a21i;  m_a[3][3] = a22r;  m_a[3][4] = -a22i;
```

```
        m_a[4][1] = a21i;  m_a[4][2] =  a21r;  m_a[4][3] = a22i;  m_a[4][4] =  a22r;
        if( !Inverse(m_a, 4) )
        {
                ErrorMessage("Error"," The Influence Coefficient Matrix is Singular.");
                free_matrix(m_a,1,4,1,4);
                m_a = NULL;
                return 0;
        }
        // express amplitudes of unbalance data as complex numbers ( real, imaginary )
        m_F[1] = m_a01 * (float)cos(ang01);  // real
        m_F[2] = m_a01 * (float)sin(ang01);  // imag
        m_F[3] = m_a02 * (float)cos(ang02);  // real
        m_F[4] = m_a02 * (float)sin(ang02);  // imag
        // find original unbalance vector R
        for( i = 1; i <= 4; i++ )
        {
                sum = 0.0f;
                for( j = 1; j <= 4; j++ )
                {
                        sum = sum + m_a[i][j] * m_F[j];
                }
                m_R[i] = sum;
        }
        m_F1mag = (float)sqrt(m_R[1]*m_R[1] + m_R[2]*m_R[2]);
        m_P1mag = (float)sqrt(m_R[3]*m_R[3] + m_R[4]*m_R[4]);
        m_We1 = m_F1mag*m_accel/(omega2*m_radii1);
        m_We2 = m_P1mag*m_accel/(omega2*m_radii2);
        m_massAngle1 = Angle( m_R[1], m_R[2] );
        m_massAngle2 = Angle( m_R[3], m_R[4] );
/*      cout << endl << "**************** Corrected masses ************************";
        cout << endl << " mass 1 = " << We1 << "   Angle 1 = " << RadToDeg(massAngle1);
        cout << endl << " mass 2 = " << We2 << "   Angle 2 = " << RadToDeg(massAngle2);  */
        free_matrix(m_a,1,4,1,4);
        m_a = NULL;

        return 1;
}
```

Two Plane Balancing Without Phase Response [6]

Qbasic Program 3 Pages

```
10   dim l0(2, 3), v0(2), v(2, 2, 3), x1(2, 2), y1(2, 2), o0(2), o1(2), p0(3), p1(3)
20   dim tl0(2, 3), tv0(2), tv(2, 2, 3)
30   dim num$(3), pln$(2)
40   key off: cls : px = 640: py = 200: bx = px / 2: by = py / 2: dx = 9: dy = 5: screen 2
50   num$(1) = "first ": num$(2) = "second ": num$(3) = "third "
60   pln$(1) = "near ": pln$(2) = "far "
100  input "enter trial mass magnitude ", tm0
110  for I = 1 to 2: for j = 1 to 3
120  print "enter location of " + num$(j) + " mass on " + pln$(i) + " plane ":
130  input "", lll: gosub 1400: lll = lll * .0174532925#
140  tl0(i, j) = lll: next j: next I
150  for j = 1 to 2
160  print " enter vibration mag. On " + pln$(j) + "plane with no trial mass":
170  input "", tv0(j): next j
180  for j = 1 to 2: for I = 1 to 3: for k = 1 to 2
190  print "vibration on " + pln$(k) + " plane with ":
200  print num$(i) + " mass on " + num$(j) + " plane":
210  input "", tv(j, k, i): next k: next i: next j
220  for I = 1 to 2: v0(i) = tv0(i): for j = 1 to 3
230  l0(i, j) = tl0(i, j)
235  for k = 1 to 2: v(k, I, j) = tv(k, I, j): next k: next j: next I
250  m0 = tm0
260  for j = 1 to 2: for I = 1 to 2: scale = 1
270  rem draw circle
380  gosub 890: beep: locate 25, 1, 0
410  print "enter desired scale, enter 0 if satisfied :"
420  input : "", a: if a = 0 then 470
440  scale = a: goto 380
470  locate 25, 1, 0
480  print "place the dot on the intersection and press home.":
490  gosub 1040
500  x = (xp - bx) / mx: y = (yp - by) / my: x1(i, j) = sqr(x ^ 2 + y ^ 2) / m0
510  x = -x: if x = 0 and y = 0 then y1(i, j) = 0
520  if x = 0 and y > 0 then y1(i, j) = 3.14159265#4 / 2
530  if x = 0 and y < 0 then y1(i, j) = -3.14159265#4 / 2
540  if x > 0 then y1(i, j) = atn(y / x)
550  if x < 0 then y1(i, j) = 3.14159265#4 - atn(y / (-x))
570  next i: next j
600  d1 = x1(1, 1) * x1(2, 2)
```

```
610   d2 = y1(1, 1) + y1(2, 2)
620   d3 = x1(1, 2) * x1(2, 1)
630   d4 = y1(1, 2) + y1(2, 1)
640   d5 = d1 * cos(d2) - d3 * cos(d4)
650   d6 = d1 * sin(d2) - d3 * sin(d4)
660   d1 = sqr(d5 ^ 2 + d6 ^ 2)
670   if d5 = 0 and d6 = 0 then d2 = 0
680   if d5 = 0 and d6 > 0 then d2 = 90
690   if d5 = 0 and d6 < 0 then d2 = -90
700   if d5 > 0 then d2 = atn(d6 / d5) * 180 / 3.141592654#
710   if d5 < 0 then d2 = 180 - (atn(d6 / (-d5))) * 180 / 3.141592654#
720   if d2 < 0 then d2 = d2 + 360
730   for k = 1 to 2
740   a = 3 - k
750   n1 = v0(k) * x1(a, a) * cos(y1(a, a)) - v0(a) * x1(k, a) * cos(y1(k, a))
760   n2 = v0(k) * x1(a, a) * sin(y1(a, a)) - v0(a) * x1(k, a) * sin(y1(k, a))
770   n3 = sqr(n1 ^ 2 + n2 ^ 2)
780   if n1 = 0 and n2 = 0 then n4 = 0
790   if n1 = 0 and n2 > 0 then n4 = 90
800   if n1 = 0 and n2 < 0 then n4 = -90
810   if n1 > 0 then n4 = atn(n2 / n1) * 180 / 3.141592654#
820   if n1 < 0 then n4 = 180 - (atn(n2 / (-n1))) * 180 / 3.141592654#
830   if n4 < 0 then n4 = n4 + 360
840   u3 = n3 / d1
850   u4 = n4 - d2 - 180: if u4 < 0 then u4 = u4 + 360
860   print "the " + pln$(k) + "plane correction has mag ", u3, " at angle ", u4, " degrees"
870   next k
880   input "press enter to continue", temp: goto 220
890   rem this rout draws 3 circles
900   b = v(j, I, 1): cls
920   for k0 = 2 to 3
930   if v(j, I, k0) < b then 950
940   b = v(j, I, k0)
950   next k0
960   s5 = v0(i) + b
970   s5 = s5 / scale: mx = .5 * px / s5: ys = dy * s5 / dx: my = .5 * py / ys
980   for k0 = 1 to 3
990   xx = v0(i) * cos(l0(i, k0)): yy = v0(i) * sin(l0(i, k0))
1000  xxp = mx * xx + bx: yyp = my * yy + by
1001  pset (xxp, yyp), 3
1010  circle (xxp, yyp), (v(j, I, k0) * mx)
1020  next k0
1030  return
```

```
1040  rem rems
1100  xp = 0: yp = 0: ttxs = 0: ttys = 0: ttep = 1
1120  gosub 1300
1130  tta$ = inkey$: if tta$ = "" goto 1130
1160  ttm = asc(tta$): if ttm <> 0 goto 1240
1170  ttm = asc(right$(tta$, 1))
1180  if ttm = 72 then ttys = -ttep: goto 1120
1190  if ttm = 75 then ttxs = -ttep: goto 1120
1200  if ttm = 77 then ttxs = ttep: goto 1120
1210  if ttm = 80 then ttys = ttep: goto 1120
1220  if ttm = 71 then return
1230  goto 1120
1240  if tta$ <> "i" and tta$ <> "I" goto 1270
1250  ttep = ttep * 2: if ttep > 100 then beep: ttep = 100
1260  goto 1120
1270  if tta$ <> "d" and tta$ <> "D" goto 1130
1280  ttep = ttep / 2: if ttep < 1 then beep: ttep = 1
1290  goto 1120
1300  rem rems
1330  pset (xp, yp), olddat
1340  xp = xp + ttxs
1350  yp = yp + ttys
1360  olddat = point(xp, yp): if olddat < 0 then olddat = 0
1370  pset (xp, yp), 3
1380  ttxs = 0: ttys = 0: return
1400  rem converts angles
1430  if lll < 0 then lll = lll + 360: goto 1430
1440  if lll > 360 then lll = lll - 360: goto 1440
1450  return
9999  end
```

Table B5.1 Maximum Residual Unbalance for Various Quality Grades [19.32]

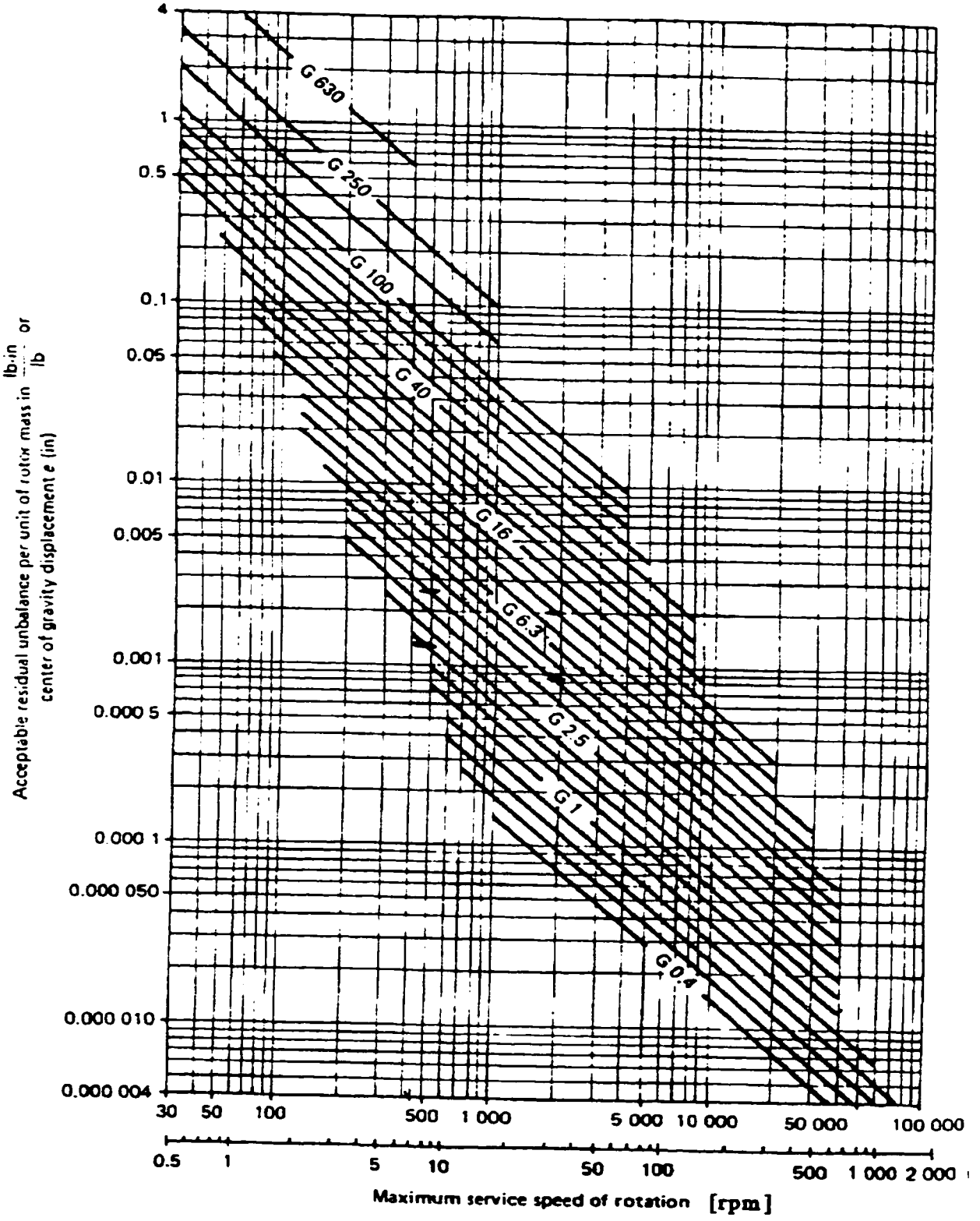

Table B5.2 Rotor Descriptions for Various Quality Grades [32]

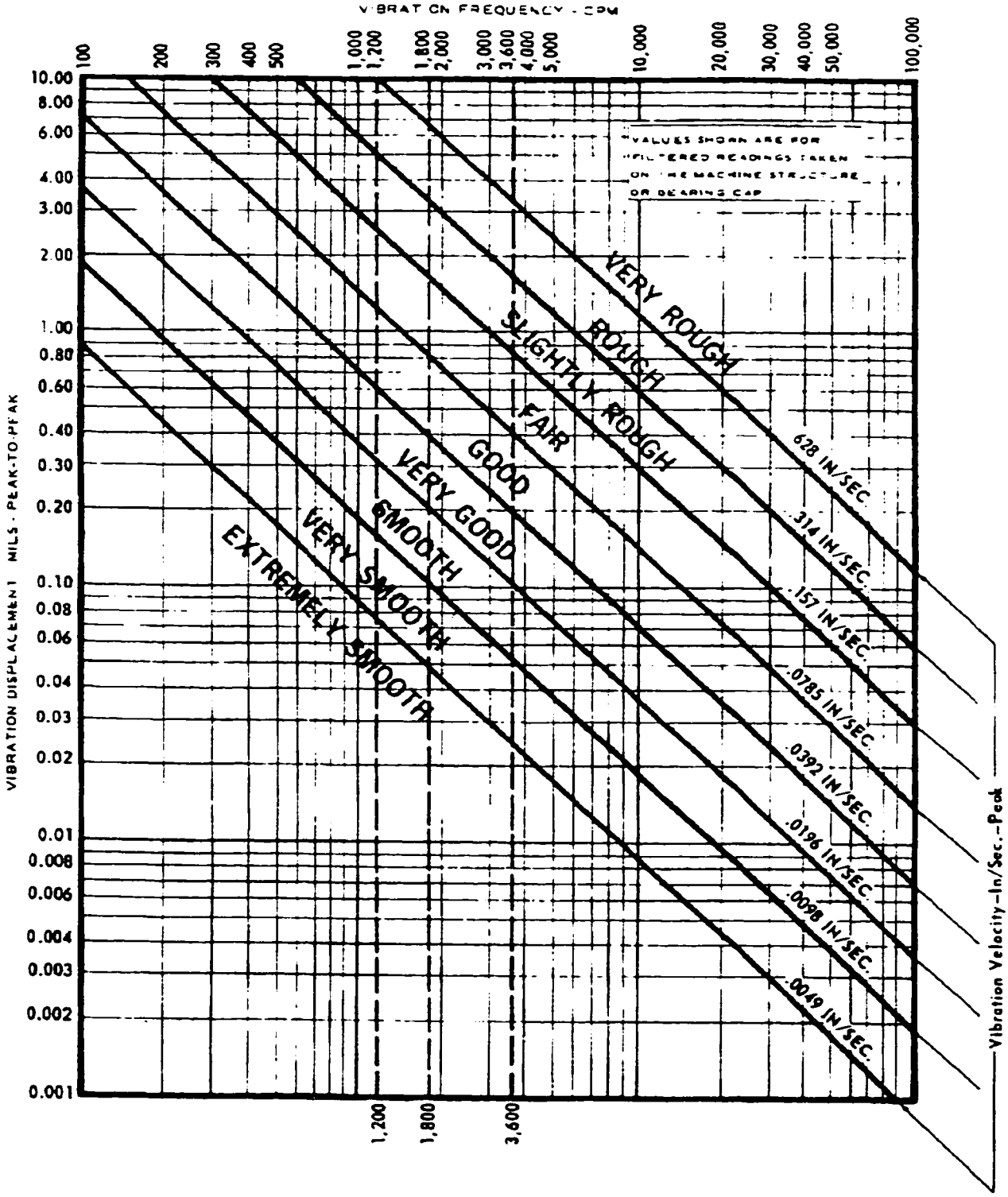

APPENDIX C

Sound Level Experiments

C. SOUND POWER CALCULATION

The analysis was performed in a *semi-reverberant* room with the machine closer to one wall than the other three. The setup was limited by the machine stand location. The machine location is shown in Figure C1.

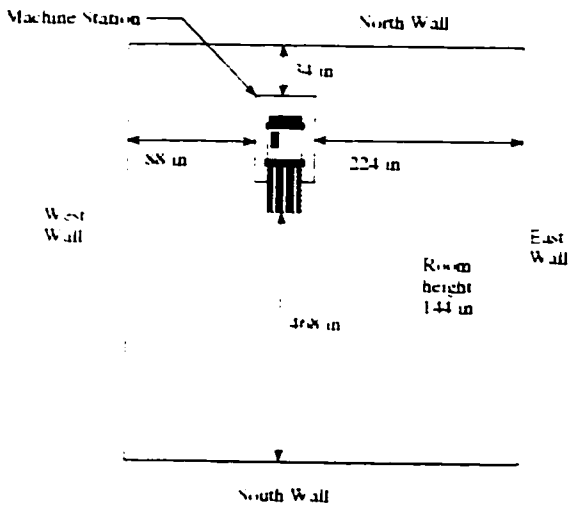

Figure C1 Room Layout

Measurements performed on the machine were recorded as a full spectrum analysis which encompasses all the frequency spectrum. If the measurements were performed over a time range, T, than an average sound pressure level would need to be calculated over the period. At the end of the period, it would have a total acoustic energy, $L_{eq,T}$. This is based on the energy principle and is defined as

$$L_{eq,T} = 10\log_{10}\frac{1}{T}\int\left(\frac{p(t)}{p_o}\right)^2 dt \qquad \text{(C1)}$$

where p_o is the reference sound pressure (20 μPa) and

p(t) is the time varying sound pressure and

T is the total measurement time.

The meter was calibrated to a sound pressure level of 93.6 dB at a frequency of 1000 Hz. The actual instantaneous measurements were setup in *[dBA]* units. This is good for determining noise sensitive to the human ear, but for actual machinery, the meter can be setup using a linear no-weight condition to obtain actual sound pressure levels in [dB].

C1.1 Noise Analysis Procedure

As shown in Figure C1, the room is a semi-reverberant space and the machine is located out of center with respect to the surrounding walls. As per the procedure, an arbitrary distance of 1 meter was selected forming a cube type space surrounding the

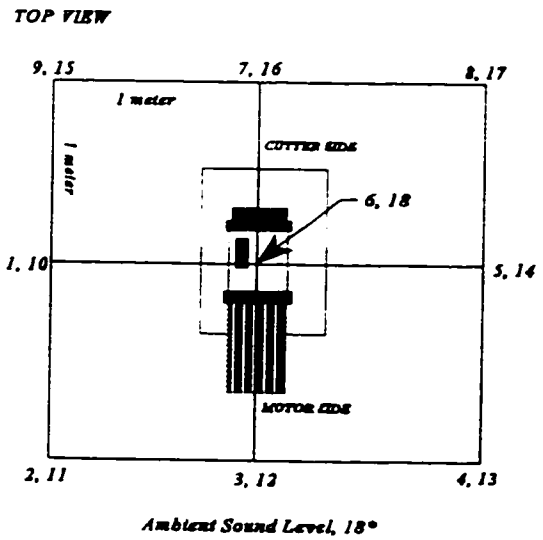

Figure C2 Top View of Experimental Layout Points

machine. This space formed a 3-D cube divided into 18 measuring points. The layout points in Figure C2 were setup such that points 1 to 5 and 7 to 9 are at a height of one meter from the shop floor, points 10 to 17 are at a height of two meters from the shop floor and points 6 and 18 are points one meter above the machine where a regular and ambient sound levels were recorded, respectively.

Instantaneous sound pressure levels were recorded at each of the points shown in Figure C2. These were recorded in *A-weighted* sound pressure levels at a full frequency spectrum. The sound level meter was placed on a stand. Each point was measured from the approximate center of the noise source. Also, an ambient sound level measurement was taken to demonstrate the relative sound level in the internal shop environment room. Table C1 shows the sound level measurements taken with respect to Figure C2.

Table C1 Sound Level Measurements

Point	SPL (dBA)	Point	SPL (dBA)
1	86.8	**10**	86.9
2	84.6	**11**	85.2
3	84.5	**12**	84.0
4	83.5	**13**	84.2
5	85.6	**14**	85.0
6	87.1	**15**	86.9
7	88.7	**16**	89.0
8	87.2	**17**	88.1
9	86.3	**18**	56.7

This chart illustrates the increased sound level as measurements are taken closer to the cutter side. The grinder interface with the face mill contributes to the noise levels significantly, but in this case noise levels are higher with proximity to the north wall.

C1.2 Sound Power Level Calculation

Assuming the experimental data given by Yang [32] and Ellison [5] is a good approximation for determining the sound power level in an ordinary room. Calculations for the machine center studied can be completed by the 17 values in Table C1 for

$$L_p = 10\log_{10}\frac{1}{17}\sum 10^{0.1L_{pi}} \tag{C2}$$

$$L_p = 10\log_{10}\left(\frac{1}{17}\left(10^{8.68}+10^{8.46}+10^{8.45}+10^{8.35}+10^{8.56}+\ldots+10^{8.81}\right)\right) = 86.4\,dBA$$

Neglecting the ground reflections, as suggested in [32] and [5], the sound power level including the effect of other room reflections is

$$L_w = L_p + 10\log_{10}(2\pi r^2) \tag{C3}$$

$$L_w = 86.4 + 10\log_{10}[2\pi(1.0)^2] = 94.4\,dBA$$

According to Yang [32] and Ellison [5], the contribution due to room reflections is approximately 3 dB at a radius of 1 meter and an A-weighted sound pressure level. Therefore the sound power level is **Lw = 94.4 dBA - 3 dBA = 91 dBA**.

C1.3 Noise Study Conclusions

The sound level of the machine was a full spectrum sound level measurement. therefore. all of the frequencies of interest are captured as a *rms* average over the entire spectrum. The average sound level was about 86 dBA. adding the radial and reflections demonstrates a sound power level of about 91 dBA.

A measurement of the noise spectrum was also performed to determine the cause of the unwanted noise. It was found through experimentation that the major contributor to the increased noise levels compare to the gear mesh frequencies of the spur gears. A complete noise analysis for the machine gears is provided in Appendix D.

APPENDIX D

Gear Noise Analysis

D. GEARING ANALYSIS

D1. Introduction

A gear mesh analysis was necessary to determine the specific frequency contribution to the overall noisiness of the machine. A full frequency analysis was performed in Appendix C of this report. However, a specific frequency analysis must be performed to determine what is causing any unwanted noise.

Factors effecting machine operation may include: rotor rub, wear / clearance problems, force or couple unbalance, bent shaft, misalignment (angular, parallel, bearing misaligned on shaft), resonance or mechanical looseness.

Factors effecting gears for the production of unwanted noise and vibration include: tooth wear, high tooth load, gear eccentricity and backlash, gear misalignment, cracked or broken tooth or hunting tooth problems.

Factors effecting motor operation or electrical problems that produce excess noise can include: stator eccentricity, shortened laminations and loose iron, eccentric rotor (variable air gap), general rotor problems around the *rotor bar pass frequency*, phasing problems or loose connector, synchronous motors or loose stator coils and general D.C. motor problems.

All of the above aforementioned problems are outlined in the illustrated vibration diagnostic chart. These charts were found in the Illustrated Vibration Diagnostic Charts [35] and are listed as Tables D2 and D3. The basic frequency plots show the analysis used to detect and cure these common problems if they exist for particular machine rotor, motor or gear system.

D1.1 *Super Finish* Gear System

The machine uses step down, step up gearing with a main planetary gear system. The motor operates at 1800 rpm geared centrally to the two planet gears. The gears orbit 180 degrees opposite with respect to each other and in turn orbit the barrel spindle. The motor is also geared to the step up grinder spindle gears. In all, there are four stages of gears allowing a barrel rotation of 420 rpm and grinder offset of 1 inch to 5823 rpm, both with respect to the motor. The gear system is shown in Figure D1. Each gear stage is represented by a number of lines through the mesh corresponding to the stage. A full set of gear stages and drawings are included in this Appendix D.

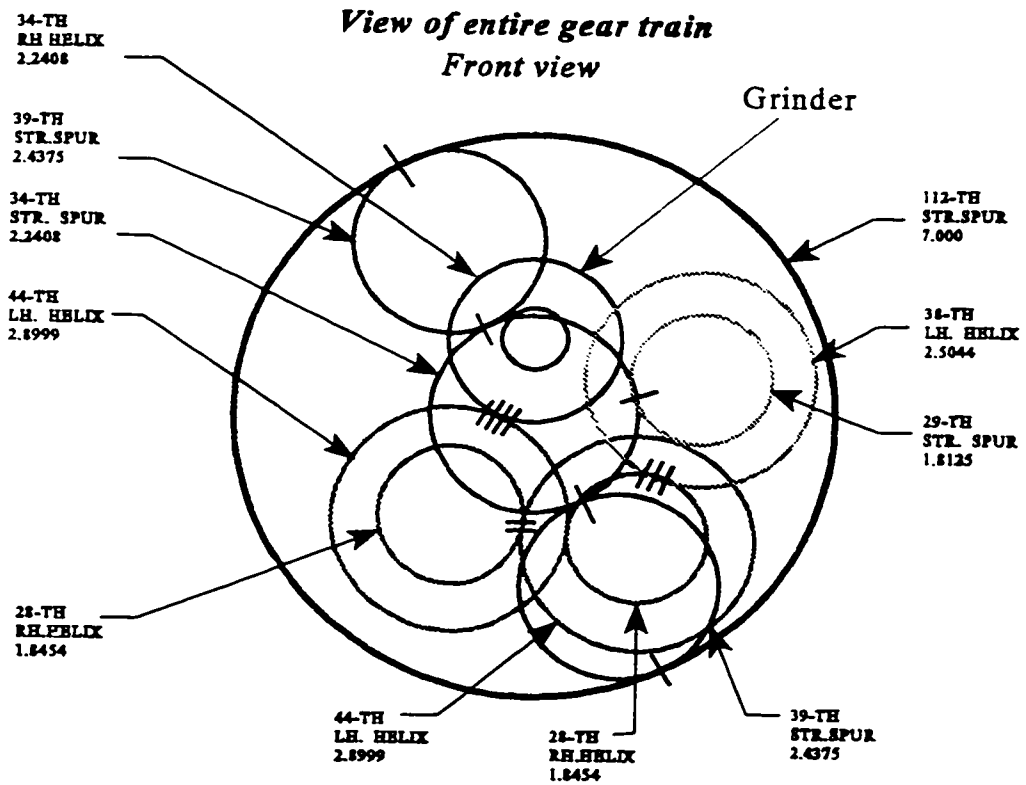

Figure D1 Front View of the Four Stage Gear Train

D1.2 Gear Frequency Analysis

The following table shows the gear frequencies which are analyzed.

Table D1 Primary and Gear Mesh Frequencies				
Gear System Type	Operation Freq. [rpm]	Operation Freq. [Hz]	Number of Teeth	Gear Mesh Frequency [Hz]
Main Planetary	420	7	112	784
Geared to motor	2110.3	35.2	38	1336.5
Geared to motor	2110.3	35.2	29	1020
R. Helix	2864	47.73	28	1336.5
L. Helix	2864	47.73	44	2100
R. Helix	4500	75	28	2100
L. Helix	4500	75	44	3300
Motor Spur	1800	30	34	1020
Planets (2) Spur	789	13.15	39	512
R. Helix	5824	97.07	34	3300

Table D1. demonstrates the frequencies of interest for the gear noise analysis. The primary gear frequency is the 1X rpm frequency of any gear. The gear mesh frequency, or *GMF*, is the product of the primary gear frequency and the number of teeth on the gear. We are also interested in multiples of these frequencies which may show possible problems in operation. The proceeding eight charts detail the analysis. Figure D2. shows the primary frequencies and the gear vibration. The letter M, G and F_L denote motor, gear and line frequencies, respectively.

This chart shows relatively high noise around the 2X and 3X line frequency and low primary gear frequency. Figure D3. is the larger size noise spectrum of figure.

Figure D4. is a comparison between the vibration and A-weighted noise of the GMF. As the chart shows, the highest GMF sound levels are produced by the 784 Hz and 392 Hz vibration. This is indicative of the stationary main planet geared to the barrel. It is also evident in Figure D5. that all the spur type geared systems are producing the majority of the noise though a 12.8 kHz spectrum. The values were taken from 1 meter in the rear motor side of the machine fixture. as shown in Figure C2 as point 3.

Figure D6. is a noise and vibration comparison at the head of the machine. Again, noise measurements were taken 1 meter from the cutter face as shown in Figure C2 as point 7. The chart shows the 7 Hz operational orbit of the grinder spindle. This spike is not produced by the unbalance, as shown in the vibration chart. the accelerometer reading was taken from plane B cutter side of Figure 7.1. Also shown are 2X, 3X and 4X, orbital frequencies.

Figure D8. depicts the vibration characteristics of the motor. Shown is the multiple line frequencies of 2X to 6X from mainly electrical interference. Again the strongest noise source from the grinder orbit.

Figure D9. shows bearing frequencies of about 15500 Hz with definite side bands. Bearing frequencies will not be calculated but equations are included in this appendix.

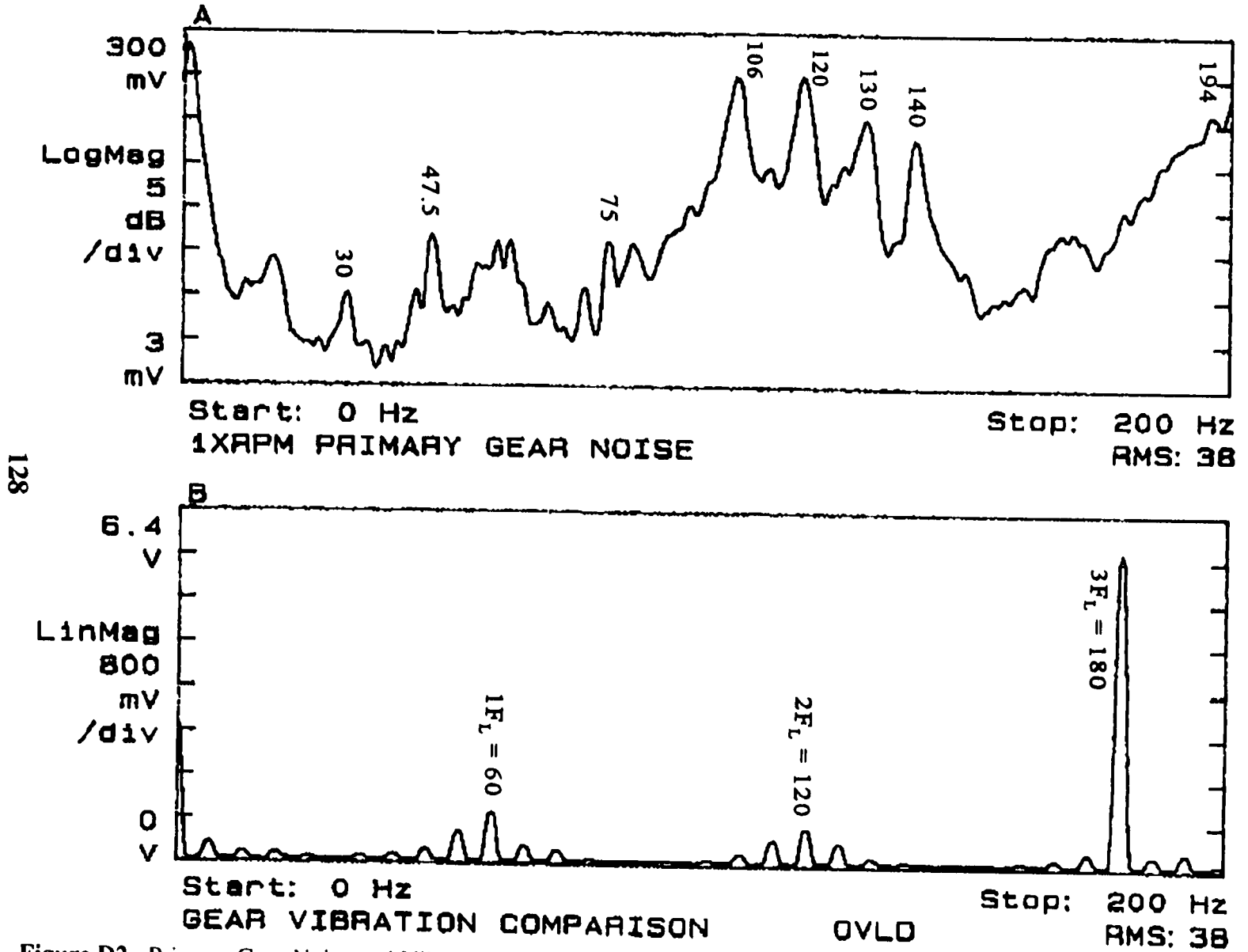

Figure D2 Primary Gear Noise and Vibration

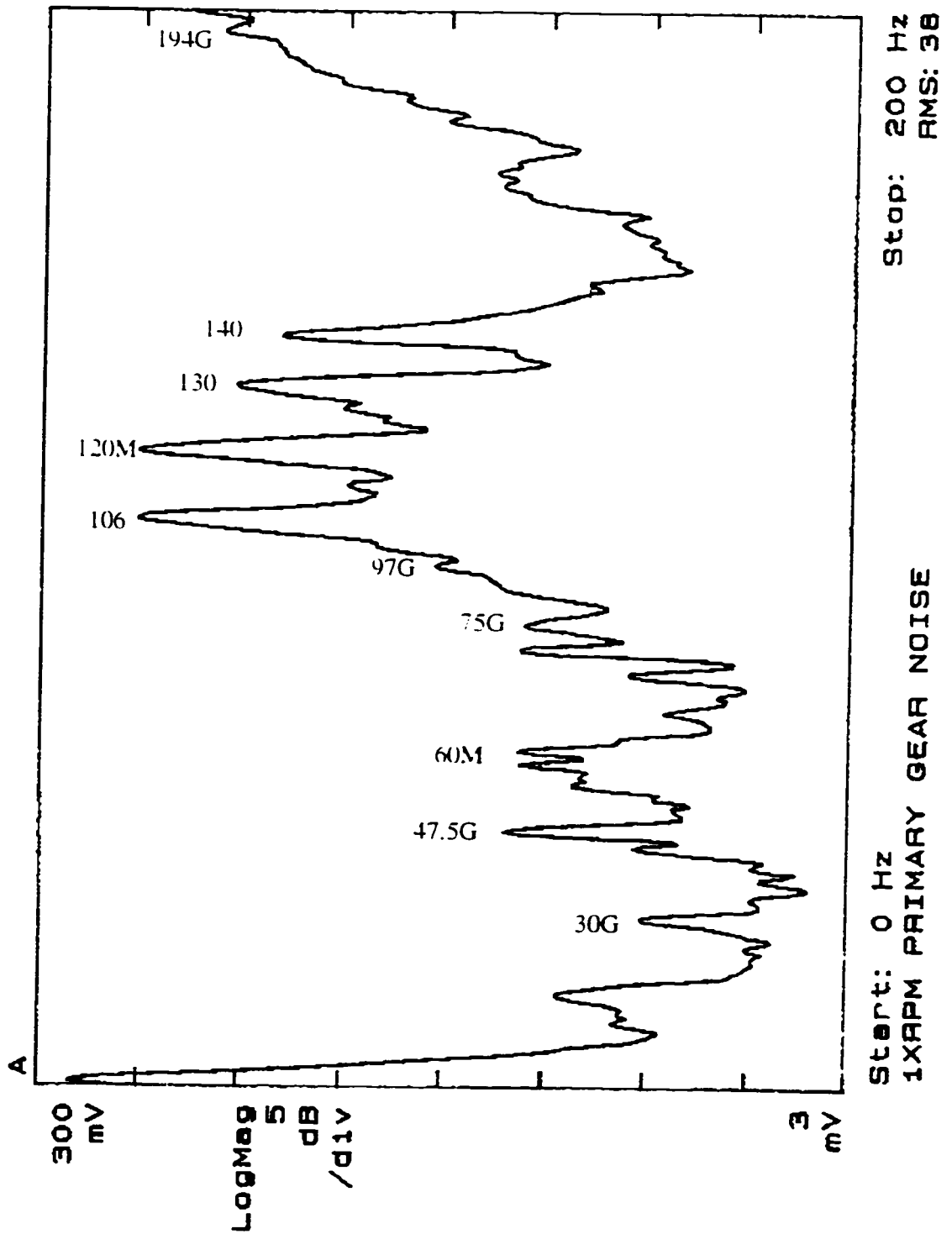

Figure D3 Primary Gear Noise Response.

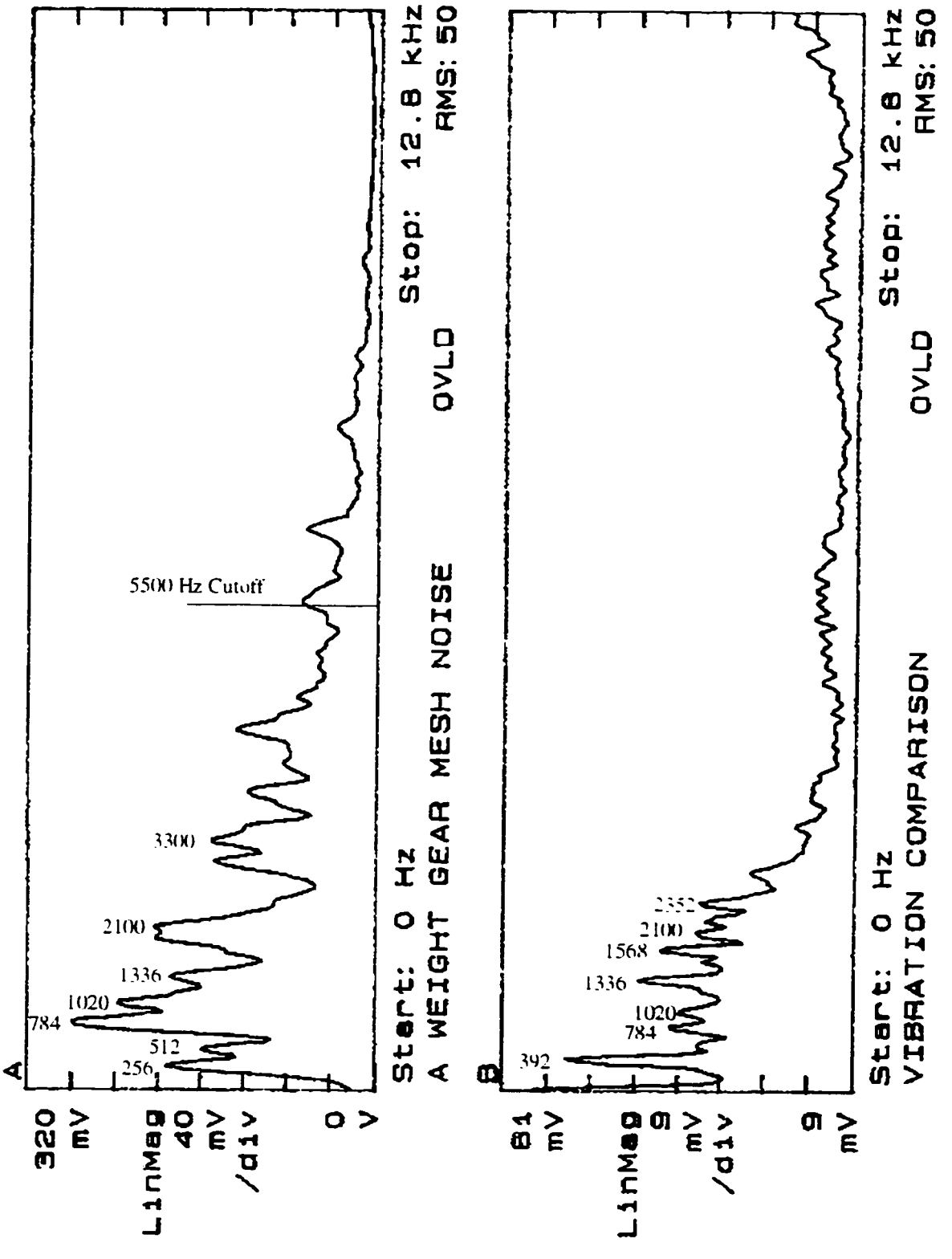

Figure D4 Gear Mesh Frequency A-weighted Noise and Vibration Response

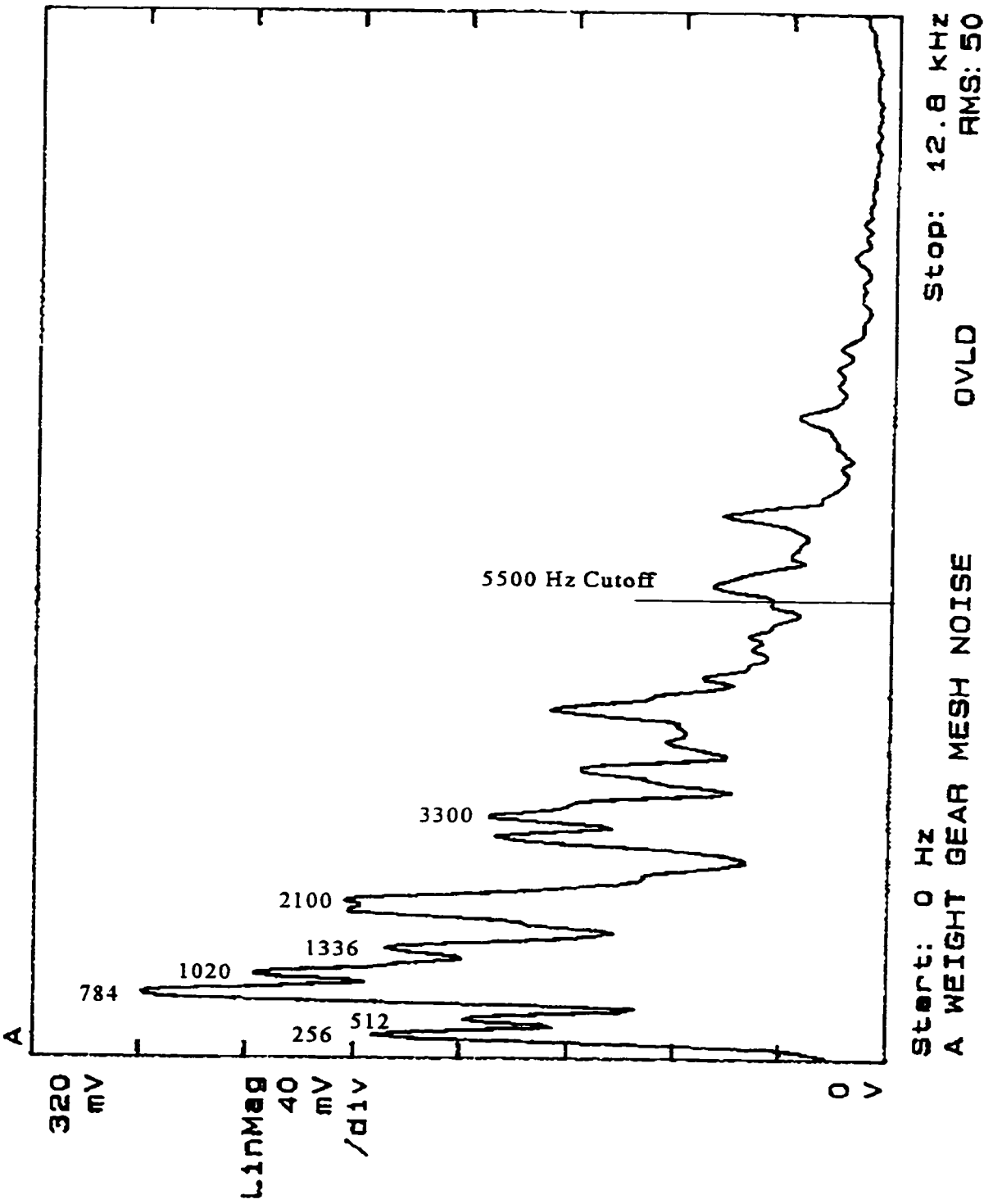

Figure D5 Gear Mesh Frequency A-weighted Noise Response

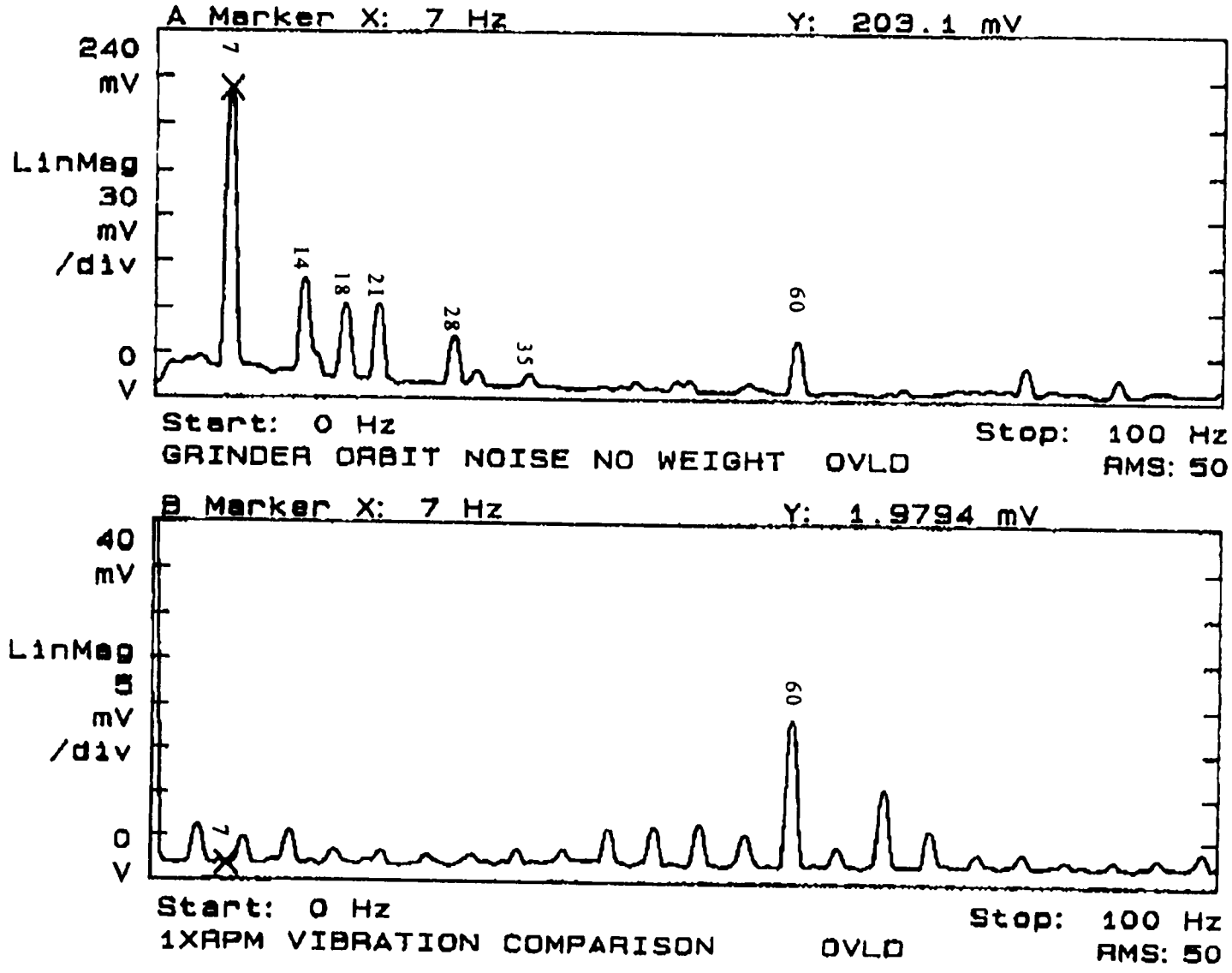

Figure D6 Cutter Head No-weight Noise and Vibration Response at Plane B

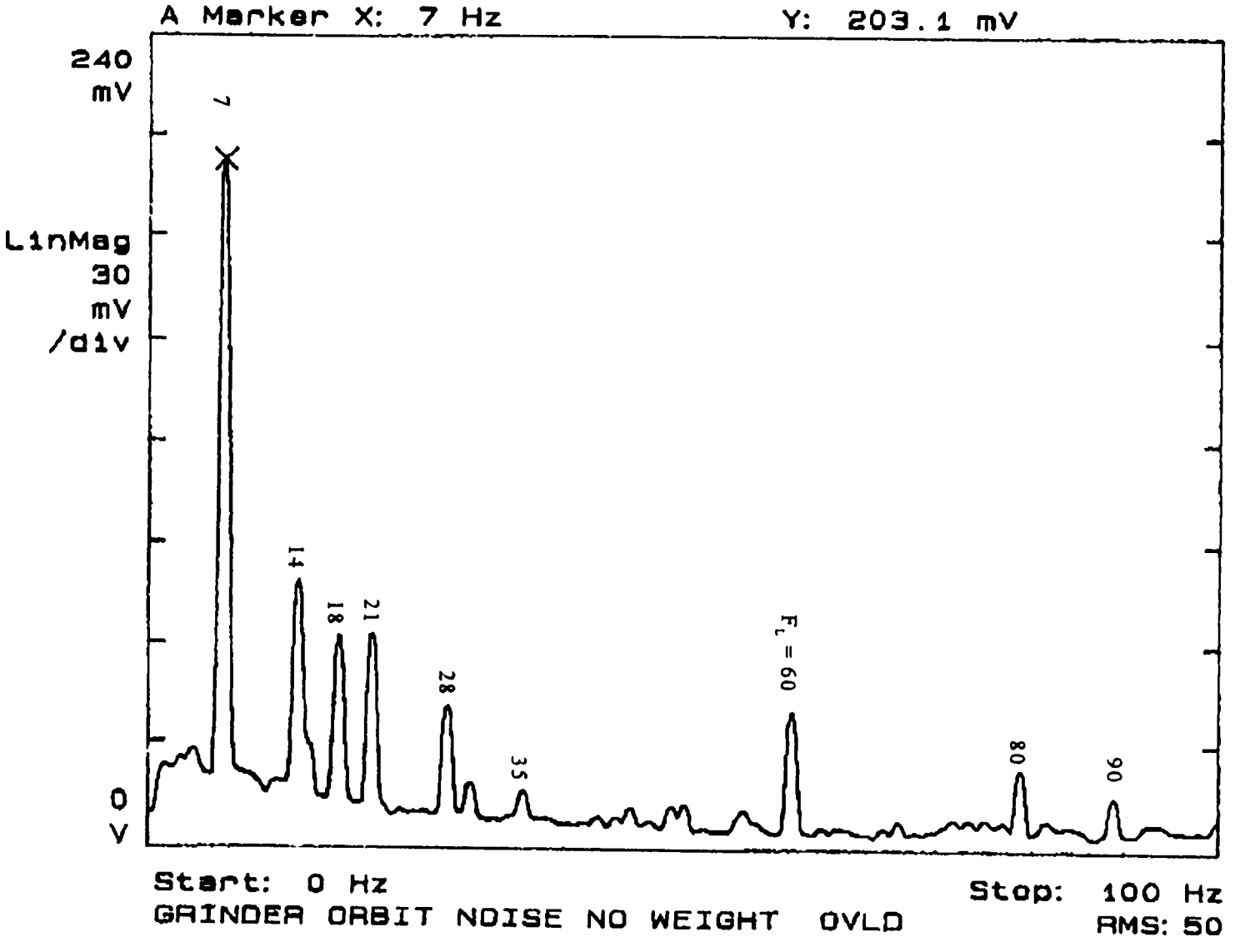

Figure D7 Cutter Head No-weight Noise Response at Plane B

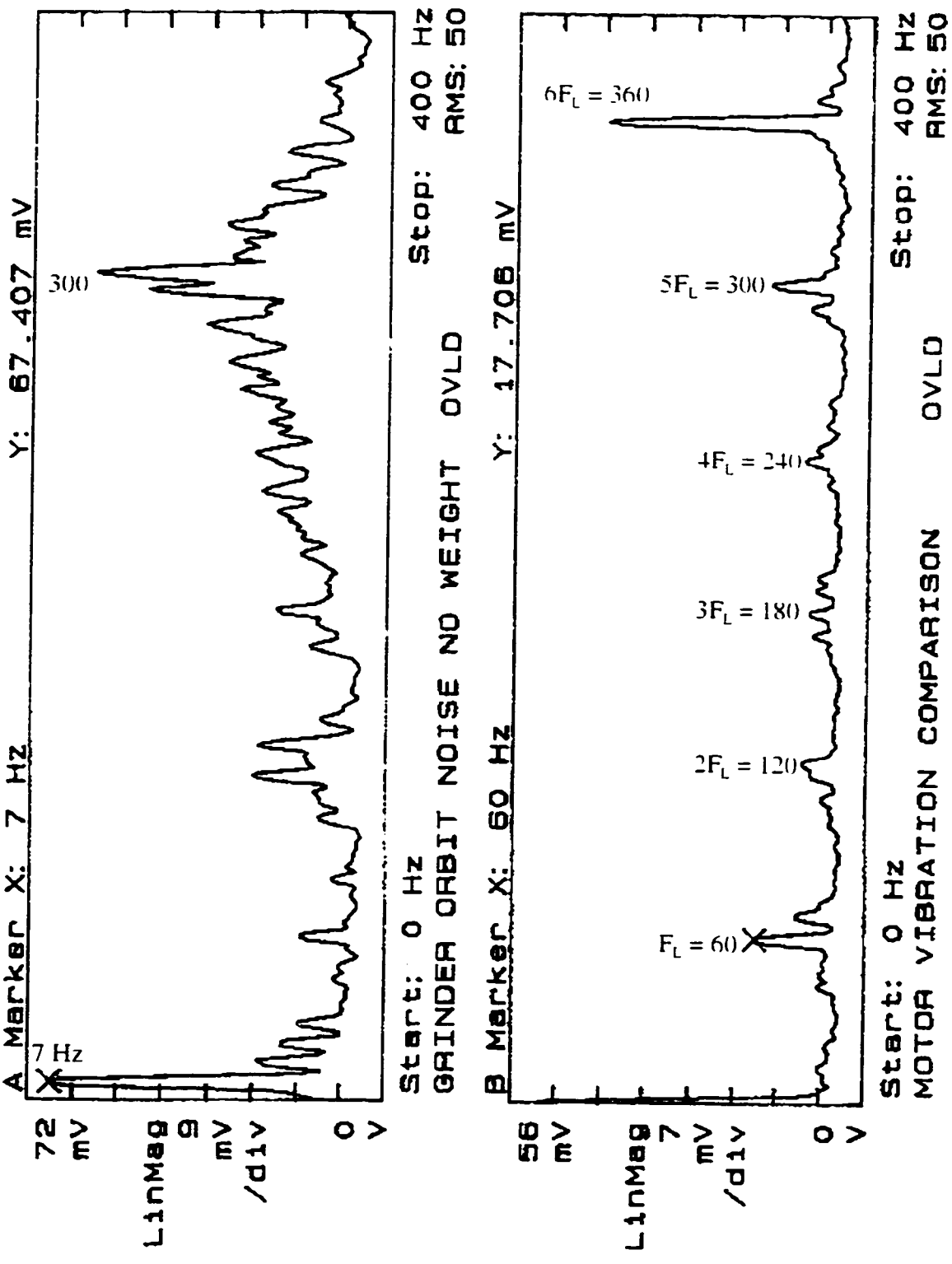

Figure D8 Motor A-weight Noise and Vibration Response at Plane B

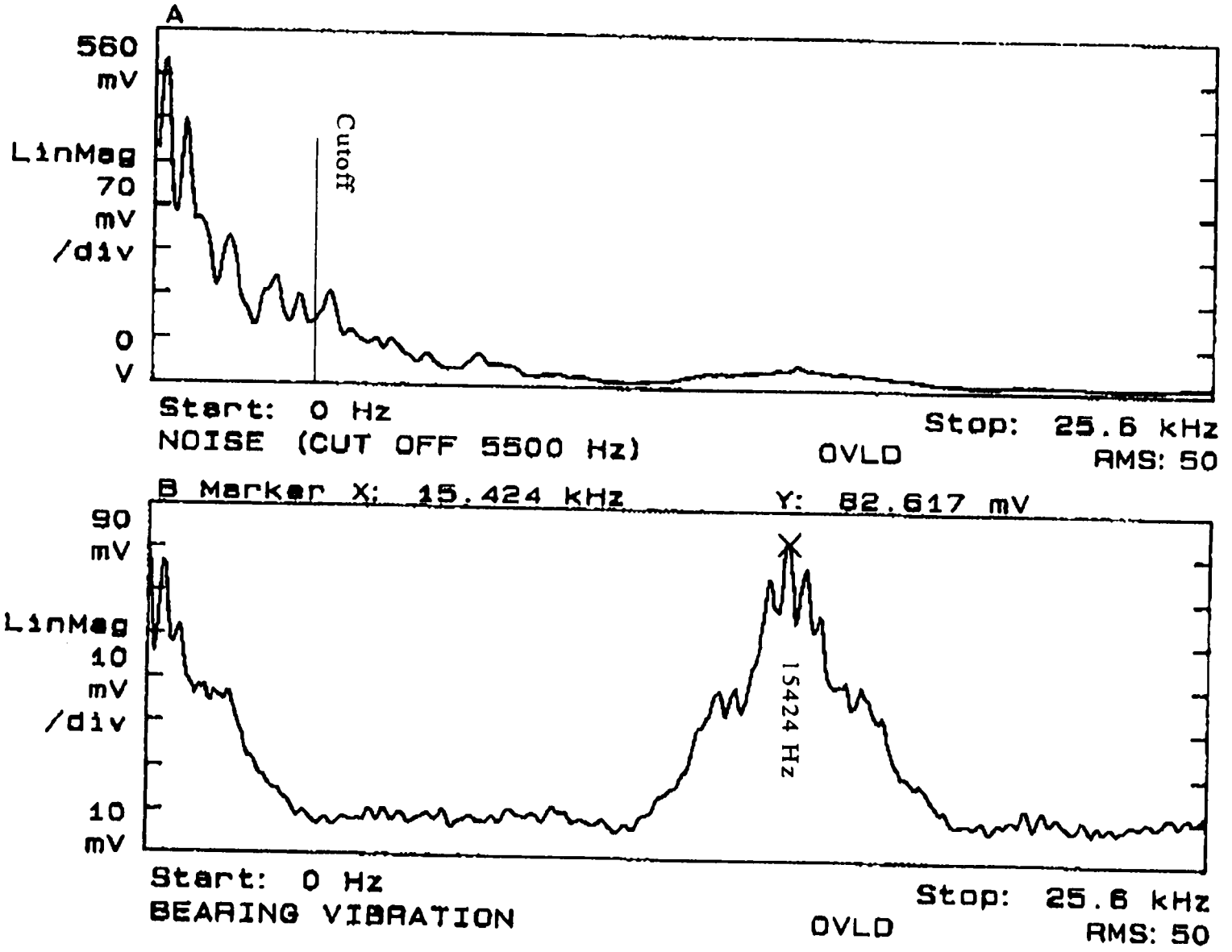

Figure D9 Bearing No-weight Noise and Vibration Response

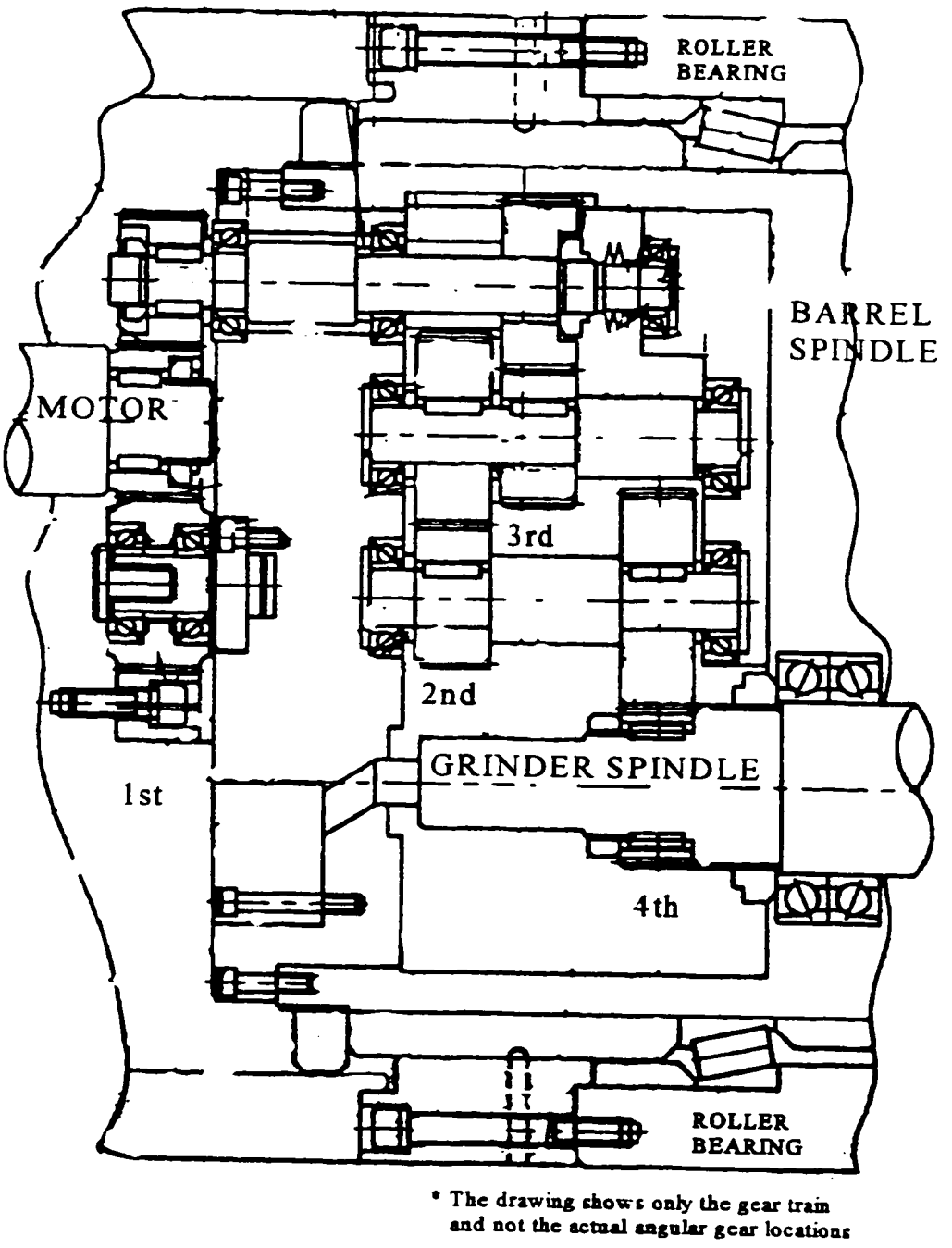

Figure D10 Side View of Gear Train

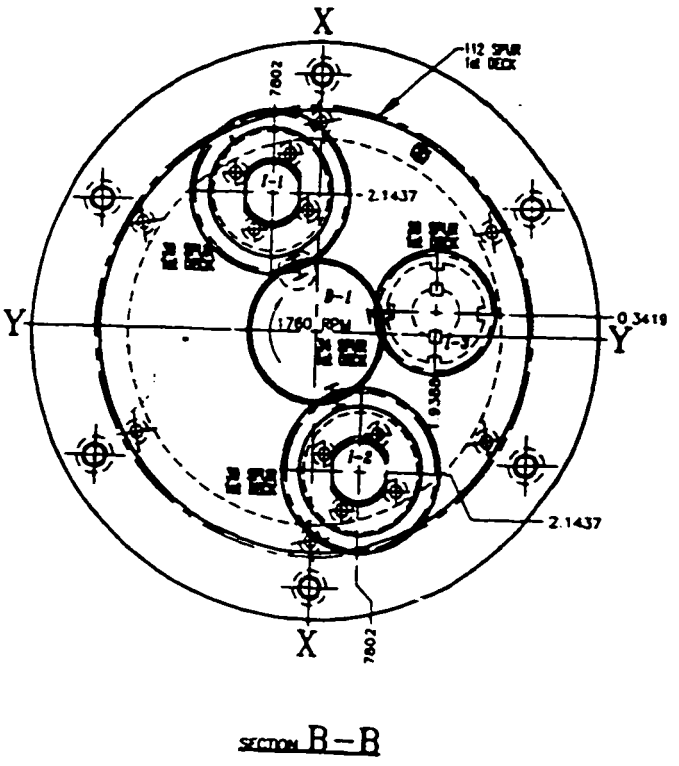

Figure D11 First Stage of Gear Train

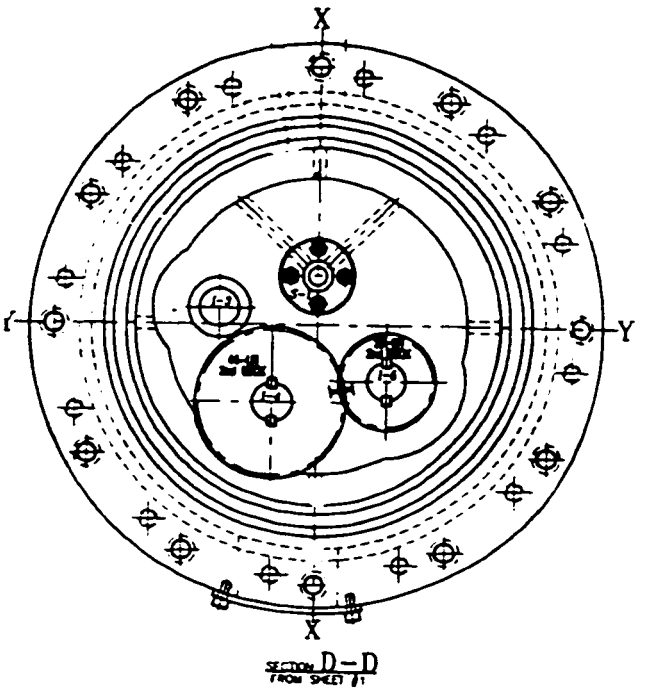

Figure D12 Second Stage of Gear Train

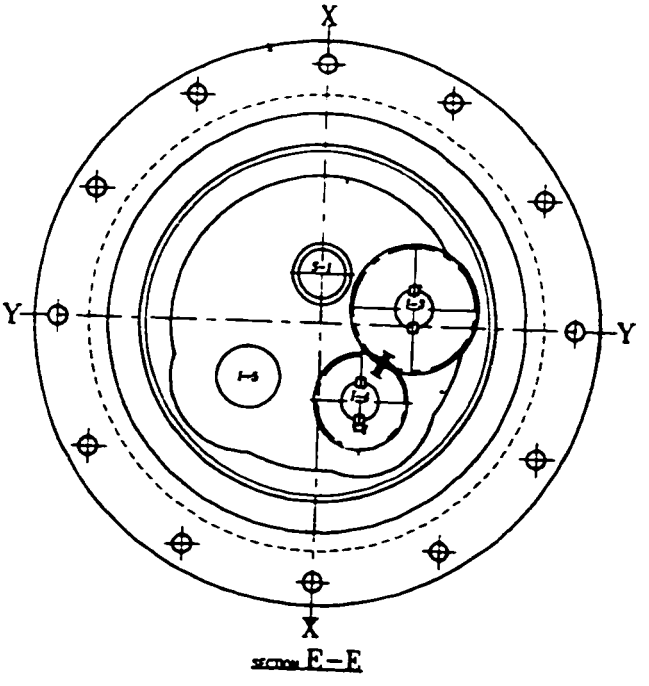

Figure D13 Third Stage of Gear Train

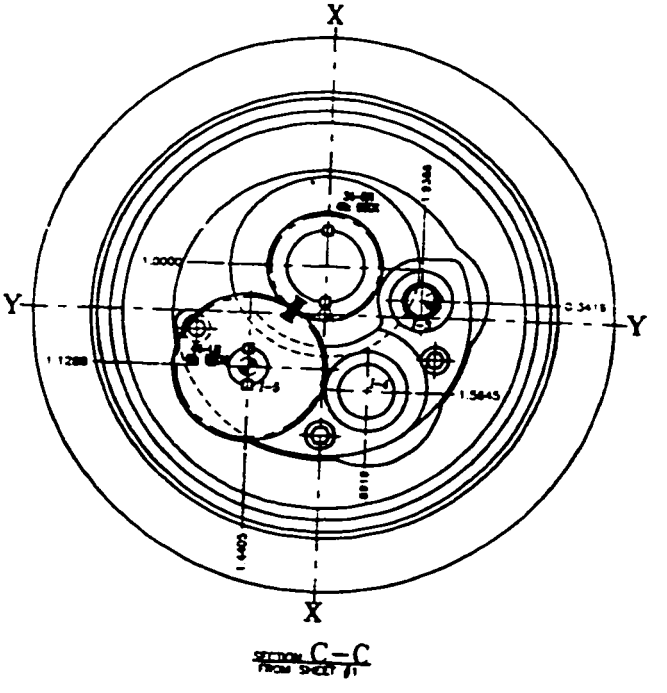

Figure D14 Forth Stage of Gear Train

Table D2.1 Illustrated Vibration Diagnostic Chart [35]

PROBLEM SOURCE	TYPICAL SPECTRUM	PHASE RELATIONSHIP
MASS UNBALANCE A. FORCE UNBALANCE		
B. COUPLE UNBALANCE		
C. OVERHUNG ROTOR UNBALANCE	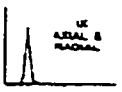	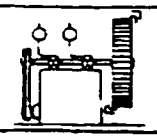
ECCENTRIC ROTOR	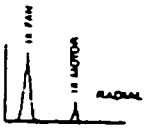	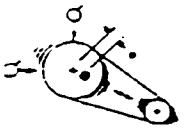
BENT SHAFT		
MISALIGNMENT A. ANGULAR MISALIGNMENT	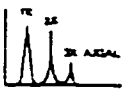	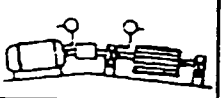
B. PARALLEL MISALIGNMENT	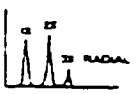	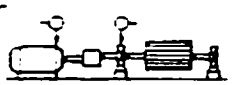
C. MISALIGNED BEARING COCKED ON SHAFT		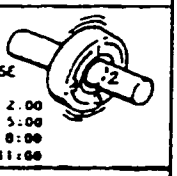
RESONANCE	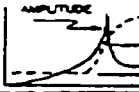	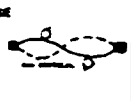
MECHANICAL LOOSENESS	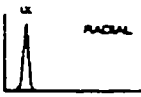 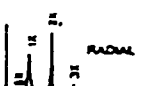 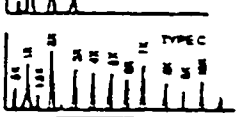	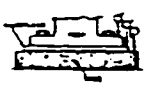  

PROBLEM SOURCE	TYPICAL SPECTRUM
ROTOR RUB	
SLEEVE BEARINGS A. WEAR / CLEARANCE PROBLEMS	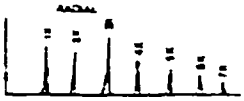
B. OIL WHIRL INSTABILITY	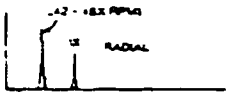 
C. OIL WHIP INSTABILITY	
ROLLING ELEMENT BEARINGS (4 Failure Phases)	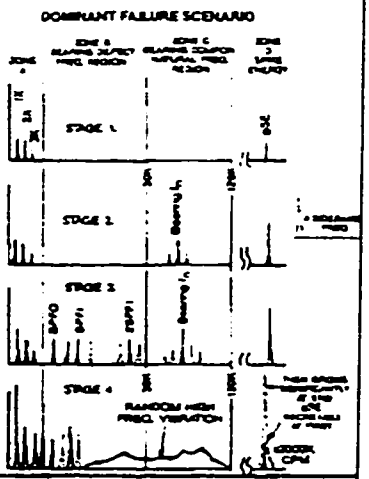
HYDRAULIC AND AERODYNAMIC FORCES A. BLADE PASS & VANE PASS	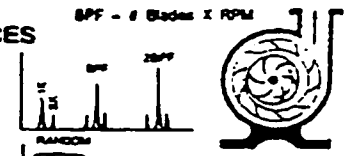
B. FLOW TURBULENCE	
C. CAVITATION	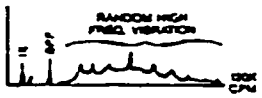

Table D2.2 Illustrated Vibration Diagnostics Chart Continued [35]

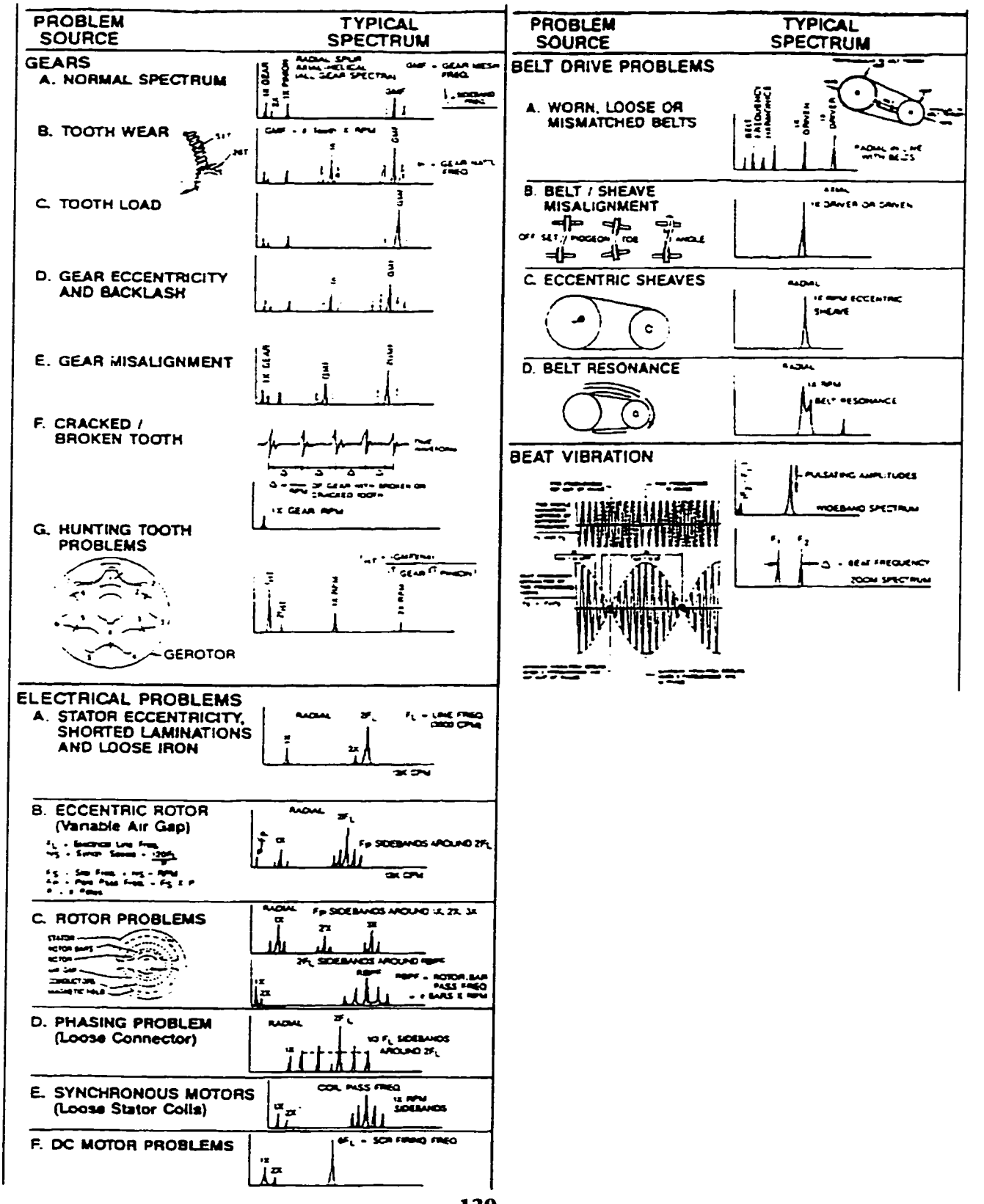

Table D3 Gear Mesh, Bearing and Belt Frequency Chart

GEAR MESH FREQUENCY

N = number of teeth on gear
RPM = shaft speed [rpm]

$$GMF = N \times RPM$$

BEARING FREQUENCIES

Inner Race Frequency

$$BPSI = \frac{N_b}{2}\left(1 + \frac{B_d}{P_d}\cos\theta\right) x\, RPM$$

Outer Race Frequency

$$BPFO = \frac{N_b}{2}\left(1 - \frac{B_p}{P_d}\cos\theta\right) x\, RPM$$

Ball Spring Frequency

$$BSF = \frac{P_d}{2B_d}\left(1 - \left(\frac{B_d}{Pd}\right)^2 (\cos\theta)^2\right) x RPM$$

Fundamental Train Frequency

$$FTF = \frac{1}{2}\left(1 - \frac{B_d}{P_d}\cos\theta\right) x RPM$$

N_b = *Number of balls or rollers*

B_d = *Ball or roller diameter*

P_d = *Bearing pitch diameter*

θ = *Contact angle*

where; $P_d \approx \frac{d_{outer} - d_{inner}}{2} + D_{inner}$

BELT FREQUENCY

RPM_{pulley} = *Pulley speed [rpm]*

P_d = *Pitch diameter of pulley*

L_b = *Length of the belt*

$$BF = \frac{\pi \cdot RPM_{pulley} \cdot P_d}{L_b}$$

APPENDIX E

Theoretical Model Development

E. DYNAMIC VIBRATION MODEL

E1. Introduction

As with any mechanical system, there is a need to mathematically model the system to determine its unique operating characteristics. The machine studied in the analysis is also very unique. It is one of the first milling machines in the North America to combine a face mill and eccentric grinder into one operation. This design involves a rotor with two spindles in rotation, each at different angular velocities. These angular velocities will produce operating frequencies that exhibit a forcing function of multiple frequency excitation. The calculations which govern the forcing function are documented in a number of texts and were combined to develop a working model of a multiple frequency type formulation.

The modeling was performed using advanced engineering dynamics described by Jerry H. Ginsberg [8] and using multiple frequency excitation formulas found in S. Graham Kelly [12]. These two texts provided most of the information needed to model the machine. Other sources were Sneck [22] and Thomson [26].

Vibrations of a mechanical system occur when a system is supplied with any external energy. Free vibrations occur when an energy source is applied and then removed while the system vibrates. Forced vibrations occur when an external source causes vibrations to occur. This external force can be of many forms: A hammer striking the floor with a periodic motion provides an external excitation to an elastic structure, but at a very low frequency.

A machine with rotating components is excited by the torque caused from a driving motor or the frequency of a force created during the operation of the machine. The fundamentals behind the vibration of a structure must be understood before modeling the machine.

A simple one degree of freedom system can be modeled as in Figure E1.

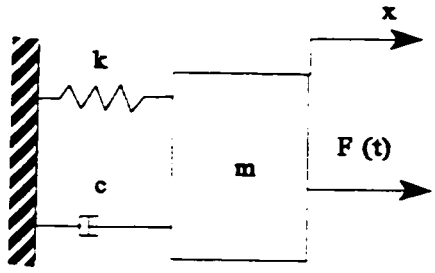

Figure E1 One-Degree-of-Freedom Vibration Model

The differential equation governing the vibration of a system in Figure E1 is simply

$$m\ddot{x} + c\dot{x} + kx = F(t) \tag{E1}$$

Through vibration theory outlined in numerous texts. [12.22.26] the forced motion of any one degree of freedom *damped* system is

$$\ddot{x} + 2\zeta\omega_n\dot{x} + \omega_n^2 x = \frac{F(t)}{m} \tag{E2}$$

where ζ is the damping ratio and ω_n is the natural frequency of the free vibration. It is also assumed that the system is under damped and. thus $\zeta < 1$. For free vibrations. the c term or damping coefficient in equation (E1) is zero and the machine experiences vibration. The solution of either equations (E1) or (E2) will yeild a transient response function and a steady-state response. respectively. The forcing function is dictated by the external or internal

machine excitation forces and controls the steady-state response function. The forcing function can be any combination of forces and frequencies. This gives rise to multi-frequency excitation response as outlined in the next section.

E2. Multifrequency Excitation

The one-degree-of-freedom system is still valid for this type of analysis. The forcing function will consist of two or more frequencies which will influence the steady-state response of the system in two components of x and y. A model of a simple multifrequency excitation is shown in Figure E2.

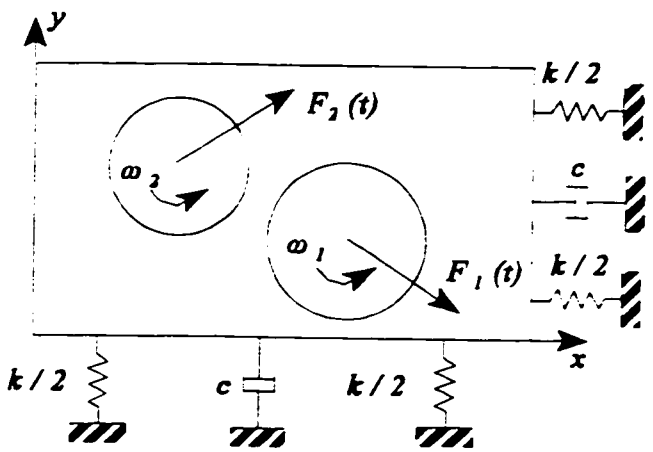

Figure E2 Multifrequency Excitation Model

Kelly [12] outlines the analysis for a multifrequency excitation and has the form

$$F(t) = \sum_{i=1}^{n} F_i \sin(\omega_i + \theta_i) \qquad \text{(E3)}$$

Without loss of generality, it is assumed that $F_i > 0$ for each i. The steady-state response due to a multifrequency excitation is obtained using the response for a single-frequency

excitation and the principle of linear superposition. The total response is the sum of the responses due to each of the individual frequency terms.

The solution to the equation (E3) in vibration terms outlined in the nomenclature are

$$x(t) = \sum_{i=1}^{n} X_i \sin(\omega_i t + \theta_i - \varphi_i) \tag{E4}$$

where

$$X_i = \frac{M_i F_i}{m\omega_n^2} \tag{E5}$$

where

$$\varphi_i = \tan^{-1}\left(\frac{2\zeta r_i}{1 - r_i^2}\right) \tag{E6}$$

and

$$r_i = \frac{\omega_i}{\omega_n} \tag{E7}$$

$$M_i = \frac{1}{\sqrt{(1 - r_i^2)^2 + (2\zeta r_i)^2}} \tag{E8}$$

An important aspect of multiple frequency excitation is that the maximum amplitude of vibration does not occur at the same instant in time [12]. For multiple frequencies the maximum is the sum of the maximum displacements for each particular frequency. Therefore the maximum displacement is of the form

$$X_{max} \leq \sum_{i=1}^{n} X_i \tag{E9}$$

This concept will be demonstrated when a graphical representation of the forcing function is plotted. Figure E2 demonstrates that the forcing functions may or may not lie in a single defining orientation. The sine terms in equations (E3) and (E4) denote the force in any angular direction, and define a rotational force vector of magnitude $me\omega^2$. For a similar

vector representation in the x and y direction. a sine and cosine term will define components of magnitude. and direction of the force with respect to the transient response of the system. The machine model can now be introduced with the calculations and explanation of the model.

E3. Machine Model

This section will introduce a model of the machine tested. It was constructed to understand the nature of the vibration when balancing a machine of this type. This gives the investigator some prior knowledge to the problem at hand. and also provides valuable information for the behavior of the system and its response to induced forces.

Figure E3 depicts the cross section of the machine tool spindles and their orientation. The calculations will demonstrate the nature of the problem when dealing with velocity. acceleration and force using a moving reference frame.

Using the suggestions from Kelly [12] a superposition model has been constructed to further demonstrate the nature of the problem. Figure E3 shows the dynamic machine model as a cross section. Figure E4 demonstrates the two spindles apart, but related to the total system of forces using the superposition theory.

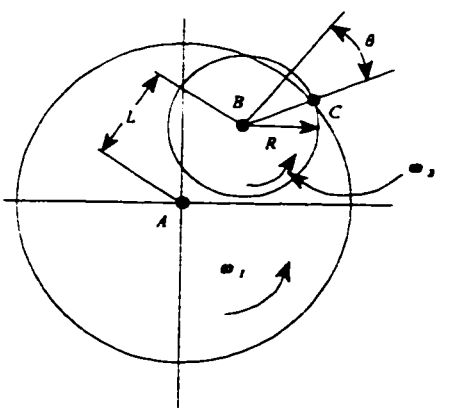

Figure E3 Dynamic Machine Model Cross Section

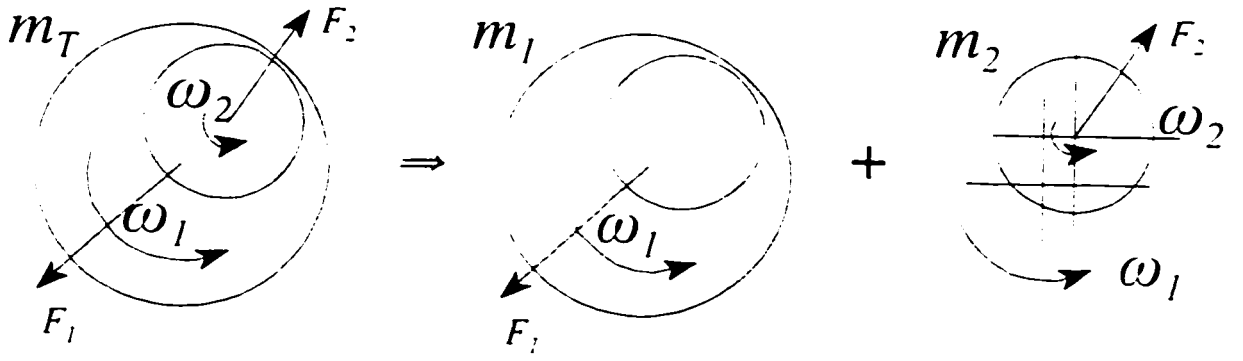

Figure E4 Superposition Model

The model consists of a dual rotor system, the first spindle is operating at one angular velocity and the rotation of a second spindle at an offset of length, *L*, at a second angular velocity. Calculations for the total force acting inside the machine will simply be an addition of the force from the barrel spindle rotating about its center of rotation and the force from the grinder spindle rotating about its center of rotation and orbiting the barrel spindle. Since there is an offset length *L*, there will also be a couple, or moment, about the center of rotation of the barrel spindle. This will be further developed in the following sections which deal with the calculations.

E4. Dynamic Model

Equation E1 shows that the forcing function governs the steady-state response of the left side of the equation. Both are governed by the internal forces within the system, the first force will be derived for the barrel spindle.

E4.1. Barrel Spindle Modeling

Considering only the barrel spindle component shown in Figure E5. It consists of a hole machined longitudinally into the page along the ***k-axis***, rotating about, O. The center of mass for the barrel however, does not correspond the center of rotation for the superposition model. Therefore, two forces will result from the model. One force, F_G, will result from the center of mass, and the force, F_{el}, will result from any eccentricity magnitude and direction left in the barrel. The eccentricity phase angle and magnitude are not known at this point in the calculations but will be considered later in the report and will be vector components with independent phases. The variables used in the calculations are found in Figure E5. The bold characters from this point on in the analysis, will symbolize vectors, with a unit coordinate system of ***i, j, k,*** representing the directions of x, y, z, respectively. Therefore for the barrel spindle, the dynamic equations are as follows:

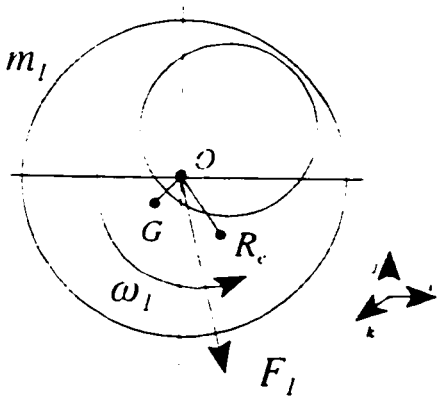

Figure E5 Barrel Spindle Variables.

$$\mathbf{F}_1 = \sum \mathbf{F} = \mathbf{F}_G + \mathbf{F}_{el}$$

$$\mathbf{a}_G = -\omega^2 \mathbf{r}_{G/O} + \alpha \times \mathbf{r}_{G/O}$$

$$\mathbf{a}_{el} = -\omega^2 \mathbf{r}_{Re} + \alpha \times \mathbf{r}_{Re/O}$$

then $$\mathbf{F}_1 = m_1 (\mathbf{a}_G + \mathbf{a}_{e1}) \qquad (E10)$$

Since the angular acceleration, $\alpha = 0$, the normal force is of positive sense, and the distance $\mathbf{r}_{R/O}$, is the remaining eccentricity unbalance $\mathbf{e}_1$, then

$$\mathbf{F}_1 = m_1 \omega_1^2 (R_{OG} \cos \gamma_1 + e_1 \cos \gamma_2) \mathbf{i} + m_1 \omega_1^2 (R_{OG} \sin \gamma_1 + e_1 \sin \gamma_2) \mathbf{j} \qquad (E11)$$

where R_{OG} is the constant distance from the center of rotation of the axis at O to the center of mass of the rotor at G. $\mathbf{F}_1$, is the force generated by the rotation of the barrel spindle at point O, and the force was also calculated in its components for additional manipulations further in the report. The second analysis is for the grinder spindle.

E4.2. Grinder Spindle Modeling

Considering the grinder spindle section shown in Figure E6. It rotates about its own axis at B and also orbits a second axis at A. The force F_2, will act at A and B and consists of various forces produced by the dual rotation of the component. The variable, L, is the distance from the center of rotation of the barrel spindle, to

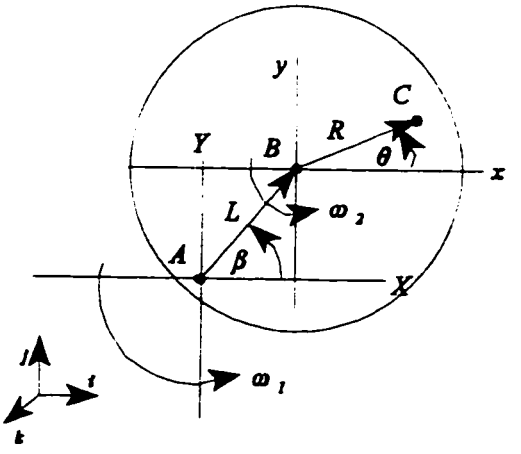

Figure E6 Grinder Spindle Variables

the center of rotation of the grinder spindle. This distance is constant and will not change. Therefore, for the grinder spindle the dynamic equations are as follows:

$\mathbf{v}_A = \mathbf{a}_A = \mathbf{0}$ and

$\omega = \omega_1 \mathbf{k}$, $\omega_{rel} = \omega_2 \mathbf{k}$

where ω and ω_{rel}, represent the angular velocity of the barrel spindle and the angular velocity of the grinder spindle relative to the barrel, respectively.

Both $\alpha_1 = \alpha_{rel} = \mathbf{0}$, since there is no angular acceleration.

Vectors,

$\mathbf{r}_{C/B} = [\, R\cos\theta\,\mathbf{i} + R\sin\theta\,\mathbf{j}\,]$ and

$\mathbf{r}_{B/A} = [\, L\cos\beta\,\mathbf{i} + L\sin\beta\,\mathbf{j}\,]$

are radial vectors depicting the distances from A to B and B to some point C.

These vectors can be added to form the vector,

$\mathbf{r}_{C/A} = \mathbf{r}_{C/B} + \mathbf{r}_{B/A}$

Therefore,

$\mathbf{r}_{C/A} = [\, R\cos\theta + L\cos\beta\,]\,\mathbf{i} + [\, R\sin\theta + L\sin\beta\,]\,\mathbf{j}$

and for the axes shown in Figure E6, the rate of change of

$\theta = \omega_2 t + \theta_0$ and $\beta = \omega_1 t + \beta_0$ (E12)

where, θ_0 and β_0, are the initial angle conditions.

To determine the relative velocity of any point C of radius R, for the frame xyz,

$(\mathbf{v}_C)_{xyz} = \omega_{rel} \times \mathbf{r}_{C/B} = \omega_2 \mathbf{k} \times [\, R\cos\theta\,\mathbf{i} + R\sin\theta\,\mathbf{j}\,] = \omega_2 [\, R\cos\theta\,\mathbf{j} - R\sin\theta\,\mathbf{i}\,]$ (E13)

To determine the relative acceleration of any point C of radius R. for the frame xyz.

$$(\mathbf{a}_C)_{xyz} = \boldsymbol{\omega}_{rel} \times (\boldsymbol{\omega}_{rel} \times \mathbf{r}_{C/B}) = \omega_2 \mathbf{k} \times (\omega_2 \mathbf{k} \times [R \cos\theta \mathbf{i} + R \sin\theta \mathbf{j}])$$

$$(\mathbf{a}_C)_{xyz} = - \omega_2^2 [R \cos\theta \mathbf{i} + R \sin\theta \mathbf{j}] \qquad (E14)$$

The absolute velocity of point C. is

$$\mathbf{v}_C = \mathbf{v}_A + (\mathbf{v}_C)_{xyz} + \boldsymbol{\omega} \times \mathbf{r}_{C/A} \qquad (E15)$$

the term $\mathbf{v}_A = \mathbf{0}$. since the velocity of the axis XYZ at A is zero. therefore

$$\mathbf{v}_C = \omega_2 [R \cos\theta \mathbf{j} - R \sin\theta \mathbf{i}] + \omega_1 ([R \cos\theta + L \cos\beta] \mathbf{j} + [R \sin\theta + L \sin\beta] \mathbf{i})$$

The absolute acceleration of point C. is (E16)

$$\mathbf{a}_C = \mathbf{a}_A + (\mathbf{a}_C)_{xyz} + \mathbf{a}_{COR} \qquad (E17)$$

where $\mathbf{a}_A$. is the acceleration of point A of the moving frame XYZ. $(\mathbf{a}_C)_{xyz}$ is the acceleration of C relative to the moving frame xyz and $\mathbf{a}_{COR}$. is the complimentary. or Coriolis acceleration.

Therefore.

$$\mathbf{a}_C = \mathbf{a}_A + (\mathbf{a}_C)_{xyz} + \boldsymbol{\alpha} \times \mathbf{r}_{C/A} + \boldsymbol{\omega} \times (\boldsymbol{\omega} \times \mathbf{r}_{C/A}) + 2 \boldsymbol{\omega} \times (\mathbf{v}_C)_{xyz} \qquad (E18)$$

there is no acceleration of point A and the angular acceleration $\boldsymbol{\alpha}$, of XYZ = 0. therefore.

$$\mathbf{a}_C = (\mathbf{a}_C)_{xyz} + \boldsymbol{\omega} \times (\boldsymbol{\omega} \times \mathbf{r}_{C/A}) + 2 \boldsymbol{\omega} \times (\mathbf{v}_C)_{xyz} \qquad (E19)$$

$$\begin{aligned} \mathbf{a}_C = \; & - (\omega_2^2 [R \cos\theta \mathbf{i} + R \sin\theta \mathbf{j}]) \\ & - \omega_1 \mathbf{k} \times (\omega_1 \mathbf{k} \times [R \cos\theta + L \cos\beta] \mathbf{i} + [R \sin\theta + L \sin\beta] \mathbf{j}) \\ & - 2 \omega_1 \mathbf{k} \times (\omega_2 [R \cos\theta \mathbf{j} - R \sin\theta \mathbf{i}]) \end{aligned} \qquad (E20)$$

Finally.

$$\mathbf{a}_c = - \omega_2^2 [R \cos\theta \mathbf{i} + R \sin\theta \mathbf{j}]$$

$$- \omega_1^2 ([R \cos\theta + L \cos\beta] \mathbf{i} + [R \sin\theta + L \sin\beta] \mathbf{j})$$

$$- 2 \omega_1 \omega_2 [R \cos\theta \mathbf{i} - R \sin\theta \mathbf{j}] \qquad (E21)$$

Relating the force $\mathbf{F}_2$ to the position of the grinder spindle as.

$$\mathbf{F}_2 = m_2 \mathbf{a}_c \qquad (E22)$$

and knowing that the eccentricity, $\mathbf{e}_2$, is a vector at some distance R. from the center of rotation of the xyz axis. R can be modeled as e_2 at some phase angle θ. Therefore.

$$\mathbf{F}_2 = - m_2 (\omega_2^2 [e_2 \cos\theta \mathbf{i} + e_2 \sin\theta \mathbf{j}]$$

$$- \omega_1^2 ([e_2 \cos\theta + L \cos\beta] \mathbf{i} + [e_2 \sin\theta + L \sin\beta] \mathbf{j})$$

$$- 2 \omega_1 \omega_2 [e_2 \cos\theta \mathbf{i} - R \sin\theta \mathbf{j}]) \qquad (E23)$$

For a particular forcing function with respect to the system. it is necessary to place equation (E23) into a time dependant function and relating equation (E12) to the system.

$$\mathbf{F}_2 = m_2 (\omega_2^2 [e_2 \cos(\omega_2 t + \theta_0) \mathbf{i} + e_2 \sin(\omega_2 t + \theta_0) \mathbf{j}]$$

$$+ \omega_1^2 ([e_2 \cos(\omega_2 t + \theta_0) + L \cos(\omega_1 t + \beta_0)] \mathbf{i} + [e_2 \sin(\omega_2 t + \theta_0) + L \sin(\omega_2 t + \beta_0)] \mathbf{j})$$

$$+ 2 \omega_1 \omega_2 [e_2 \cos(\omega_2 t + \theta_0) \mathbf{i} - e_2 \sin(\omega_2 t + \theta_0) \mathbf{j}]) \qquad (E24)$$

and resolving equations (E24) and combining (E11) into components using the principle of superposition and using the positive sense with respect to force.

$$\mathbf{F}_T(t) = [m_1 \omega_1^2 [R_{cg} \cos(\omega_1 t + \gamma_{0.1}) + e_1 \cos(\omega_1 t + \gamma_{0.2})]$$

$$+ m_2 \omega_2^2 e_2 \cos(\omega_2 t + \theta_0) + m_2 \omega_1^2 [e_2 \cos(\omega_2 t + \theta_0) + L \cos(\omega_1 t + \beta_0)]$$

$$+ 2 m_2 \omega_1 \omega_2 e_2 \cos(\omega_2 t + \theta_0)] \mathbf{i}$$

$$+ [m_1 \omega_1^2 [R_{cg} \sin (\omega_1 t + \gamma_{0,1}) + e_1 \sin (\omega_1 t + \gamma_{0,2})]$$

$$+ m_2 \omega_2^2 e_2 \sin (\omega_2 t + \theta_0) + m_2 \omega_1^2 [e_2 \sin (\omega_2 t + \theta_0) + L \sin (\omega_1 t + \beta_0)]$$

$$+ 2 m_2 \omega_1 \omega_2 e_2 \sin (\omega_2 t + \theta_0)] \mathbf{j} \qquad \text{(E25)}$$

As shown in equation (E25), the phase angles multiplied to the constant radius, L, and centroidal radius, R_{cg}, are 180 degrees opposite to each other, therefore some magnitude cancellation will take place and $\gamma_{0,1} = \beta_0 + 180$. The phase angles multiplied to the eccentricity terms e_1, and e_2, are both arbitrary and can start at the same phase angle of 0 degrees, or in the maximum force starting position. These positions and calculations will be discussed in section eight of the study as a modeling comparison. The final defining equation for the system shown in Figure E3 for the y-direction is

$$m_T d^2y/dt^2 + c\, dy/dt + k\, y = m_1 \omega_1^2 [R_{cg} \sin (\omega_1 t + \gamma_{0,1}) + e_1 \sin (\omega_1 t + \gamma_{0,2})]$$

$$+ m_2 \omega_2^2 e_2 \sin (\omega_2 t + \theta_0) + m_2 \omega_1^2 [e_2 \sin (\omega_2 t + \theta_0) + L \sin (\omega_1 t + \beta_0)]$$

$$+ 2 m_2 \omega_1 \omega_2 e_2 \sin (\omega_2 t + \theta_0) \qquad \text{(E26)}$$

This equation can be modeled at two planes where the variables defined such as e_1 and e_2 will also change in magnitude and direction at both planes and conclusions made for the model will be discussed in chapter eight.

E4.3 Moment Considerations

The moment produced by the grinder spindle can also be modeled dynamically. It is documented that the moment about any point O, is produced by a force F, at any perpendicular distance r, from point O. Therefore, only a force which acts about point O will cause a moment. If a force acts through point O or normal to O, there is an acceleration of point O, but not a moment. This machine exhibits many of these properties. Since we are interested in the moments about the center of rotation of the barrel spindle, from Figure E3, any forces acting through point A, in this case, will not contribute to the moment at A, since they are normal to A. Only the eccentricity vector $\mathbf{e_2}$, from $\mathbf{F_2}$, will contribute to the moment about A. However, defining the moment is definitely evident in the radial direction but, since the analysis is extended to two planes, this also gives rise to another moment axially. Therefore, there will be a definite moment about each axis as M_x, M_y, and M_z such that there exists a moment of inertia $I\alpha$, radially. Since the analysis for the rotors consists of determining only the forcing function $\mathbf{F}(t)$ and balancing these forces, the moments about A, will not be considered in the scope of this study.

These equations seem very ideal for a real system and must be investigated experimentally to determine if the variables accurately depict the system. This requires the use of sensitive instrumentation and further studies in this area.

GLOSSARY OF TERMS [3,19,32]

Balancing Plane - The axial rotor position were balance weights are applied radially.

Correction Mass - A mass which can be added or removed from a specified axial, radial and angular position on the rotor.

Couple Unbalance - (rocking couple) an unbalance rotor condition in which the principle axis of a shaft intersects at the center of gravity.

Critical Speed - Synchronous natural frequency of a rotor.

DSA - Digital Signal Analyzer

Dynamic Runout - The amount runout remaining from subtracting the static runout from the total runout

Dynamic Unbalance - An unbalance rotor condition when the principal axis and the rotating shaft centerline do not coincide or touch.

FFT - Fast Fourier Transform

Flexible Rotor - A rotor which operates above its first bending critical speed.

Flexible Rotor Balancing - Balancing of a rotor which operates around or above its first natural frequency. This means that the rotor operates between its first and second mode shape.

FRF - Frequency Response Function

GMF - Gear Mesh Frequency

Influence Coefficient Balancing - An entirely empirical, flexible rotor balancing method which uses known trial masses to experimentally determine the sensitivity of a rotor; and subsequently uses this sensitivity information to determine a set of discrete correction masses that will minimize synchronous vibration amplitudes.

Measurement Error - Random or bias vibrations in empirical vibration measurements which are due to electrical and mechanical noise and other uncontrollable, variable physical parameters.

Measurement Plane - Rotor axial position where unbalanced response measurements are made.

Mode Shape - Shape of the response of a rotor-bearing system at a critical speed.

Phase Angle - A measurement used to define the circumferential location of a trial or correction mass, or unbalance response peak amplitude, relative to a specific angular reference position on the rotor.

Plane Transposition - The process of moving the two correction weights on a rigid rotor to different axial planes.

Quasi-static Unbalance - An unbalance rotor condition which the principle axis intersects the shaft axis at a point other than the center of gravity.

Reciprocity - A property of linear static or dynamic response whereby two points in a structure exhibit identical sensitivity to one another, regardless of which is used as the forcing point and which as the response point.

Residual Unbalance - The unbalance response of a rotor remaining after the completion of one or more balancing operations.

Rigid Rotor - A rotor which operates substantially below its first critical speed.

Rotor Balancing - The application of any of a variety of methods for reducing the unbalance response of a rotor through the addition of correction masses to adjust the rotor's mass centroidal axis.

Runout - the total linear displacement measured on the outside diameter in the radial direction and indicated on a dial indicator as the part is slowly turned.

SLM - Sound Level Meter

Static Runout - That part of the total runout that is due to synchronous structural and electrical sources, and does not change with rotational speed (and is thus not a function of unbalance); generally significant only for displacement sensors.

Static Unbalance - An unbalance rotor condition when the principal mass axis is displaced parallel to the shaft axis.

Sub-critical Speed - System vibration occurring at integer sub-multiples of the main system critical speed (1/2 ω_c , 1/3 ω_c , ... 1/10 ω_c) arising from stiffness non-linearity, such as a 'flat' shaft.

Super-critical Rotor - A rotor that operates above one or more critical speeds.

Synchronous Response - Rotor whirl whose frequency is identical to its rotational frequency.

Total Runout - The total synchronous component of the measured signal from a vibration sensor.

Trial Mass - A single mass, or group of masses, of known magnitude installed in a rotor at a specific balancing plane and angle, to generate data used for calculating influence coefficients of the rotor-bearing system for this balancing mass location at speeds and measurement planes at which data are taken.

Unbalance - The generally accepted term for the eccentricity of the center of mass of a rotor relative to its center of rotation.

Unbalance Response - Synchronous response of a rotor due to a lack of concentricity of its mass centroidal axis, with respect to its center of rotation.

Uncorrected Rotor - Rotor condition at the beginning of a balance step, with no trial or correction masses installed.

REFERENCES

[1] Broch, Jens T., *On the Frequency Analysis of Mechanical Shocks and Impulses*, Bruel and Kjaer Technical Review, Vol. 3, 1970.

[2] Crawley, P., *The Accuracy of Frequency Response Function Measurements Using FFT-Based Analyzers With Transient Excitation*, Journal of Vibration, Acoustics, Stress, and Reliability in Design, Vol. 108, January 1986.

[3] Darlow, Mark, S., *Balancing of High Speed Machinery*, Spinger-Verlag, 1989.

[4] Dudley, D. W., *Handbook of Practical Gear Design* - Gear Noise by Donald Houser, McGraw-Hill , New York, 1984.

[5] Ellison, A. J., Moore, C. J. and Yang, S. J., *Methods of Measurement of Acoustic Noise Radiated by an Electric Machine*, Proc. IEE 116, 1419-31, 1969.

[6] Everett, Louis, J., *Two-Plane Balancing of a Rotor System Without Phase Response Measurements*, Journal of Vibration, Acoustics, Stress, and Reliability in Design, Vol. 109, April 1987.

[7] Foiles, W. C., *Balancing With Phase Only (Single- Plane and Multi-Plane)*, Journal of Vibration, Acoustics, Stress, and Reliability in Design, Vol. 110, April 1988.

[8] Ginsberg, J. H., *Advanced Engineering Dynamics*, Harper and Rom Publishers, New York, 1988.

[9] Goodman, T. P., *A Least-Squares Method for Computing Balance Corrections*, Journal of Engineering for Industry, August 1964.

[10] Gupta, K., Gupta K. D., Athre, K., *Unbalance Response of a Dual Rotor System: Theory and Experiment*, Journal of Vibrations and Acoustics, Vol. 115, October 1993.

[11] Halfen, Earl M., *Shop Balancing Tolerances a Practical Guide*, Reliability Magazine, November/December 1994.

[12] Kelly, S. G., *Fundamentals of Mechanical Vibrations*, McGraw Hill, New York, 1993.

[13] Larsen, Holger. *Reverberation Process at Low Frequencies*. Bruel and Kjaer Technical Review, Vol. 4, 1978.

[14] Lees, A. W., *Vibration Spectra From Gear Drives*. Reliability Magazine, 1980.

[15] Licht, Torben. *Acoustic Emission*. Bruel and Kjaer Technical Review, Vol. 2, 1979.

[16] Lund, J. W., Tonnesen, J., *Analysis and Experiments on Multi-Plane Balancing of a Flexible Rotor*. Journal of Engineering for Industry, February 1972.

[17] Parkinson, A. G., *Balancing of Rotating Machinery*. Journal of Mechanical Engineering Science, January 1991.

[18] Randall, R. B., Upton R., *Digital Filters and FFT Techniques in Real Time*. Bruel and Kjaer Technical Review, Vol. 1, 1978.

[19] Rieger, N. F., Crofoot, J. F., *Vibrations of Rotating Machinery Part 1: Rotor-Bearing Dynamics*. Rochester Institute of Technology, New York, November 1977.

[20] Serridge, Mark, *Ten Crucial Concepts Behind Trustworthy Fault Detection in Machine Condition Monitoring*. Bruel and Kjaer.

[21] Singleton, Ken, *Tutorial on Experimental Modal Analysis*, Vibrations, Eastman Chemical Company, Vol. 11 No. 2, 1995.

[22] Sneck, Henry, J., *Machine Dynamics / Dynamics of Machinery*, Prentice Hall, 1991.

[23] Spur, G., Kirchheim, A., Schule, A., *Monitoring the Cutting Process in Multi-Spindle Lathes*, Technical University of Berlin.

[24] Tessarzik, J. M., Badgley, R. H., *Experimental Evaluation of the Exact Point- Speed and Least-Squares Procedures for Flexible Rotor Balancing by the Influence Coefficient Method*, Journal of Engineering for Industry, May 1974.

[25] Tessarzik, J. M., Badgley, R. H., Anderson, W. J., *Flexible Rotor Balancing by the Exact Point-Speed Influence Coefficient Method*, Journal of Engineering for Industry, February 1972.

[26] Thomson W. T., *Theory of Vibrations with Applications*, Prentice Hall, Third Edition, 1988.

[27] Vaughan, John. *Static and Dynamic Balancing Using Portable Measuring Equipment*. Bruel and Kjaer Application Notes. Second Edition. 1984.

[28] Westphal, G.. *Laboratory Tests of the Dynamic Performance of a Turbo-Charger Rotor-Bearing System*. Bruel and Kjaer Technical Review. Vol. 4. 1973.

[29] Williams, J. H.. *Fundamentals of Applied Dynamics*. John Wiley and Sons. 1996.

[30] Wort, J. F. G.. *The Rationale of Dynamic Balancing by Vibration Measurement*. Bruel and Kjaer Technical Review. Vol. 3. 1979.

[31] Wort, J. F. G.. *The Fundamentals of Industrial Balancing Machines and Their Applications*. Bruel and Kjaer Technical Review. Vol. 1. 1981.

[32] Wowk, Victor. *Machinery Vibration Balancing*. McGraw-Hill, Inc.. 1995.

[33] Yang, S. J.. Ellison, A.J.. *Machinery Noise Measurement*. Oxford University Press. New York. 1985.

[34] *General Motors Vibration Standards*. 1989.

[35] Technical Associates of Charlotte, Inc. *Illustrated Vibration Diagnostic Chart*. 1990.

VITA AUCTORIS

Name:	Jason Kyle Kushniruk
Place of Birth:	Windsor, Ontario, Canada
Year of Birth:	August 1972
Education:	University of Windsor Windsor, Ontario, Canada 1991 - 1995 B.A.Sc. Mechanical Engineering (Honours)

IMAGE EVALUATION
TEST TARGET (QA-3)

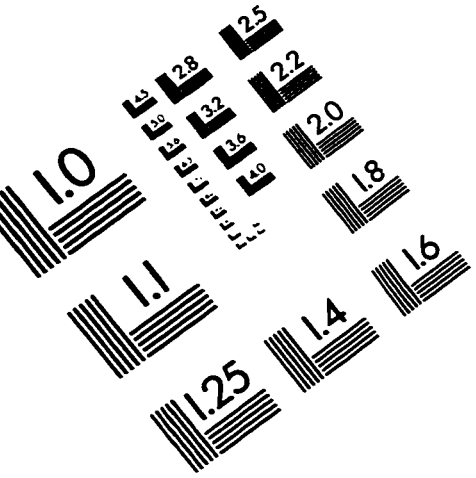

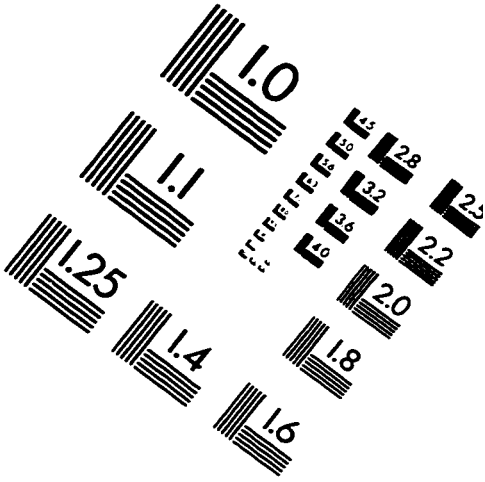

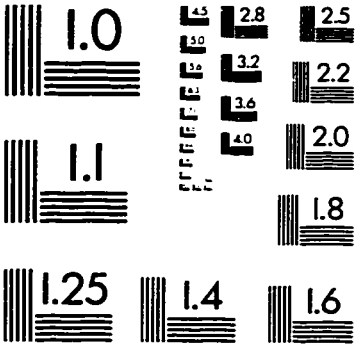

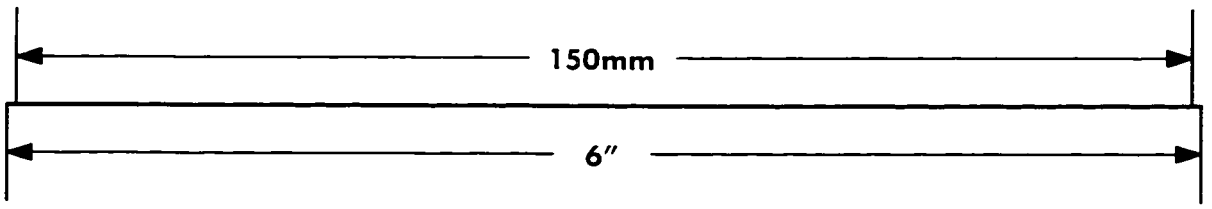

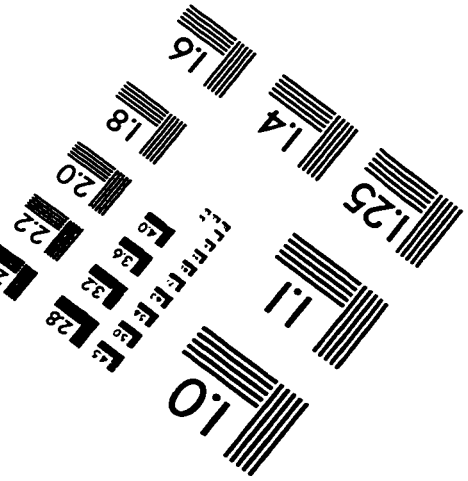

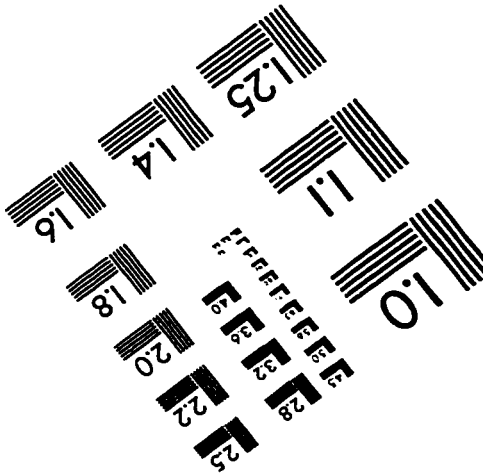

APPLIED IMAGE, Inc
1653 East Main Street
Rochester, NY 14609 USA
Phone: 716/482-0300
Fax: 716/288-5989